



72
P.S.



AVSCOM REPORT NO. TR76-23

**A COMPARISON OF VARIOUS NON-DESTRUCTIVE
INSPECTION PROCESSES USING HOT ISOSTATICALLY
PRESSED POWDER TURBINE PARTS**

AD A 040333

Donald E. Nulk
General Electric Company
Aircraft Engine Group
Lynn, Massachusetts 01910

December 1976

Final Report

Contract Number DAAJ01-75-C-0894

AD No. []
DDC FILE COPY,

Prepared for
US ARMY AVIATION SYSTEMS COMMAND
St. Louis, Missouri 63166

US ARMY AVIATION SYSTEMS COMMAND
St. Louis, Missouri 63166

DDC
RECEIVED
JUN 8 1977
B

DECLASSIFICATION STATEMENT A
Approved for public release,
Distribution Unlimited

1473

The findings in this report are not to be construed as an official Department of the Army position, unless so designated by other authorized documents.

Mention of any trade names or manufacturers in this report shall not be construed as advertising nor as an official indorsement or approval of such products or companies by the United States Government.

DISPOSITION INSTRUCTIONS

Destroy this report when it is no longer needed. Do not return to the originator.

REPORT DOCUMENTATION PAGE

READ INSTRUCTIONS
BEFORE COMPLETING FORM

1. REPORT NUMBER 19 TR76-23 ✓	2. GOVT ACCESSION NO. 18	3. RECIPIENT'S CATALOG NUMBER USAAVSCOM
4. TITLE (and Subtitle) 6 A COMPARISON OF VARIOUS NON-DESTRUCTIVE INSPECTION PROCESSES USING HOT ISOSTATICALLY PRESSED POWDER TURBINE PARTS.		5. TYPE OF REPORT & PERIOD COVERED Final Report 6/75 6/76
7. AUTHOR(s) 10 Donald E. Nulk		8. CONTRACT OR GRANT NUMBER(s) 15 DAAJ01-75-C-0894
9. PERFORMING ORGANIZATION NAME AND ADDRESS General Electric Company Aircraft Engine Group Lynn, Mass. 01910		10. PROGRAM ELEMENT, PROJECT, TASK AREA & WORK UNIT NUMBERS AMCMS CODE 1497.94.5 S7096.(XZ5)
11. CONTROLLING OFFICE NAME AND ADDRESS US Army Aviation Systems Command Attn: DRS AV-PUEB P.O. Box 209, St. Louis, Mo. 63166		12. REPORT DATE 11 Dec 1976
14. MONITORING AGENCY NAME & ADDRESS (if different from Controlling Office) 12 173 p.		13. NUMBER OF PAGES 171
		15. SECURITY CLASS. (of this report) Unclassified
		15a. DECLASSIFICATION/DOWNGRADING SCHEDULE
16. DISTRIBUTION STATEMENT (of this Report) Approved for public release Distribution unlimited		
1 <i>Final report June 75 - June 76</i>		
17. DISTRIBUTION STATEMENT (of the abstract entered in Block 20, if different from Report) -		
18. SUPPLEMENTARY NOTES -		
19. KEY WORDS (Continue on reverse side if necessary and identify by block number) Non Destructive Evaluation Photon Scattering Acoustical Holography Hot Isostatically Pressed Powder Ultrasonic Testing Turbine Rotating Hardware Fluorescent Penetrant Radiographic Tomography Neutron Radiation		
20. ABSTRACT (Continue on reverse side if necessary and identify by block number) Four emerging NDE (non destructive evaluation) processes were explored using aircraft turbine rotating hardware or simulated samples as test specimens. The material was a high strength nickel-base alloy, Rene' 95, which was made by hot isostatically pressing powder. The bases of comparison were conventional FPI (fluorescent penetrant inspection) and conventional ultrasonic testing.		

Unclassified

A 00

S/C 403329

20 (Continued)

Neutron radiography and radiographic tomography appear to have insufficient capabilities for NDE of this type of turbine hardware. Conversely, acoustical holography and photon scattering (Compton) methods offer much promise. Both are readily adaptable to fully automatic inspection of hardware. Both appear cost effective based on projected production inspection costs. Both make it possible to reduce metal envelopes of raw material thus decreasing material costs.

The acoustical holography process represents a later stage of development than the photon scattering method but both processes require additional development effort to obtain a production process. Much of this effort is in computer hardware and software which would reduce inspection time and permit calibration of equipment.

Results of inspection scans of test specimens are presented and compared to this report. Specific recommendations for continued effort is also outlined.



A-000

Unclassified

TABLE OF CONTENTS

<u>Title</u>	<u>Page No.</u>
SUMMARY	i
ACKNOWLEDGEMENTS	iii
FOREWORD	iv
LIST OF ILLUSTRATIONS	v
LIST OF TABLES	ix
INTRODUCTION	
HIP Powder Process	1
NON-DESTRUCTIVE EVALUATION	
General	5
Conventional Ultrasonics And Improved Techniques	10
Fluorescent Penetrant Inspection	28
Holosonics Intensity Mode Ultrasound	53
Holosonics Acoustical Holography	92
Intercom Rad Tech Neutron Radiography	100
Intercom Rad Tech - Compton Scattering	104
Radiographic Tomography	124
Comparison Of NDE Processes	138
EQUIPMENT MODIFICATIONS FOR PRODUCTION CAPABILITY	146
CONCLUSIONS AND RECOMMENDATIONS	148
BIBLIOGRAPHY	150
APPENDICES	151
DISTRIBUTION	159

SUMMARY

This contract was awarded to evaluate several emerging NDE (Non-Destructive Evaluation) processes and compare them with conventional ultrasonics and FPI (fluorescent penetrant inspection). The specimens evaluated were HIP (Hot Isostatically Pressed) powder Rene' 95⁽¹⁾ alloy like that used in the high pressure turbine of the T700 Aircraft Gas Turbine engine.

The evaluation of NDE processes for this contract revealed:

- o The prime method for evaluating cracks or similar defects open to the surface is an advanced method of FPI. This process requires an acid etch followed by an ultra high sensitivity penetrant, hydrophilic remover and non-aqueous developer.
- o An advanced technique of conventional ultrasonics was evaluated which increased ability to receive signals from small defects. However, a reliable evaluation of defect size and location is difficult at this time. For some scans, false indications exceeded those from known defects. Sensitivity to small size defects appeared to be erratic.
- o One of the new processes evaluated makes use of the intensity mode ultrasound using special equipment and some important modifications in ultrasonic techniques. Increased sensitivity or ability to find small defects has been demonstrated and the visual display that was employed contributes to ease and reliability of the inspection process. This NDE method appears to be the only one that offers improvement over conventional ultrasonics and can be ready for production NDE after some equipment modification and appropriate calibration effort.
- o Two new processes are very promising but require more development prior to the calibration phase. Both promise improvements in detectability, ease of interpretation and low costs. Additional development is recommended to bring these processes into production reality. The two NDE methods are Acoustical Holography and Compton Scattering Evaluation.
- o Two other new processes demonstrated limited applications to aircraft engines and no application to rotating turbine hardware. Some special applications were identified but were of peripheral interest to this contractual effort. These two NDE methods are Radiographic Tomography and Neutron Radiography.

(1) See Appendix I

With regard to the needs of NDE of HIP T700 hardware:

- o Non Metallic Inclusions - The most promising solution to NDE of non-metallic particle is the use of intensity mode, coherent pulse, coherent transmit Hologonic equipment ultrasound. Much work is necessary to calibrate equipment and perform parallel inspection with conventional ultrasonics before this improved NDE can be ready for production.
- o Cracks & Surface Defects - The improved FPI method described above appears to be superior to any other NDE method. For all methods evaluated, even when crack locations were known, the only process revealing entire cracked areas was the improved FPI method. Parts of various cracks were missed with all other methods. If crack inspection were assigned to this FPI method some shear sweeps of ultrasonic testing, now justified primarily for cracks, could be eliminated.
- o Porosity - Indications of porosity from sample P1 ⁽²⁾ were obtained with conventional ultrasonics and intensity mode modified ultrasonics using Hologonic equipment. However the number of indications were so numerous as to be confused with background or structure. No method has been established better than the current thermally induced porosity test, TIP⁽¹⁾ and density measuring method. One could project that the Compton Scattering Method has the sensitivity for accurately measuring density; however, this work needs development and would not be available for two or more years.

The work performed under this contract indicates the need for:

- o A calibration effort, appropriate fixturing and software effort to convert intensity mode, coherent pulse, coherent transmit ultrasound, (Hologonics, Inc. equipment) to production inspection capability.
- o A development effort with acoustical holography NDE to solve some of the software problems associated with turbine hardware and defect size being evaluated in the non rectilinear shapes. This process is probably two years behind the intensity mode described above.
- o A development effort to explore the problems of reliably inspecting turbine hardware by Compton Scattering Evaluation. More effort is needed prior to the calibration phase.

Note that both of these last two processes offer the possibility of a very quick, low cost, and reliable automatic inspection process. It may be desirable to avoid the intermediate modified ultrasonic step and go directly to acoustical holography.

(1) See Appendix I

(2) See Page 5

ACKNOWLEDGEMENTS

The Holosonic effort of this report represented the work of Dr. Victor Neeley and Norman Nutter of Holosonic Inc. of Richland, Washington. The neutron radiography was performed at IRT of San Diego, California by Howard Harper. For subsequent work on photon scattering measurements at the same company we are indebted to Mr. Hans Weber and Dr. Joseph Jon. The radiographic tomography process was examined by Mr. John Zurbrick of General Electric, Evendale who also supervised the work on high gain ultrasonics using graytone recording. Mr. Angelo Chiango, of General Electric, Lynn supervised the study of FPI and the standard ultrasonics effort. For the coordinating text, we are indebted to many contributors too numerous to mention.

FOREWORD

In the manufacture of high performance gas turbine engines, like the General Electric T700, it is normal practice to inspect all critical rotating parts by radiographic or ultrasonic methods. The ultrasonic inspection technique is currently used on most General Electric applications and, therefore, is currently applied to hot isostatically-pressed (HIP) parts under development (reference Contract No. DAAJ02-73-C-0106). (1)

The ultrasonic inspection technique represents the best current NDE (Non-Destructive Evaluation) method in production for forgings, but there are questions as to its value in a HIP component. The technique is more applicable to ingot casting defects, internal forging tears and center bursts that could be present in forgings but are not present with the HIP process. With a HIP component, no internal defects would be expected due to metal shearing because of the hydrostatic nature of stresses imposed.

Since all powder passes through a 60 mesh screen during powder processing, normal contaminants from the process (e.g. sprue erosion) would tend to be below .010 inch in diameter, a size difficult to reliably inspect with ultrasonics. Needle shaped defects could have one dimension much greater than .010 inch. Work is in progress to evaluate the impact of such small particles on mechanical properties. Also unintentional contamination can occur. An NDE process program must be in place while the quality aspects of this new process are being resolved. Later it will be used to monitor process quality to the standards being developed. (A more detailed analysis of possible HIP defects is given later in this report).

There is another consideration with ultrasonic inspection that is reason for concern. The high noise from the surface tends to hide responses from defects near the surface. To circumvent this problem, ultrasonic envelopes are frequently specified to permit gating out surface responses and later removing this material by machining. This is an expensive solution to an NDE problem especially with turbine alloys high in cost and difficult to machine. It is desirable to develop an NDE process that will not require a "throw away" envelope.

The basic purpose of this contractual program was to evaluate several emerging NDE processes and determine relevance for HIP turbine components, especially for the T700 engine. These NDE processes were compared with conventional ultrasonic and surface penetrant processes. It was anticipated that a process would emerge that would be as good or better than ultrasonic techniques currently used and not have some of its limitations when inspecting HIP hardware.

(1) See Bibliography

LIST OF ILLUSTRATIONS

<u>Figure No.</u>	<u>Title</u>	<u>Page No.</u>
1	Basic Dimensions Of HIP'd Rene' 95 Disk Used For NDE Samples	6
2	Map Of Hole Pattern Of Drilled Holes (.020 inch) In Sample S1	7
3	Description Of S2 Sample Having A Series Of Top Drilled And Side Drilled Holes	8
4	Description Of S3 Sample Having Holes As Indicated	9
5	Sketch Of S3 Showing Typical Hole Locations	14
6	Hole Plan Of S ₃ Sample Made With Groups Of Drilled Holes Of Three Different Sizes	15
7 & 8	Calibration Data For High Gain Ultrasonics	19 & 20
9	Summary Of Results Of 52 Scans Of S3 Sample	21
10	The C-Scan Number 2 (S3)	23
11	Examples Of Typical B Scans Probes Of S3	24
12	These 4 C-Scans And 2 B-Scans Illustrate A Wide Variation In Size And Shape Of The Signals From Holes Numbers 1 and 2	25
13	Scans Of S3 - Note Relative Shift Of #3 And #8	26
14	Scan Of S3 - Note #3 And #8 Compared To Figure 13	26
15	Examples Of False Indications (Arrows) On Various Scans	27
16-29	FPI Comparisons On Block C1	29 - 42
30	Schematic Drawing Of The System 200 Imaging Modes	57
31	Plan View Or C-Scan Of Selected Region Of Specimen D1	57
32	Electronic Section Or B-Scan View Of Selected Region Of Specimen D1	57
33	3-D Perspective Image Of Specimen D1	58

LIST OF ILLUSTRATIONS (CONT.)

<u>Figure No.</u>	<u>Title</u>	<u>Page No.</u>
34	Plan View Of C-Scan Image In Figure 33	58
35	Resolution Standard S 2	60
36	Plan View Of All (14) Drill Holes In Resolution Standard (S2) Back Surface Included For Reference	61
37	Same As 36 With Back Surface Gated Out	62
38	Reoriented Plan View And Section View Of Quadrant III	63
39	3-D Scan Of Quadrant III	64
40	Doped Specimen D 1; Description Of Gating Technique	66
41	Slice #1; D 1	67
42	Slice #2; D 1	68
43	Slice #3; D 1	69
44	Slice #3 - Lower Gain Setting	70
45	Slice #4; D 1	71
46	Slice #5; D 1	71
47	S3 Sample Showing Indications Of .007 Inch Holes	73
48	Defect Identification In HIP'd Disks - Serial - 45	74
49	Source As 48 From Opposite Side	75
50	Diagram Showing Preferential Electrochemical Attack Of A Surface With Non-Metallic Inclusions	77
51	Examples Of Small Non-Metallic Inclusions Found By Metallographic Evaluation Of Holographic Defect Indications	78 - 79
52	Spacial Illustration Of Defects	80
54	Sample 414; Identified Indications From A Selected Gate; C Scan And Simulated B Scan	82

LIST OF ILLUSTRATIONS (CONT.)

<u>Figure No.</u>	<u>Title</u>	<u>Page No.</u>
55	Sample 412; Exposure Similar To Figure 54	83
56	Full Width Scan Of Sample #413	84
57	Partial Scans Of #413; Ref. Figure 56	85
58	Sample 416 - Partial Scan Showing Innumerable Indications (Suitering Malfunction)	86
59 - 60	Two Methods Of Evaluating Cracks	88
61	Holosonic Ultrasound View Of C1 Specimen At High Gain. Method Of Figure 60 Was Used	89
62	Same As Figure 61 Except Method Of Figure 59 Was Used	89
63	Specimen C 2 Inspected With Method Illustrated In Figure 59	90
64	Image Of A Known Simulated Crack 1/4" Deep In A 1 1/2" Thick Test Sample Using The Same Set-Up As For Figure 63	90
65	Sample P 1 Gated To Record A Small Depth Increment	91
66	Transmitted Ultrasonic Beam From One Scanned Transducer Focussed At The Surface Of A Test Specimen	93
67	Typical Set-Up For Making An Acoustical Hologram	93
68	This Pattern Is Very Similar To That Obtained By Making An Acoustical Hologram Of A Point Source	95
69	Schematic Diagram - Optical Reconstruction Of An Acoustical Hologram	95
70	11MHz Acoustical Hologram Of Two Side Drilled Holes In Resolution Standard S 1	97
71-73	Reconstructed Image Of Figure 70	98
74	Neutron Radiography Exposure Of S2	102
75	Schematic Representation Of A Photon-Scattering Gage In Comparison To A Transmission Gage	106

LIST OF ILLUSTRATIONS (CONT.)

<u>Figure No.</u>	<u>Title</u>	<u>Page No.</u>
76	Schematic Representation Of Geometrical Arrangement Used For The Conceptual Model	112
77-80	Results Of Photon-Scattering Evaluation	116-119
81	Exposure Table & Diagram Of Exposure Technique	125
82	Shaper Sub System And Marker	126
83	Viewer For Radiographic Tomography	127
84	Density vs Exposure Curve Comparison	131

LIST OF TABLES

<u>Table No.</u>	<u>Title</u>	<u>Page No.</u>
I	List Of Scans Used For Gray Scale, High Gain Ultrasonic Testing Of S3 Sample	16-17
II, III & IV	Non-Destructive Test Evaluation Of Diametrically Cracked Block	45-51
V	Comparison Of Conventional Ultrasonics With Intensity Mode Holographic Ultrasonic Inspection	54
VI	Intentionally Doped Disks Of Rene' 95 Material (Contaminant Additions)	81
VII	Results From NDE Of Disks (From Table VI)	81
VIII	Table of Angles Used (Tomography)	133
IX	Description of S3 Disk and Results of Inspection	136

INTRODUCTION

The prime purpose of this contract was to evaluate some of the emerging or improved NDE processes. The specimens used were all Rene' 95 material, a turbine disk alloy prepared by the new HIP powder process. Improvements in two factors of inspection technique are desirable; first to reliably detect small defects to permit life extension of the advanced high strength alloys, and, second to be more cost effective.

HIP Powder Process

This basic NDE program is addressed to the emerging powder metallurgy program in which a container is filled with high quality alloy powder, evacuated and sealed. The container is then exposed to high temperatures and high pressures (typically 2125°F at 15,000 PSI pressure in argon) and sintered in a manner that yields 100% density, the container shrinking as the powder sinters. After appropriate heat treatment, the product has mechanical and physical properties very close to a forged disk. The nickel-base alloy used for this contract is a high strength high temperature disk alloy, Rene' 95.

Since the process involves isostatic pressures at elevated temperatures, internal shear forces, during processing, are essentially non-existent. The types of defects that could normally occur from the process are the following:

- o Non Metallic Inclusions - This is probably the most significant defect needing monitoring in the HIP process. The major source of non-metallics are oxides which come from mold washers, sprue erosion, ceramic container particles or unintentional shop dirt. Theoretically, no defect larger than .010 inch in diameter can occur since all powder is passed through a 60 mesh screen during powder processing. However, an NDE process is necessary for larger particles until or unless it is proven that basic process control could eliminate accidental occurrence of such defects.

First, there is the necessity of establishing an applicable morphology (size, shape and distribution) for non-metallic particles to permit a proper NDE target. Such work is in process. There are some opinions that reliable identification to .010 inch would be useful. Current capabilities of reliable inspection of defects are well above .010 inch in size. Reliable inspection of this size inclusion (if necessary) poses a difficult NDE problem. So the current program includes an evaluation of NDE capabilities to identify small non-metallic particles.

It may be necessary to establish powder cleaning procedures to eliminate most of these oxides present in the powder process. But the expeditious evaluation of this need requires better NDE processes than are represented by current production procedures.

(1) Appendix I

- o Porosity (or less than 100% density) - The major source of this type of defect is equipment malfunction or, argon contamination from the atomizing process. Process control appears to be solution to the malfunction problem. The processing of powders involve outgassing which should eliminate occluded gases. These remaining gases could contribute to small pockets of porosity which, if not agglomerated, would be of the order of .002 inch in diameter or smaller.

Porosity of this size tends to be outside the range of current NDE process capabilities. Two process control devices are used to monitor this possible malfunction. First, density measurements are made to insure 100% density to five significant figures in weighing accuracy. Secondly, a TIP (thermally induced porosity) test is run on each powder lot and on each lot of parts. This involves exposing a compacted sample to temperatures near the melting point. At these temperatures, any internal argon gas has maximum pressure and alloy yield strength is at a minimum. Thus, expansion of hole size of any internal porosity occurs. On subsequent cooling to room temperature, any porosity increase at temperature results in a density decrease at room temperature, thus improving accuracy of density evaluation for gas porosity.

Thus, for gas porosity there appears to be process control methods in place that may be more powerful than existing NDE methods. Nevertheless, evaluation of void identification is a part of this contract.

- o Cracks or surface defects - Such defects are primarily the result of improper quenching techniques during heat treatment but also can occur by improper cut off techniques.

Surface penetrant techniques are generally considered most applicable for this type of defect. However, some inspection errors have been made especially when cracks present are so tight that penetrants do not go into the defects of the specimen. In some instances, defects missed by penetrant methods have been found by ultrasonic testing and vice versa. This program will involve a critical look at capabilities of various NDE methods, penetrant and otherwise, to inspect for defects open to the surface.

NDE METHODS OF INSPECTION

- o Ultrasonic Inspection - This is the reference NDE method. Acoustical holography, neutron radiography, and radiographic tomography were compared with conventional ultrasonics.

Some experimental ultrasonic techniques were also used to assess future ultrasonic capabilities.

- o Penetrant Inspection - Various penetrant inspection processes have been used for years with good results. Difficulties have occurred primarily with two extreme defect types: very tight cracks and very open defects. A very tight crack may not be filled with penetrant and a very open crack will sometimes have all penetrant washed out prior to development sequence of inspection. A variety of solutions are available and some of the newer ones were evaluated for this report.

- o Acoustical Holography - This process combines the ultrasonic inspection process with holographic concepts to yield an imaging portrayal of the object illuminated by ultrasound. A transducer is used to focus ultrasonic energy on the surface of the part. Sound is transmitted through the part and signals are reflected back from defects and surfaces to the transmitting transducer (pulse-echo technique). The transducer traverses the object with the aid of appropriate scanners and bits of intelligence are received and recorded from a series of discrete positions.

These bits of intelligence are in the form of a series of superimposed sine waves differing from each other in intensity and phase. They appear as Fourier type wave patterns. These information units are combined with an ultrasound wave (single frequency) which results in an electronic interference signal. These signals vary in intensity and phase shift with time.

Upon completion of the scanning operation, the bits of intelligence are displayed on a cathode ray tube. This reconstructed image defines the part and any defects reflecting the ultrasound energy. The part can be displayed as if viewed from various directions. A basic view similar to C-scan in ultrasonic testing can be rotated to approximate the results of a B-scan. In this manner, the exact location of defects can be readily identified.

- o Intensity Mode Ultrasonic Inspection Using Holosonic Equipment- The Holosonic electronic equipment is capable of a modified ultrasonic inspection. The process, used for much of the Holosonic Inc. effort for this report, was intensity mode ultrasonic inspection using pulse-echo techniques similar to conventional ultrasonics. However, transducers with broad band frequency response were used and driven (not resonated at their resonate frequency) at the desired frequency using a coherent pulse. The reflected signal was analyzed using a coherent transmit mode which permitted analysis of phase shift as well as intensity. Whereas 5 MHz is the effective frequency limit of most current conventional ultrasonic equipment, this Holosonic inspection was performed at 5 to 11.2 MHz, a frequency range that appears to offer some advantages in reduced wave length and increased resolution.

- o Neutron Radiography - This is a process of producing a radiographic image similar to conventional X-radiography. The difference lies in the energy source, a neutron emitter rather than X-ray emitter. The source of neutrons for this work was Californium 252.

Several differences between neutron and X-ray radiography are described briefly below:

- o Neutrons have different capture cross section than X-rays. Heavy metals are effective in impeding X-rays but tend to be quite transparent to neutrons. Light metals or atoms, Beryllium, Hydrogen, Nitrogen and Oxygen as examples, tend to impede neutrons but have little effect on X-rays.
- o With X-rays, the X-rays themselves that pass through the object, impinge and expose the film. The film is transparent to neutrons but is exposed by neutrons passing through object and film, activating the film backing strip and exposing the film by reflected radiation. The backing material is typically gadolinium.
- o Generally, exposure times are longer with neutron radiography.
- o Since radiation from the californium involves γ rays in addition to neutrons, new and different shielding techniques are useful to prevent film fogging.
- o Compton Scattering Evaluation - This is a very new technique developed within the last 12 months. The original IRT-Army contract was modified to include a small effort of HIP'd Rene' 95 hardware. It involves the measurement of the scattered radiation from a collimated X-ray beam generated by a cobalt 60 source.
- o Radiographic Tomography - This process involves an imaging technique with conventional radiography similar to a stereoscopic projection. A stack of several X-ray films are used for this evaluation. A series of exposures are made with different impinging angles of the X-ray source. Then with the aid of reference dots on the film and a special trimming device, the films are cut into discrete parallelograms. These trimmed films are placed into a special cassette in front of a conventional viewer. By manipulating the relative position of the film stack, using a special device, it is possible to bring any part of the object into focus. There are claims that unwanted portions of the part can be placed out of focus and focus concentrated on the portion being evaluated so that the effective clarity of picture is enhanced.

NON DESTRUCTIVE EVALUATION

GENERAL

The following HIP'd Rene' 95 samples were used in this evaluation:

- o P 1 T700 turbine disk blank, see Figure 1 that was compacted yielding low density due to an equipment malfunction.
- o D 1 & D 2 Two 6 inch diameter, 2 inch thick disks were compacted with intentionally added oxides. These were to be used to evaluate capabilities of identifying non-metallic particles. Unfortunately numerous particles were added making definitive analysis of a few defects impractical. As indicated later in this report, other samples were used for this preliminary calibration.
- o S1, S2 & S3 Three disks were made with hole patterns drilled to form reference defects in various sizes, locations, and orientations. These are presented in Figures 2, 3 and 4.
- o C1 & C2 Two cracked samples were used, one similar in shape to D1 and one a rectangular block approximately 1 1/2 X 3 1/2 X 11 1/4 inches in size.

In addition, six turbine blanks like Figure 1, were used. Additional samples were introduced later in the program.

In the following sections, the results are given of non-destructive evaluation of the samples described above using the various NDE methods. It was the intent of the program to develop satisfactory procedures with these intentionally defected samples and apply the processes to the six HIP T700 disks. Comparative evaluation was planned for all processes. Early effort demonstrated that, after initial evaluation, some processes did not warrant further effort and so evaluation was discontinued.

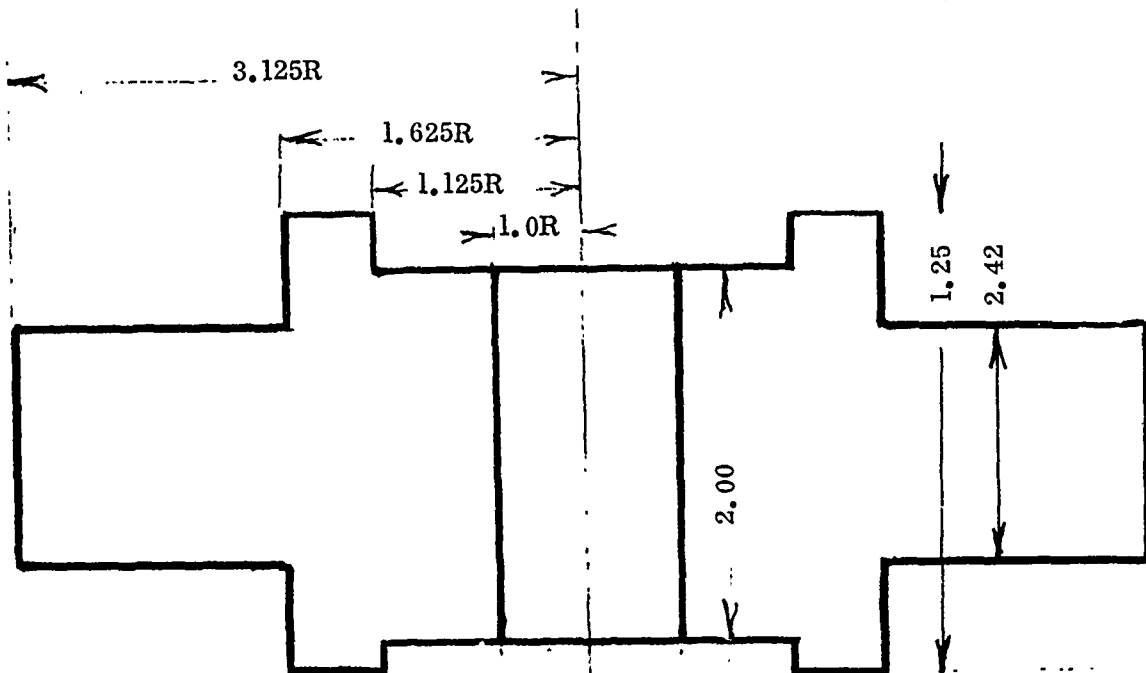


Figure 1: Basic Dimensions Of HIP'd Rene' 95 Disk Used For NDE Samples.

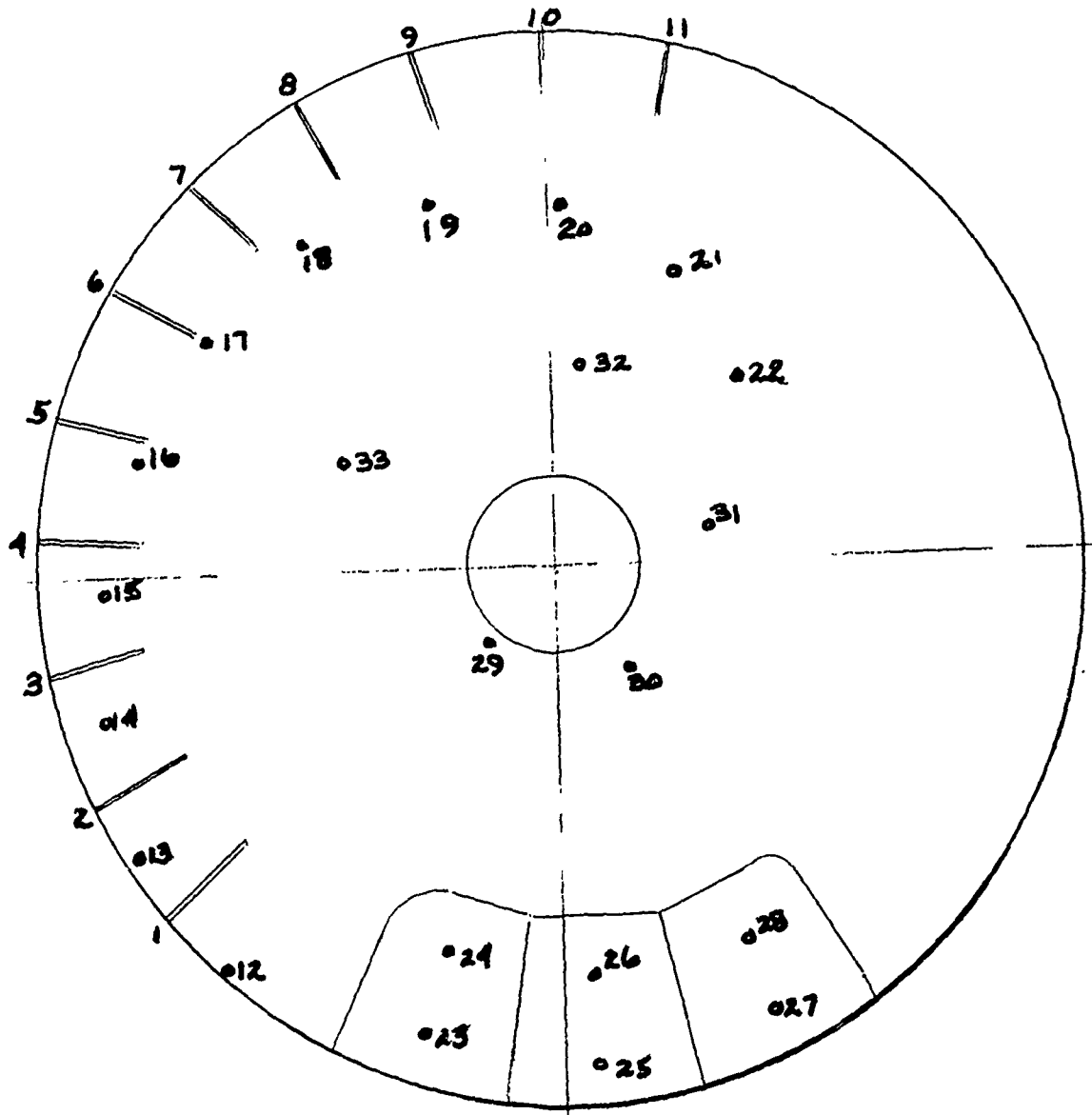
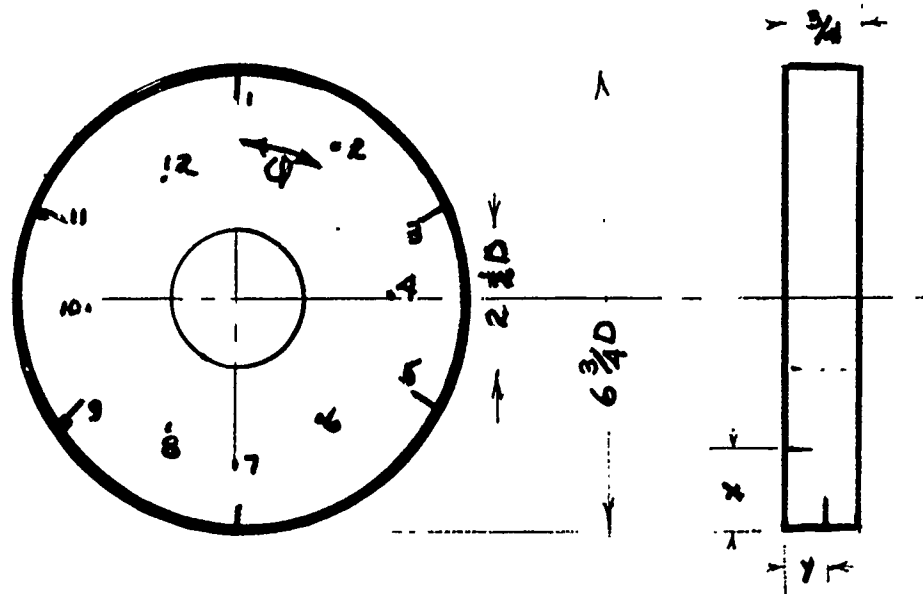


Figure 2: Map Of Hole Pattern Of Drilled Holes (.020 inch)
In Sample S-1.

BDD COPY



Hole #	Depth In	X (Mils)	Y (Mils)	Q
1	.500	-	579	0
2	.500	1012	-	30
3	.500	-	491	60
4	.400	1083	-	90
5	.500	-	400	120
6	.300	1100	-	150
7	.500	-	310	180
8	.200	-	-	210
9	.500/.300*	-	202	240
10	.100	1115	-	270
11	.500/.100	-	110	300
12	.600	1115	-	330

* 2 Holes

Figure 3: Description Of S 2 Sample Having A Series Of Top Drilled And Side Drilled Holes.

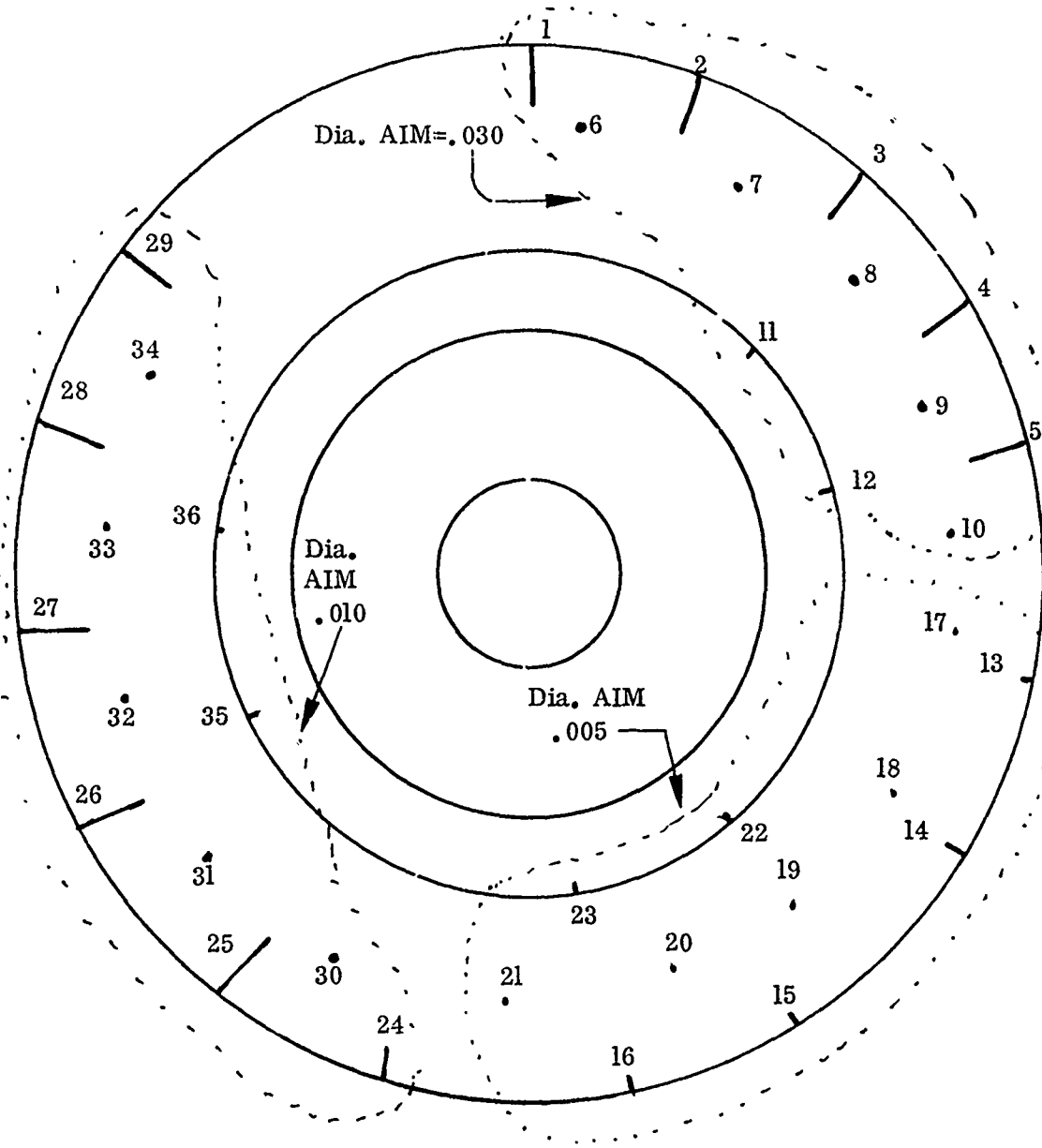


Figure 4: Description Of S 3 Sample Having Three Families Of Holes As Indicated Above. Cross Section Is The Same As Figure 1.

CONVENTIONAL ULTRASONICS AND IMPROVED TECHNIQUES

The ultrasonic testing described below was to be used as a comparison standard for all the new NDE processes.

The same ultrasonic technique that is specified for the T700 program was used to evaluate these samples. The technique is described in the G.E. specification P3TF1. ⁽¹⁾ The gain setting was adjusted to give a 80% full scope indication from a .020 inch side drilled hole. Any single point indication above 40% was considered rejectable. Any indication at 30% and 1/2 inch long was considered rejectable.

Results

The D1 and D2 samples were examined but found to have too many indications to make plotting practical. It was the original intent of this test to have a discrete number of oxides added to make D1 and D2 samples. Thus the evaluation of sensitivity of this process to these small defect sizes was not possible with the samples prepared.

The C1 and C2 cracked samples were examined using the standard procedure which gated out on 1/8 inch of the surface, the region known as the ultrasonic envelope. Several segments of the known crack were missed. By inspecting with a nonstandard shear wave technique without the gate, most of the crack was revealed. This inspection included the normal four shear scans, two circumferential tilt, clockwise and counter clockwise, and two axial tilt. Portions of the cracks were still missed indicating the need to have near perpendicular orientation of the shear wave to the crack in order to be effective. Another non-standard longitudinal scan revealed portions of the crack extended as far as 3/8 inch below the surface but still some portions were missed with the initial inspection scans. Considering the fact that crack locations were known and could be seen visually, little confidence can be placed on ultrasonics to identify such defects.

S1, S2 and S3 - There was no difficulty in identifying all .020 inch drilled holes in S1 and S2. The S3 disk had holes varying from .007 to .030 inch in diameter. Not all .007 inch holes were revealed by conventional ultrasonics.

HIGH GAIN ULTRASONICS

General Electric has been pursuing various approaches to high gain ultrasonics for the last few years. This has included work to standardize transducer response and electronic response of the ultrasonic equipment. Electronic modifications and additions have been employed to get high fidelity signal response.

(1) Appendix II

Previous attempts to use higher gain have been thwarted by high "noise" which is really a mixture of electronic malfunction and unintelligible signals. To improve interpretation, effort has been made to perfect computer processing of signal response which ignores confusing signals and concentrates on prime signal response which is then displayed with devices that are more readily interpreted. One such display is called "High Resolution Gray Scale Recording" and is described below.

The S3 sample was intensively evaluated using this process to examine some of its merits and to compare results with some of the new NDE processes. It is noteworthy that the scanning development with computer analysis and visual display is effort that is applicable to other emerging processes such as Acoustical Holography and Compton Scattering Analysis.

Gray Scale Recording - Process Description

These gray scale recordings used to evaluate S3 contain information directly related to the peak echo amplitude of each pulse received from the bulk material of the disk. The peak amplitude is recorded as 15 levels of gray tone, typically with black representing very low echo amplitudes (5% of full CRT) and white very high echo amplitudes (95% of full CRT) with the grays linearly spread between. Each data point is laid down exactly at the position the ultrasound beam entered the disk surface when the echo was received. The projected view of all the data contains the observed surface area of the scan (known as a C-scan) for two dimensions, plus the amplitude gray levels. Depth position of the echo, the third dimension, is not recorded. Normally the depth (time) gate window is set to include the material just behind the front surface to just ahead of the back surface, excluding front and back-surface reflection echoes. Where depth information is also desired, the depth gate window is narrowed to a convenient thickness of material, i.e., 1/8 to 1/4 in. so that only echoes occurring from one layer are recorded. A series of scans and recordings covering the total sequence of layers from front to back provides the full set of data.

Full-depth gated, and section or layer-gated C-scans were both used in evaluating conventional ultrasonic detectability of the holes in S3. By this means a set of data was produced which could be directly compared with Hologosonics intensity mode and acoustical holographic mode results.

The output of the ultrasonic instrument is fed into a dot generator which converts the major amplitude of the signal to a gray scale tone. Dry facsimile paper having the inherent capacity to produce a maximum of 15 shades of gray using a dot-tone format provides the image record. The paper is essentially a black base coated with a white overlay. The overlay is burned away by an electric current upwards of 250 volts. Because the "blackness" of each

burned spot is constant, only the length and width of the dot varies to produce the impression of grayness. "Gray" as seen by the eye is the percent of black area against a white background over a specific area of interest. As the percent of black area increases, the percent of white area decreases, giving 15 shades from essentially pure white to pure black.

A practical gray scale computer module (analog) and writing driver system was designed and fabricated at GE/AEG in the Evendale lab for application in composite blade and metal disk inspection programs over the past three years. One of these same systems was used in the S3 disk inspections. Practical time and cost considerations dictated that a .020 inch line-to-line spacing (scanning index) in the recordings be used, a common spacing known to sacrifice very little in image gray-tone quality or data content. Line-to-line spacing ranges from .005 to .030 inch for maximum to minimum image fidelity.

Inspection Plan

Ultrasonic inspection of engine disks is controlled in general by GE/AEG Specification P3TF1⁽¹⁾ as described in the preceding section. The inspection of S3 disk was conducted within this specification. The inspection plan was established to first accomplish P3TF1 calibrations and scans on S3 which would be typical of production inspection conditions using the .020 inch index for purposes of gray scale recording. A typical full-depth time gate window was used.

Second, the ultrasonic instrument receiver gain was increased by 12db (4X voltage ratio) for longitudinal mode scans and 6db (2X voltage ratio) for shear mode scans. In these cases instrument gain was near maximum. Again, a typical full-depth time gate window was used.

Third, the section-gate technique was applied. When depth-section scanning is used, the ultrasonic instrument gain setting can be adjusted to the calibration value for that depth, thereby offering the best relationship between recorded echo amplitude and defect size. Also, the series of adjacent layer scans generally give equal tones for equal defect size, regardless of depth. To effect the most capability out of conventional ultrasonic inspection, in this comparison effort with the Hologonics' capabilities (in terms of drilled-hole detection), the ultrasonic instrument gain was maximized. This was done by using maximum instrument gain for the near-front-surface and deepest layers, with lowered gains for the between layers, while keeping grain structure and front-surface ringing noise to no greater than 20% of full CRT amplitude.

(1) Appendix II

Disk S3 was placed on the turntable with the axially drilled holes entering from the lower surface, Figure 5. Observed from above, the hole positions appeared as in Figure 6. The 52 actual scans accomplished are listed in Table I, grouped according to the three scan groups described above. Scan numbers represent the chronological order in which the scans were produced, and identify the individual scan gray-scale recordings.

Part attitude with respect to V/S beam all inspections made on this surface.

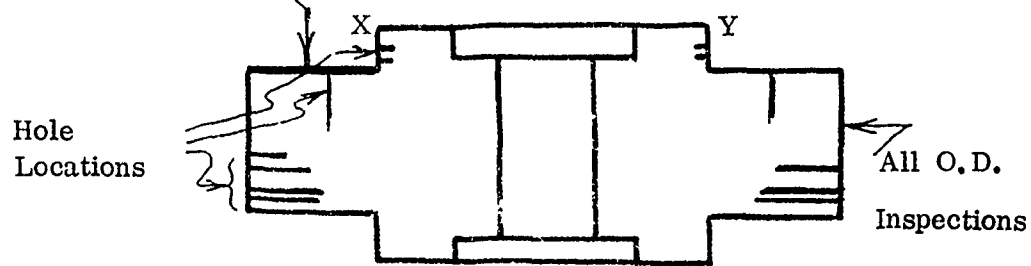


Figure 5. Sketch of S3 Showing Typical Hole Location. Note that holes in X and Y were considered Too Shallow to detect without special setups.

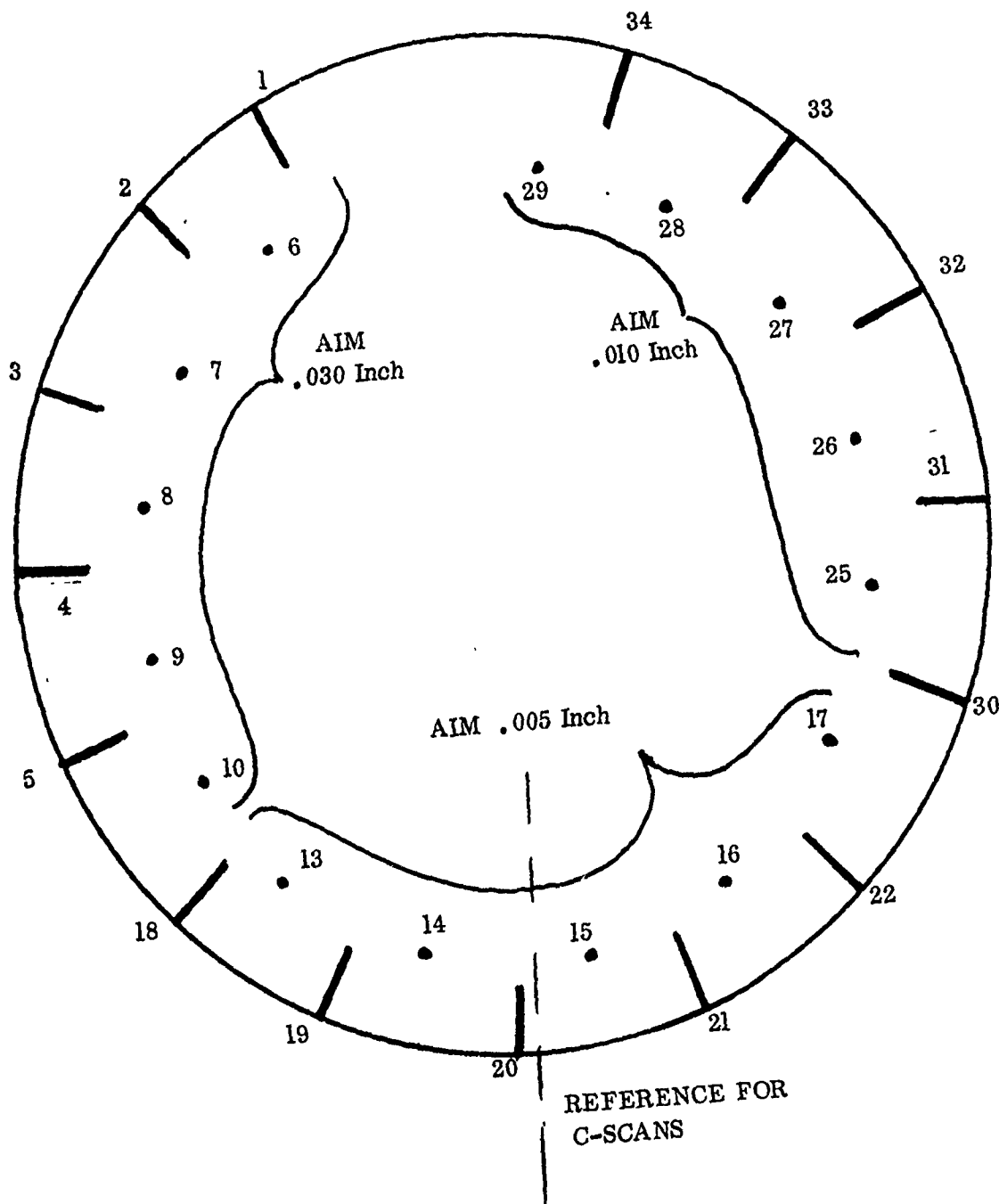


FIGURE 6 . Hole Plan Of S-3 Sample Made With Groups Of Drilled Holes Of Three Different Sizes.

TABLE 1

<u>SCAN NO.</u>	<u>MODE</u>	<u>FACING DIRECTION</u>	<u>CALIBRATION GAIN</u>	<u>TIME GATE WINDOW</u>
<u>FIRST*</u>				
1	Longitudinal	Top Normal	170 P3TF1	Full Depth
3	Circum. Shear	Top CW 19°	450 P3TF1	Full Depth
4	Circum. Shear	Top CCW 19°	450 P3TF1	Full Depth
7	Radial Shear	Top In 19°	450 P3TF1	Full Depth
9	Radial Shear	Top Out 19°	450 P3TF1	Full Depth
11	Longitudinal	O.D. Normal	200 P3TF1	.125 to 1.5
15	Circum. Shear	O.D. CW 19°	450 P3TF1	.125 to 1.5
13	Circum. Shear	O.D. CCW 19°	450 P3TF1	.125 to 1.5
<u>SECOND</u>				
2	Longitudinal	Top Normal	680 P3TF1+12db**	Full Depth
6	Circum. Shear	Top CW 19°	900 P3TF1+6db	Full Depth
5	Circum. Shear	Top CCW 19°	900 P3TF1+6db	Full Depth
8	Radial Shear	Top in 19°	900 P3TF1+6db	Full Depth
10	Radial Shear	Top Out 19°	900 P3TF1+6db	Full Depth
12	Longitudinal	O.D. Normal	800 P3TF1+12db	.125 to 1.5
16	Circum. Shear	O.D. CW 19°	900 P3TF1+6db	.125 to 1.5
14	Circum. Shear	O.D. CCW 19°	900 P3TF1+6db	.125 to 1.5
<u>THIRD</u>				
34	Longitudinal	Top Normal	420 P3TF1+8.9db	.25 to .50
35	Longitudinal	Top Normal	900 P3TF1+15.5	.50 to .75
36	Longitudinal	Top Normal	1000 P3TF1+15.9	.75 to 1.00
37	Longitudinal	Top Normal	1000 P3TF1+15.4	1.00 to 1.25
43	Circum. Shear	Top CW 19°	920 P3TF1+12db	0 to .25
44	Circum. Shear	Top CW 19°	920 P3TF1+12db	.25 to .50
45	Circum. Shear	Top CW 19°	1000 P3TF1+10.7db	.50 to .75
36	Circum. Shear	Top CW 19°	1000 P3TF1+7db	.75 to 1.00
47	Circum. Shear	Top CW 19°	1000 P3TF1+7db	1.00 to 1.25
38	Circum. Shear	Top CCW 19°	920 P3TF1+12db	0 to .25
39	Circum. Shear	Top CCW 19°	920 P3TF1+12db	.25 to .50
40	Circum. Shear	Top CCW 19°	1000 P3TF1+10.7db	.50 to .75
41	Circum. Shear	Top CCW 19°	1000 P3TF1+7db	.75 to 1.00
42	Circum. Shear	Top CCW 19°	1000 P3TF1+7db	1.00 to 1.25

TABLE I (Cont.)

<u>SCAN NO.</u>	<u>MODE</u>	<u>FACING DIRECTION</u>	<u>CALIBRATION GAIN</u>	<u>TIME GATE WINDOW</u>
48	Radial Shear	Top Out 19°	920 P3TF1+12db	0 to .25
49	Radial Shear	Top Out 19°	920 P3TF1+12db	.25 to .50
50	Radial Shear	Top Out 19°	1000 P3TF1+10.7db	.50 to .75
51	Radial Shear	Top Out 19°	1000 P3TF1+7db	.75 to 1.00
52	Radial Shear	Top Out 19°	1000 P3TF1+7db	1.00 to 1.25
23	Longitudinal	O.D. Normal	560 P3TF1+12db	.25 to .50
24	Longitudinal	O.D. Normal	750 P3TF1+14db	.50 to .75
25	Longitudinal	O.D. Normal	1000 P3TF1+16.5db	.75 to 1.00
26	Longitudinal	O.D. Normal	1000 P3TF1+15.4db	1.00 to 1.25
27	Longitudinal	O.D. Normal	1000 P3TF1+14db	1.25 to 1.50
17	Circum. Shear	O.D. CW 19°	920 P3TF1+12db	0 to .25
18	Circum. Shear	O.D. CW 19°	920 P3TF1+12db	.25 to .50
19	Circum. Shear	O.D. CW 19°	1000 P3TF1+10.7db	.50 to .75
20	Circum. Shear	O.D. CW 19°	1000 P3TF1+7db	.75 to 1.00
21	Circum. Shear	O.D. CW 19°	1000 P3TF1+7db	1.25 to 1.50
28	Circum. Shear	O.D. CCW 19°	920 P3TF1+12db	0 to .25
29	Circum. Shear	O.D. CCW 19°	920 P3TF1+12db	.25 to .50
30	Circum. Shear	O.D. CCW 19°	1000 P3TF1+10.7db	.50 to .75
31	Circum. Shear	O.D. CCW 19°	1000 P3TF1+7db	.75 to 1.00
32	Circum. Shear	O.D. CCW 19°	1000 P3TF1+7db	1.00 to 1.25
33	Circum. Shear	O.D. CCW 19°	1000 P3TF1_2.6db	1.25 to 1.50

* These scans are typical P3TF1 procedures.

** Production reliability has not yet been established for this process.

Equipment

The following equipment was used to produce the conventional ultrasonic pulse-echo data:

MANIPULATOR-TANK SYSTEM:

Automation Industries

4' X 6" X 3' Tank
US640 Bridge (X & Y)
US740 Vertical (Z) Axis and Gimbal
US942 Polar/Drum Recorder and Turntable

ULTRASONIC INSTRUMENT:

Automation Industries

UM721 Reflectoscope S/N 3163-8
10N Pulser-Receiver
E550 Transigate
Transducer 57A4705 SIL - 3/4" dia
15 MHz S/N 21452. Approximately 7 inch focal length in water

RECORDING SYSTEM:

GE/AEG Gray Scale Computer Module
Bogen MT60 Booster Amplifier
Wavetek Model 130 Function Generator
Fitchburg Timeface NDR Facsimile Paper

Calibration

Calibration was performed according to Specification P3TFl in order to relate all scan data to production inspection instrument gain levels. The standard calibration block No. XNB of Inconel 718 was used for this purpose. Calibration Sheets Figure 7 and 8 are included. Additional reference data were obtained from a cylinder of Rene' 95 PM material as follows:

CALIBRATION DATA

DV 240-A

Equipment Description:						
Chassis S/N	Pulser S/N	Transd. S/N	Gate S/N	Calib. Blk. S/N & Material	Linearity Check Date	P/M Date
3163-8		21452		XN: IN718		

Calibration Conditions:						
Delay Range Setting	Water Path	Frequency Settings	Scanning Gain Setting	Mat'l. Calibration Setting	Delay Setting	Course Delay Setting
	5	5 MHz				

T.C.G. Information:			General Information:		
Delay Setting	Near Gain Setting	Slope Setting	Calibration Date	Inspector	Time
			2-13-76		1st 2nd

CALIBRATION

	.125	.250	.375	.500	.625	.750	.875	1.00	1.250
LONGITUDINAL	620	250	260	240	250	290	280	260	500
recheck									
SHEAR									
recheck									
ABLE									
recheck									
	1.50	1.750	2.00	2.125	2.250	2.375	2.500	2.750	2.875
LONGITUDINAL	350								
recheck									
SHEAR									
recheck									
ABLE									
recheck									

Percent Merge of .125" longitudinal @ scanning gain level _____

Problems: (Mach. Malfunction, Part Non-Conformance, etc.)

List changes in equipt: (Pulser, Receiver, Scope, Gate, Transducer, etc.)

Note: Any changes in equipment requires a new calibration sheet

Reason for change:

Figure 7

CALIBRATION DATA

DV 240-A

Equipment Description:										
Chassis S/N	Pulser S/N	Transd. S/N	Gate S/N	Calib. Bk. S/N & Material	Linearity Check Date	P/M Date				
3163-8		21452		XNB 12/13						
Calibration Conditions:										
Delay Range Setting	Water Path	Frequency Settings	Scanning Gain Setting	Mat'l. Calibration Setting	Delay Setting	Course Delay Setting				
	6.125	5 MHz								
T.C.G. Information:			General Information:							
Delay Setting	Near Gain Setting	Stop Setting	Calibration Date	Inspector	Time					
			2-16-70	PARKER	1st 2nd					
CALIBRATION										
		.125	.250	.375	.500	.625	.750	.875	1.00	1.250
LONGITUDINAL		330	150	150	140	150	150	160	150	170
	rocheck									
SHEAR 45°		230	230	210	230	280	290	330	450	450
	rocheck									
ABLE										
	rocheck									
		1.50	1.750	2.00	2.125	2.250	2.375	2.500	2.750	2.875
LONGITUDINAL		200								
	rocheck									
SHEAR		740								
	rocheck									
ABLE										
	rocheck									
Percent Merge of .125" longitudinal @ scanning gain level _____										
Problems: (Mech. Malfunction, Part Non-Conformance, etc.)										
List changes in equip: (Pulser, Receiver, Scope, Gate, Transducer, etc.)										
Note: Any changes in equipment require a new calibration sheet										
Reason for change:										

LONGITUDINAL:

<u>Hole</u>	<u>Gain</u>	<u>Amplitude</u>	<u>Water Path</u>
1/4"	230	80%	4.375"
1"	230	80%	4.375"

SHEAR:

<u>Hole</u>	<u>Gain</u>	<u>Amplitude</u>	<u>Water Path</u>
1/4"	350	80%	4.375"

Results

The complete set of 52 gray-scale C-scans were reviewed and hole numbers entered on them where echo images appeared. This information was then transferred to Figure 9 as a summary of individual hole detectability by the longitudinal mode and the shear mode with its four facing directions. Full depth gated and section level gated echo occurrences were presented together in Figure 9 to express the value of retaining the third dimension information.

Scan No. 6 revealed all holes although No. 28 was weak. The next largest number of indications (29) on one single scan record occurred in Scan No. 5, circumferential shear, facing counterclockwise, P3TF1 calibration plus 6db (2X voltage) increased sensitivity, full-depth gated. Maximum possible is 30 with hole no. 28 as the only one not detected in this scan. Similar success was obtained in Scan No. 4 (28 indications), No. 10 (28 indications), No. 9 (27 indications), No. 47 (27 indications), and No. 42 (26 indications) all in the shear mode.

A typical C-scan is shown in Figure 10. A typical B-scan is shown in Figure 11. The biggest problem areas are associated with interpretation. For example, a given size defect appears to vary widely in size by the indications in the views of Figure 12. Figure 13, shows two shear scans, one clockwise and one counterclockwise. Note the relative positions of 3 and 8. If depth were known, the defect location could be depicted graphically, but it is not too accurate. Clear and concise presentation of location does not exist. Figure 14 is a similar distortion illustrated by the shear angle rotated 90°. Then finally, false indications are sometimes greater than indications from known defects as illustrated in Figure 15.

Even with this advanced method of ultrasonic inspection, the major problems are interpretation and reliable identification of all defects. This problem is discussed in the NDE comparison section.

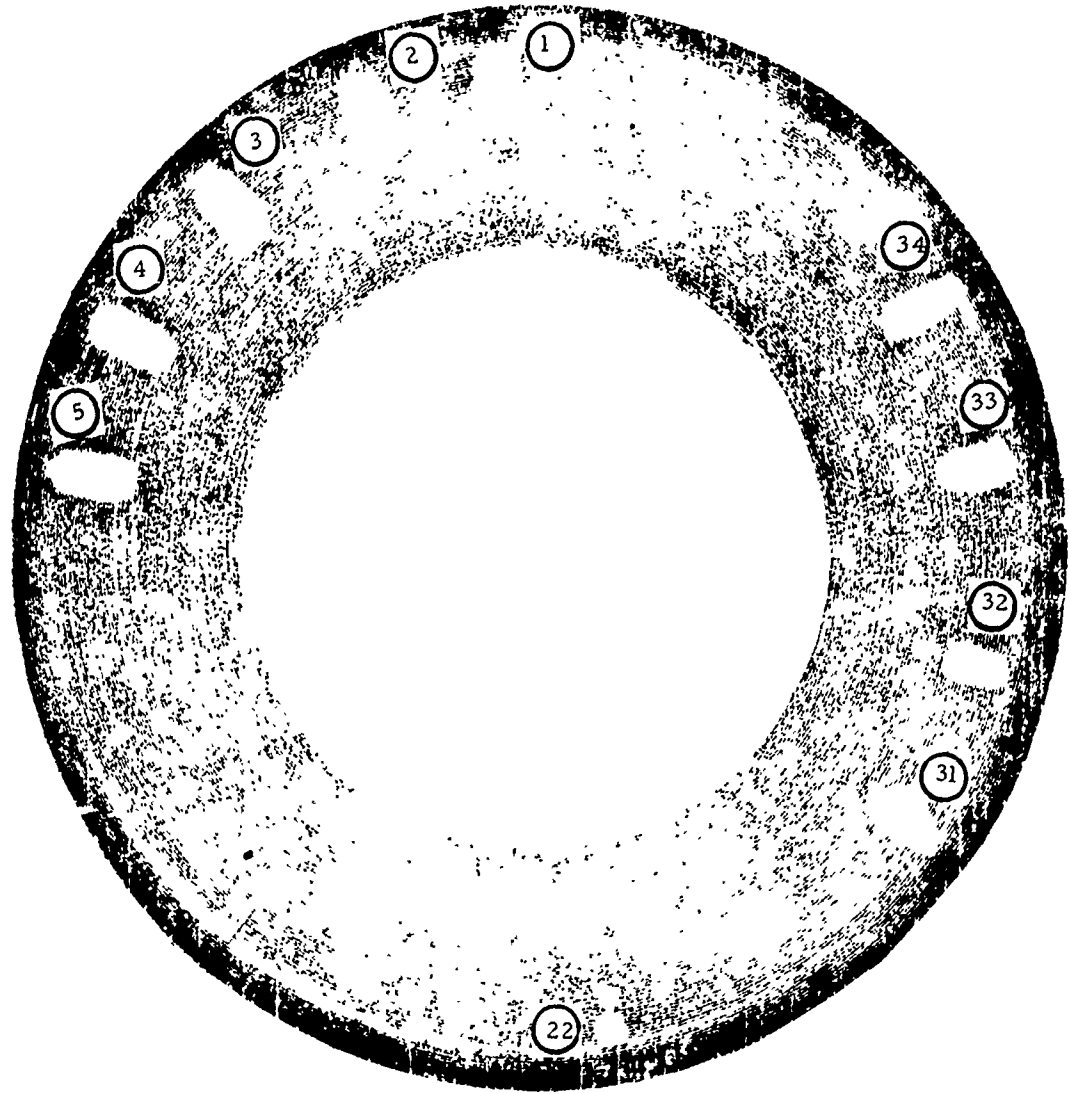


Figure 10. The C-scan Number Two. The Circled Numbers Refer to Indications From Numbered Holes in S3 Sample.

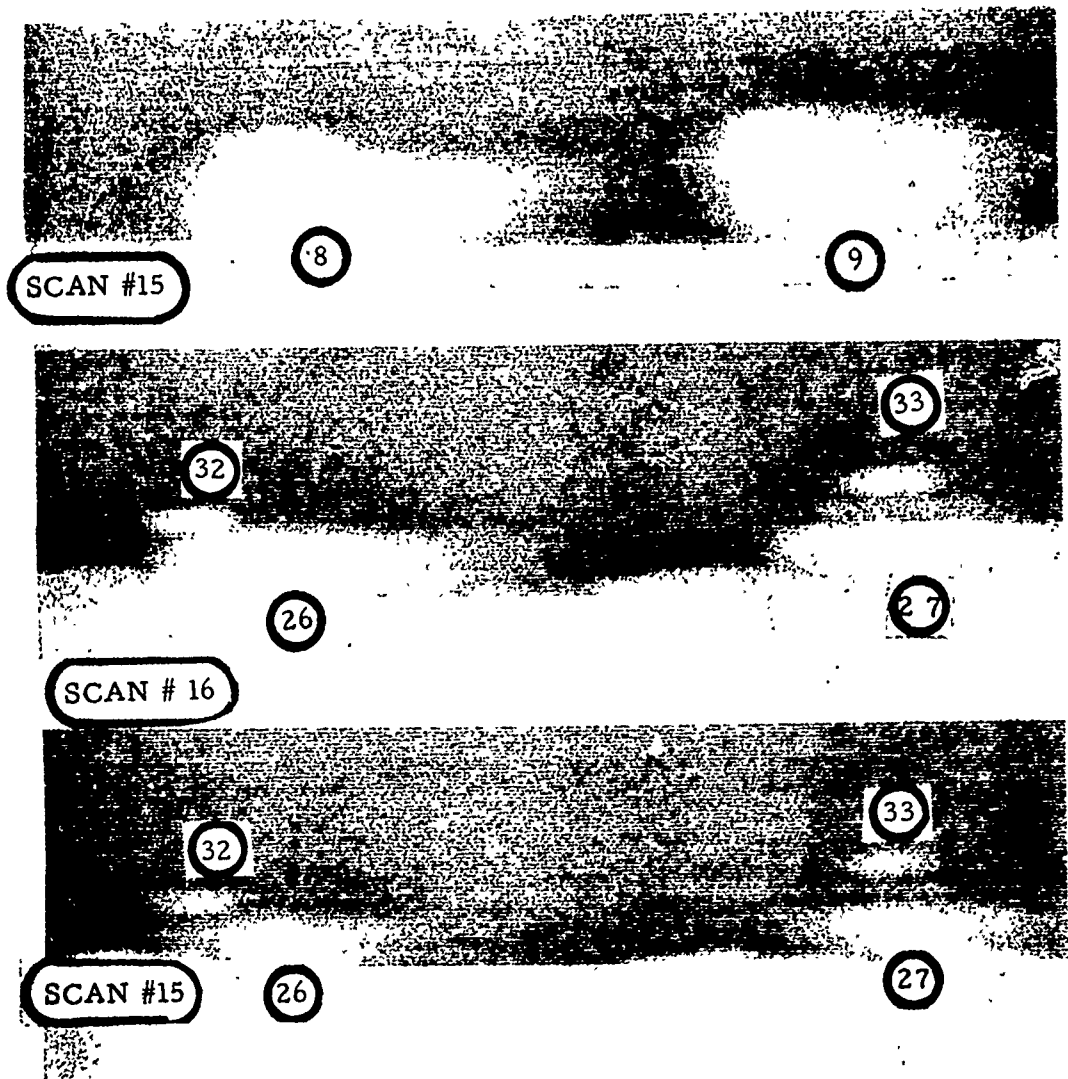


Figure 11. Examples of Typical B-Scan Probes of S3.

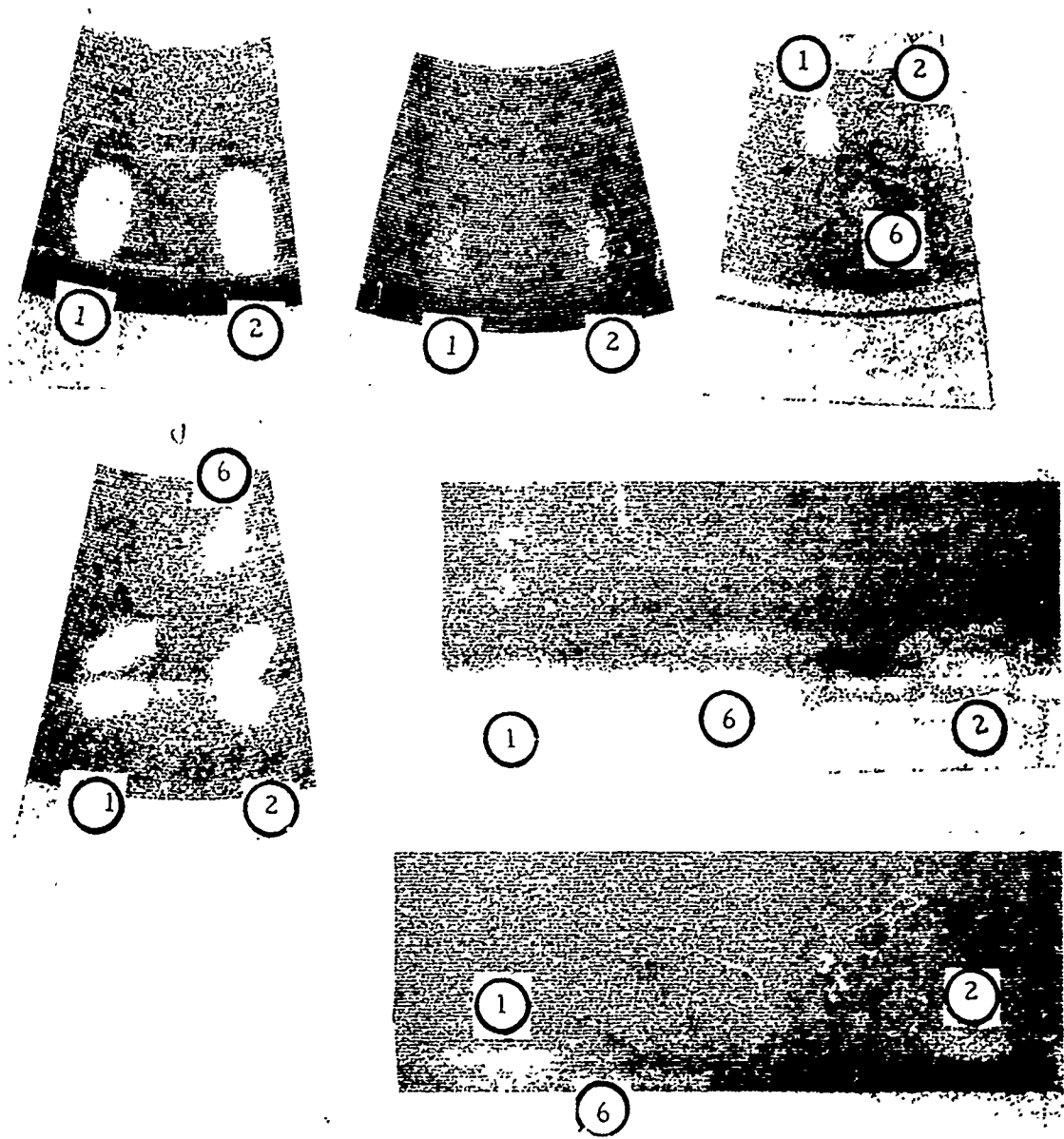


Figure 12. These 4 C-scans and 2 B-scans illustrate a wide variation in size and shape of the signals from holes numbers 1 and 2.

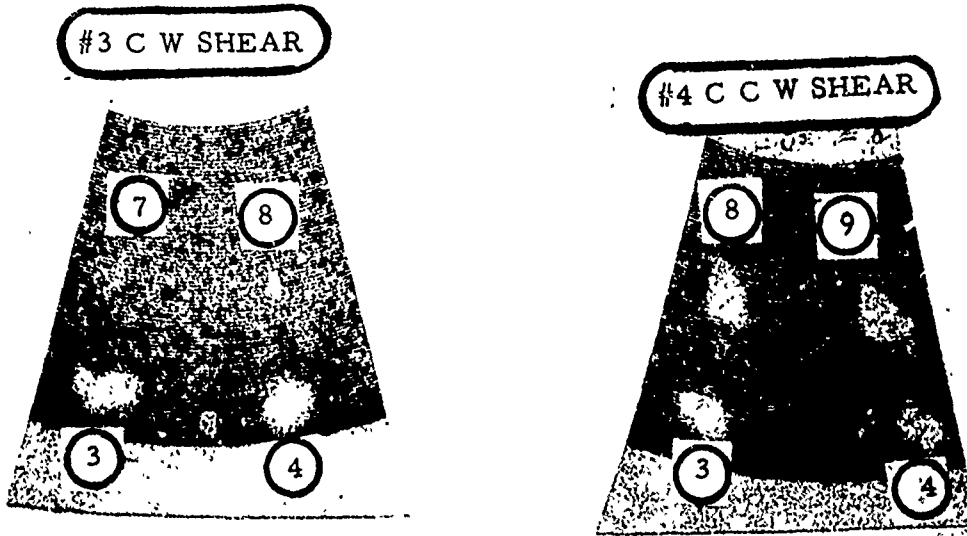


Figure 13. Scans of S3 - Note Relative Shift of #3 and #8.

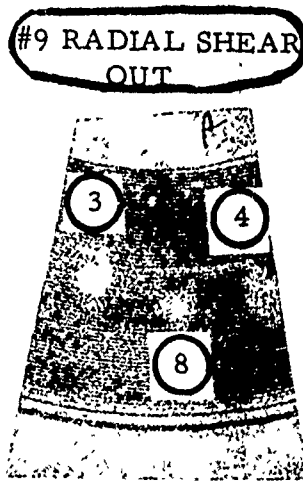


Figure 14. Scan of S3 - Note #3 and #8 Compared to Figure 13.

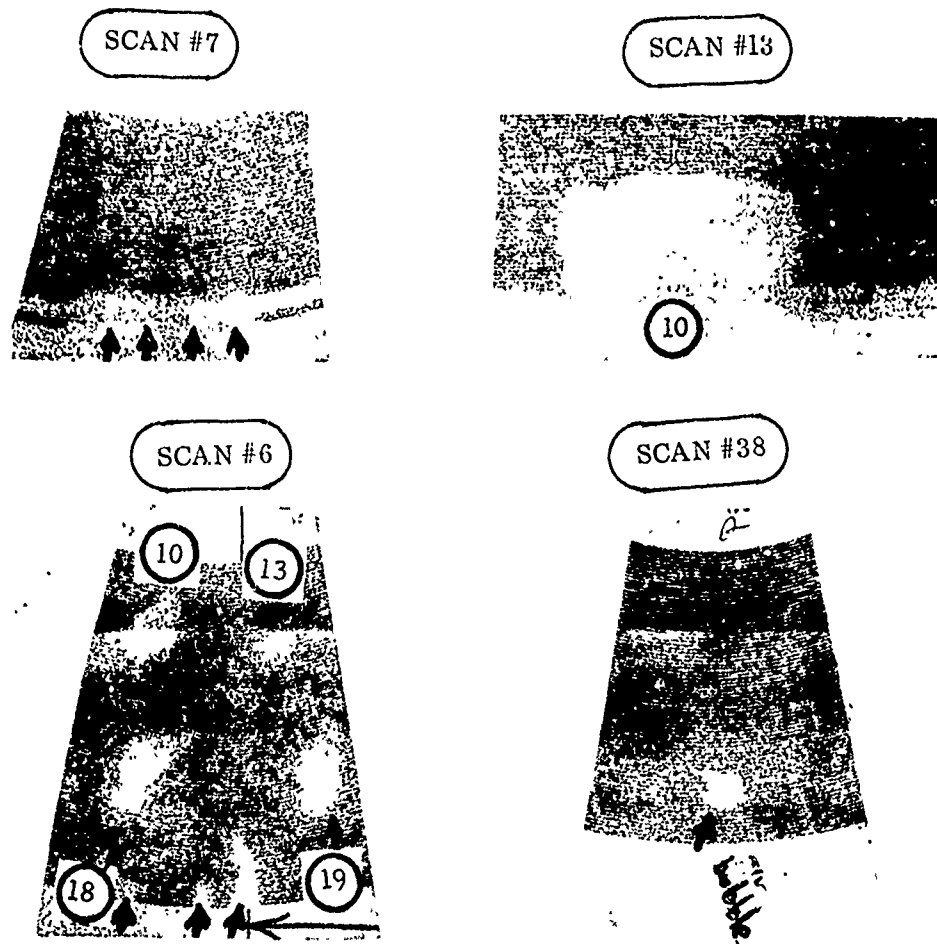


Figure 15. Examples of False Indications (arrows) on Various Scans.

EVALUATION OF FPI SYSTEMS ON AS-HIP' D RENE' 95

Purpose

This section and accompanying photos represents the investigation conducted to assess various fluorescent penetrant inspection (FPI) systems sensitivity in detecting quench cracks in AS-HIP Rene' 95 material. Since fluorescent penetrant inspection is a relatively conventional type of NDT tool and thereby readily available in AEG, the investigation/experiments were embarked upon with the objective of building upon years of application to optimize the sensitivity of a fluorescent penetrant type of surface inspection.

Description Of Process Approaches

A block of Rene' 95, 2" X 6" in diameter, containing an extremely tight quench crack across the entire face of the block was methodically subjected to various FPI systems in the unetched and etched conditions. In each case, the impact on crack sensitivity was assessed by comparing penetrants, emulsifiers/removers and developers. While this study is based on one defective specimen, the nature of the defect permitted dramatic comparisons of the sensitivities of FPI systems. The degree of sensitivity between the least sensitive to optimum sensitivity ranged from no visibility whatsoever of the crack to complete and extremely brilliant representation of the crack.

The reference inspection penetrant processes are considered the best production approaches and involve pre-etching the sample, using conventional P41 penetrant, E41 hydrophilic remover and either aqueous ZP4A or non aqueous developer. The subsequent comparison program evaluated effects of the following variables.

- o Unetched vs etched sample preparation
- o Conventional P41 penetrant vs high penetrating fluids ZL22A or AL30A.(1)
- o Conventional ZE4A emulsifier vs E41 hydrophilic remover
- o Aqueous AP4A vs non-aqueous developer (NAWD)

Results and Conclusions

The results of this FPI study are presented in Tables II, III and IV and shown pictorially in Figures 16-29. The crack involved could be seen by the unaided eye but it was very tight and so was not delineated completely by ultrasonic inspection using either conventional or advanced methods. With the advanced solutions used the crack was clearly delineated giving credence to the contention that surface defects can best be inspected with advanced FPI methods. One surface technique that was not used in this comparison was eddy current testing.

- (1) The solutions used in this report represented classes of inspection solutions which probably have several equivalents. See appendix II.

RENE' 95 CALIBRATION BLOCK

POST EMULSIFICATION VS. HYDROPHILIC

BLOCK NO. CI

COMMENTS/OBSERVATIONS

Indication sharp with seperation at tail.

Porosity showed slightly when Z.4. developer was used.

EXHIBIT # V - 1



<u>TYPE</u>	<u>PENETRANT</u>	<u>PRE-RINSE</u>	<u>EMULSIFIER/REMOVER</u>	<u>DEVELOPER</u>	<u>ETCHED/UNETCHED</u>
	<u>P41</u>	Yes	<u>F41</u>	<u>ZP4A</u>	Local etch
<u>TIME</u>	<u>30 Min</u>		<u>30 sec.</u>	<u>7 min.</u>	

Figure 16

RENE' 95 CALIBRATION BLOCK

POST EMULSIFICATION VS. HYDROPHILIC

BLOCK NO. C1

EXHIBIT # V - E

COMMENTS/OBSERVATIONS

1. Indication sharp and complete.
2. Corrosion is sharper and greater than with ZP's developer.
3. Indications appear very sharp in second of contact with non-aqueous developer.

Notes:

Non-aqueous developer's ZP's developer, provides better results of the indications.



DEVELOPER
Non-aqueous
10 min

EMULSIFIER/REMOVER
E41
30 sec

PRE-RINSE
Yes

PENETRANT
P41
30 min

ETCHED/UNEETCHED
Local etched.

Figure 17

RENE' 95 CALIBRATION BLOCK

POST EMULSIFICATION VS. HYDROPHILIC

BLOCK NO. CI

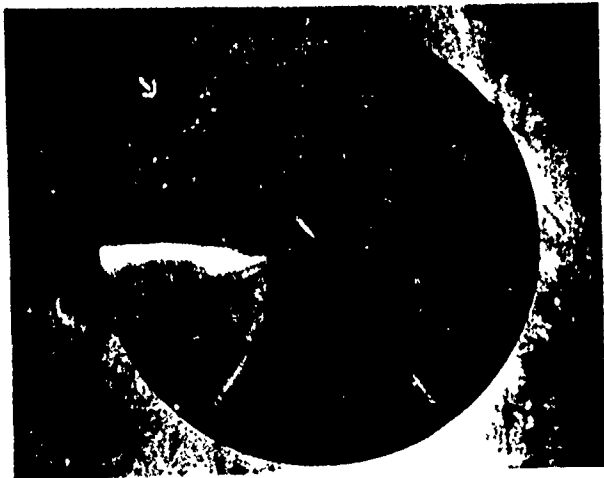
EXHIBIT # V - C

COMMENTS/OBSERVATIONS

Indication noted only at machined slot in etched condition.
(see arrow)

ORIENT:

0 in acetone solvent face of block is 100% by mass of
production of inspectors.



<u>PENETRANT</u>	<u>PRE-RINSE</u>	<u>EMULSIFIER/REMOVER</u>	<u>DEVELOPER</u>	<u>ETCHED/UNETCHED</u>
<u>21 22A</u>	<u>NO</u>	<u>ZE4A</u>	<u>ZP4A</u>	<u>unetched</u>
<u>30 min</u>		<u>1.5 min</u>	<u>7 min</u>	

Figure 18

RENE' 95 CALIBRATION BLOCK

POST EMULSIFICATION VS. HYDROPHILIC

BLOCK NO. C1

EXHIBIT # V - E

COMMENTS/OBSERVATIONS

Indication sharp at machined slot (see arrow) but not sharp across face of block.

Comment:

Indication could be missed by production IPI inspectors or interpreted as a scratch.



Pg. 32

<u>TYPE</u>	<u>PENETRANT</u>	<u>PRE-RINSE</u>	<u>EMULSIFIER/REMOVER</u>	<u>DEVELOPER</u>	<u>ETCHED/UNETCHED</u>
	<u>2122A</u>	<u>No</u>	<u>2F4A</u>	<u>Non-aqueous</u>	<u>unetched</u>
<u>TIME</u>	<u>30 min</u>		<u>1.5 min</u>	<u>10 min</u>	

Figure 19

RENE' 95 CALIBRATION BLOCK

POST EMULSIFICATION VS. HYDROPHILIC

BLOCK NO. C1

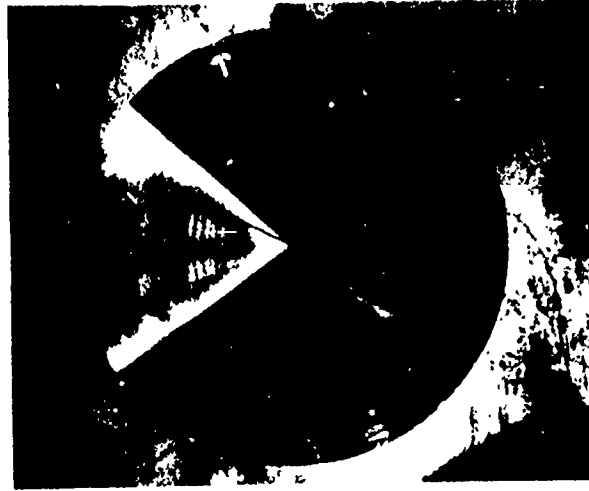
EXHIBIT # V - E

COMMENTS/OBSERVATIONS

1. Sharp indication noted only at machined slot (see arrow) that has been etched.
2. No indication noted on face of block.

Comments:

Indication would be missed by production rpi inspectors
71 30 was no improvement over 2.22 with dry developer.



<u>TYPE</u>	<u>PENETRANT</u>	<u>PRE-RINSE</u>	<u>EMULSIFIER/REMOVER</u>	<u>DEVELOPER</u>	<u>ETCHED/UNETCHED</u>
	<u>Z130A</u>	<u>Ho</u>	<u>ZE-A</u>	<u>ZP4A</u>	<u>unetched</u>
<u>TIME</u>	<u>30 min</u>		<u>1.5 min</u>	<u>7 min</u>	

Figure 20

RENE' 95 CALIBRATION BLOCK

POST EMULSIFICATION VS. HYDROPHILIC

BLOCK NO. C1

EXHIBIT # V - F

COMMENTS/OBSERVATIONS

Indication noted on face of block within seconds of first contact with non-aqueous developer.

Comments:

Indication would be found by production MPI inspectors but would be missed using ZP4A developer as noted in exhibit IV-E.



<u>PENETRANT</u>	<u>PRE-RINSE</u>	<u>EMULSIFIER/REMOVER</u>	<u>DEVELOPER</u>	<u>ETCHED/UNETCHED</u>
<u>ZL30A</u>	<u>0</u>	<u>ZE4A</u>	<u>Non-aqueous</u>	<u>unetched</u>
<u>30 min</u>		<u>1.5 min</u>	<u>10 min</u>	

Figure 21

RENE' 95 CALIBRATION BLOCK

POST EMULSIFICATION VS. HYDROPHILIC

BLOCK NO. C1

EXHIBIT # V - 3

COMMENTS/OBSERVATIONS

Penetration slant at 45 degrees (see also) and faint but not complete across bottom of block.

Comments: (1) Penetration at 45 degrees (see also) and faint but not complete across bottom of block.



<u>TYPE</u>	<u>PENETRANT</u>	<u>PRE-RINSE</u>	<u>EMULSIFIER/RENOVER</u>	<u>DEVELOPER</u>	<u>ETCHED/UNETCHED</u>
	<u>P41</u>	<u>Yes</u>	<u>E41</u>	<u>ZB4A</u>	<u>unetched</u>
<u>TIME</u>	<u>30 min</u>		<u>30 sec</u>	<u>7 min</u>	

Figure 22

RENE' 95 CALIBRATION BLOCK

POST EMULSIFICATION VS. HYDROPHILIC

BLOCK NO. C1

EXHIBIT # V - H

COMMENTS/OBSERVATIONS

1. Indication sharp but incomplete.
2. Indication as sharp on first contact with the non-aqueous developer.

Comments:

Indication could have been interpreted as a crack with the non-aqueous developer by production line inspectors. The non-aqueous developer with the hydrophilic gives us better visibility of the indication.



pg. 36

<u>TYPE</u>	<u>PENETRANT</u>	<u>PRE-RINSE</u>	<u>EMULSIFIER/REMOVER</u>	<u>DEVELOPER</u>	<u>EICHER/UNETCHED</u>
P41		Yes	E61	Non-aqueous	unetched
<u>30 min</u>			<u>30 sec</u>	<u>10 min</u>	

Figure 23

RENE' 95 CALIBRATION BLOCK

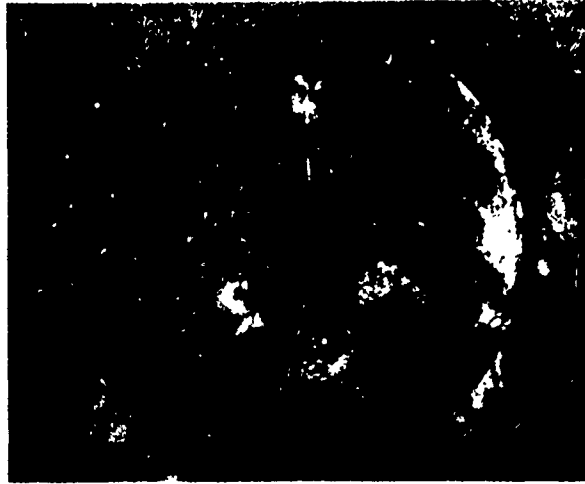
POST EMULSIFICATION VS. HYDROPHILIC

BLOCK NO. C1

EXHIBIT # V - I

COMMENTS/OBSERVATIONS

1. Indication faint and not complete.
2. 7022: It is a developer in a better condition gives us better results as it indicates top up in the unetched condition.



<u>TYPE</u>	<u>PENETRANT</u>	<u>PRE-RINSE</u>	<u>EMULSIFIER/REMOVER</u>	<u>DEVELOPER</u>	<u>ETCHED/UNETCHED</u>
<u>2122A</u>	<u>2122A</u>	No	<u>ZE4A</u>	<u>ZP4A</u>	Etched
<u>30 min</u>	<u>30 min</u>		<u>1.5 min</u>	<u>7 min</u>	

Figure 24

RENE' 95 CALIBRATION BLOCK

POST EMULSIFICATION VS. HYDROPHILIC

BLOCK NO. CI

COMMENTS/OBSERVATIONS

Indication sharp and 95 complete compared to using Z122A with ZP4 developer.

EXHIBIT # V-1



<u>TYPE</u>	<u>PENETRANT</u>	<u>PRE-RINSE</u>	<u>EMULSIFIER/REMOVER</u>	<u>DEVELOPER</u>	<u>ETCHED/UNETCHED</u>
	<u>Z122A</u>	No	<u>ZE4A</u>	Non-aqueous	Etched
<u>TIME</u>	<u>30 min</u>		<u>1.5 min</u>	<u>10 min</u>	

Figure 25

RENE' 95 CALIBRATION BLOCK

POST EMULSIFICATION VS. HYDROPHILIC

BLOCK NO. C1

COMMENTS/OBSERVATIONS

Improved visibility over 7120s with dry developer. Note no separation of indications in center

EXHIBIT # V - K



<u>TYPE</u>	<u>PENETRANT</u>	<u>PRE-RINSE</u>	<u>EMULSIFIER/REMOVER</u>	<u>DEVELOPER</u>	<u>ETCHED/UNETCHED</u>
	<u>Z130A</u>	<u>no</u>	<u>ZE-4A</u>	<u>ZF4A</u>	<u>Etched</u>
<u>TIME</u>	<u>30 min</u>		<u>1.5 min</u>	<u>7 min</u>	

Figure 26

RENE' 95 CALIBRATION BLOCK

POST EMULSIFICATION VS. HYDROPHILIC

BLOCK NO. C1

COMMENTS/OBSERVATIONS

Indication sharp and quite an improvement over 7L22A and ZL30A using P41 developer.

EXHIBIT # V - M



<u>TYPE</u>	<u>PENETRANT</u>	<u>PRE-RINSE</u>	<u>EMULSIFIER/REMOVER</u>	<u>DEVELOPER</u>	<u>ETCHED/UNETCHED</u>
	P41	Yes	E41	ZP4A	Etched
<u>TIME</u>	30 min		30 sec	7 min	

Figure 27

RENE' 95 CALIBRATION BLOCK

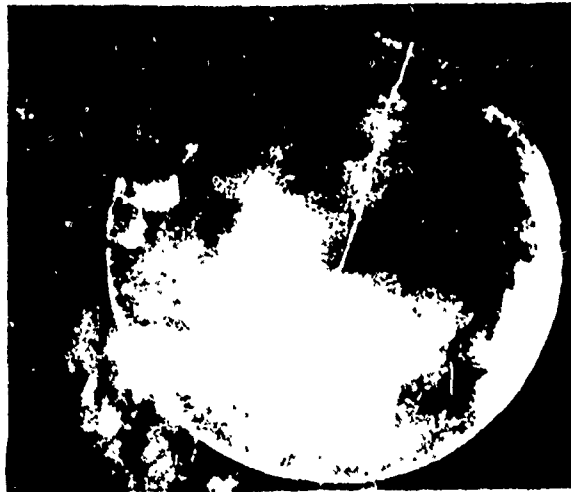
POST EMULSIFICATION VS. HYDROPHILIC

BLOCK NO. C1

COMMENTS/OBSERVATIONS

Indication is visible with no improvement over 7122A with non-aqueous developer.

EXHIBIT # V - L



<u>TYPE</u>	<u>PENETRANT</u>	<u>PRE-RINSE</u>	<u>EMULSIFIER/RENOVER</u>	<u>DEVELOPER</u>	<u>ETCHED/UNETCHED</u>
	<u>Z130A</u>	<u>No</u>	<u>ZE4A</u>	<u>Non-aqueous</u>	<u>Etched</u>
<u>TIME</u>	<u>30 min</u>		<u>1.5 min</u>	<u>10 min</u>	

Figure 28

RENE 95 CALIBRATION BLOCK

POST EMULSIFICATION VS. HYDROPHILIC

BLOCK NO. C1

EXHIBIT # V - N

COMMENTS/OBSERVATIONS

1. Indication sharp and complete.
2. Indication was sharp on first contact with the non - aqueous developer as is 10 minutes later when photograph was taken.

Comments:

Visibility of the indication is better with hydrophilic and non - aqueous developer than with post emulsification etching.



DEVELOPER
Non-aqueous
10 min

ETCHED/UNETCHED
Etched

EMULSIFIER/REMOVER
E41
30 sec

PRE-RINSE
Yes

PENETRANT
K41
30 min

TYPE
TIME

Figure 29

This process may prove competitive but it still suffers from the need to consider defect orientation. The following conclusion were obtained from this data;

1. Present day fluorescent penetrant inspection with modifications can be an effective surface inspection for Rene' 95.
2. It has been previously established and here substantiated that etching prior to FPI yields a large improvement in crack detection. See direct comparisons.

Figure 18 vs Figure 24

Figure 19 vs Figure 25

Figure 20 vs Figure 26

Figure 21 vs Figure 27

Figure 22 vs Figure 28

Figure 23 vs Figure 29

3. Non-aqueous wet developers improved sensitivity when compared to dry developers. This was evident for all penetrants used in both the etched and unetched conditions.

See direct comparisons.

Figure 16 vs Figure 17

Figure 18 vs Figure 19

Figure 20 vs Figure 21

Figure 22 vs Figure 23

Figure 24 vs Figure 25

Figure 26 vs Figure 27

Figure 28 vs Figure 29

4. The improvement in sensitivity achieved with NAWD was not as great as that realized as a result of etching.
5. The hydrophilic FPI system was slightly better than an FPI system comprised of a high sensitivity penetrant and post emulsification when compared in the unetched condition.

See direct comparisons.

Figure 22 vs Figure 20

Figure 23 vs Figure 21

6. The hydrophilic system in etched conditions is far superior to a post emulsification system. Indications/cracks appear bright and distinct, due to the absence of background fluorescence commonly associated with post emulsification systems on etched surfaces.

See direct comparisons.

Figure 28 vs Figure 26

Figure 29 vs Figure 27

7. The optimum fluorescent penetrant inspection observed in this evaluation was comprised of a high sensitivity penetrant, hydrophilic remover and a non-aqueous wet developer applied to an etched surface.

NOTE: Refer to the attached tables and figures which support the conclusions listed above.

Comparison of FPI With Ultrasonic Inspection Of Cracked Disks

In the conventional ultrasonic inspection and associated FPI of two disk samples, Block 22 and C1 (the latter disk is a part of this program) rather deep cracks were missed. See Table III. After removal of .035-.300 inch from these disks, cracks were noted visually. This started a series of ultrasonic and FPI investigations summarized in Tables II, III and IV.

The FPI evaluation (Table II was covered in the preceding section. The initial and final ultrasonic evaluations are summarized in Tables III and IV. Several facets of this program are significant:

- o Significant cracks were missed by normal high quality FPI and ultrasonic inspection on a 63 microinch surface. (1 in Table III).
- o Initial reinspection did not indicate that cracks were deep. (I in Table IV).
- o Using GE's "best" FPI method, cracks were readily detectable. See Figure 2 and 3.
- o Cracks could not be identified by ultrasonic inspection if 0.125 inch of the surface was gated out. (1 in Table III).
- o After several modifications of ultrasonic techniques, e.g. use of surface wave, the complete crack was identified but not with a strong indication. Also, true depth of cracks were not observed with ultrasonic techniques. Noise contributed to loss in resolution.

TABLE II
NON DESTRUCTIVE TEST EVALUATION OF Diametrically Cracked Block

SEQUENCE	DESCRIPTION OF INSPECTION	INSPECTION PARAMETERS	PURPOSE	RESULTS
1	Etch local area.	Macro etch 35 seconds, 9 parts HCL to 1 part H ₂ O ₂ solution.	Eliminate "possible" masking effect of Crucible grinding operation.	Indication observed under White light.
2	FPI local area.	P3TF2 Class "D" P4I Penetrant Pre-rinse E4I Hydrophilic remover ZP4A developer Clean	To determine presence of surface cracking using what was considered best FPI inspection based on previous T700 Rene'95 study.	Refer to Figure 2.
3	FPI local area.	P3TF2 Class "D" P4I Penetrant Pre-rinse E4I Hydrophilic remover Non Aqueous developer	Same	Refer to Figure 3.
4	Machine slot.	Slot machined .200 x .100	To determine if machining will eliminate crack.	
5	Etch slot and visual 10x.	Macro etch 35 seconds, 9 parts HCL to 1 part H ₂ O ₂ solution.	Eliminate "possible" masking effect of machining of slot.	Indication still existed under white light. Crack deeper than machined slot.
6	FPI inspect 100% unetched condition.	P3TF2 Class "D" ZL22A Penetrant ZE4A Emulsifier ZP4A Developer Clean	Evaluate effect of various penetrants/developer combinations especially post emulsification vs. hydrophilic.	Refer to Figure 4.

TABLE II - Continued
 NON DESTRUCTIVE TEST EVALUATION OF Diametrically Cracked Block

SEQUENCE	DESCRIPTION OF INSPECTION	INSPECTION PARAMETERS	PURPOSE	RESULTS
7	FPI inspect 100% unetched condition.	P3TF2 Class "D" ZL22A penetrant ZE4A emulsifier	Evaluate effects of various penetrants/developer combinations especially post emulsification vs. hydrophilic.	Refer to Figure 5
8		Non Aqueous Developer Clean	Same	
9	FPI inspect 100% unetched.	P3TF2 Class "D" ZL30A penetrant ZE4A emulsifier ZP4A developer Clean	Same	Refer to Figure 6
10	FPI inspect 100% unetched condition.	P3TF2 Class "D" ZL30A penetrant ZE4A emulsifier Non-aqueous developer Clean	Same	Refer to Figure 7
11	FPI inspect 100% unetched condition	P3TF2 Class "D" P4I penetrant Pre-rinse E4I hydrophilic remover ZP4A developer Clean	Same	Refer to Figure 8
12	FPI inspect 100% unetched condition	PTF2 Class "D" P4I penetrant Pre-rinse E4I hydrophilic remover Non-aqueous developer Clean	Evaluate effects of various penetrants/developer combinations especially post emulsification vs. hydrophilic	Refer to Figure 9

TABLE II - Continued
 NON DESTRUCTIVE TEST EVALUATION OF Diametrically Cracked Block

SEQUENCE	DESCRIPTION OF INSPECTION	INSPECTION PARAMETERS	PURPOSE	RESULTS
13	Etch complete and visual inspect.	Macro etch 35 seconds, 9 parts HCL to 1 part H ₂ O ₂ solution.	Eliminate "possible" masking effect of Crucible grinding operations.	Cracks visible to naked eye.
14	FPI inspect 100% etch.	P3TF2 Class "D" ZL22A penetrant ZE4A emulsifier ZP4A developer Clean	Evaluate effects of various penetrants/developer combinations especially post emulsification vs. hydrophilic.	Refer to Figure 10.
15	FPI inspect 100% etch.	P3TF2 Class "D" ZL22A penetrant ZE4A emulsifier Non-aqueous developer Clean	Evaluate effects of various penetrants/developer combinations especially post emulsification vs. hydrophilic.	Refer to Figure 11.
16	FPI inspect 100% etch.	P3TF2 Class "D" ZL30A penetrant ZE4A emulsifier ZP4A developer Clean	Same	Refer to Figure 12.
17	FPI inspect 100% etch.	P3TF2 Class "D" ZL30A penetrant ZE4A emulsifier Non-aqueous developer Clean	Same	Refer to Figure 13
18	FPI inspect 100% etch	P3TF2 Class "D" P4I penetrant Pre-rinse E4I hydrophilic remover ZP4A developer Clean	Same	Refer to Figure 14
19	FPI inspect 100% etch.	P3TF2 Class "D" P4I penetrant Pre-rinse E4I hydrophilic remover Non-aqueous developer Clean	Same	Refer to Figure 15

TABLE III INITIAL APPRAISAL & VERIFICATION
OF SURFACE DEFECTS
OF TWO DISKS

BLOCK	DESCRIPTION OF INSPECTION	INSPECTION PARAMETERS	COMMENTS	RESULTS
22 & C1	Ultrasonic inspection upon receipt from Crucible.	Both faces @ 12Db Circumferential - 2 Dir. Radial - 2 Dir. Longitudinal OD @ 12 Db Circumferential - 2 Dir. Axial Longitudinal - Slight Record groove finish Did not permit high sensitivity		No rejectable indications observed.
1	Envelope - .150+ Finish - Better than 63 some scratches on faces.			
2	Ultrasonic inspection after Hooksett machining .035 in from cracked face & .300 in from uncracked face. Block 22	Local reinspection performed circumferential shear on face at cracked areas.	Gate start set to include surface.	Could detect cracks in circumferential shear on face at surface. <u>No depth</u> seen.
3	Etch local area block C1 Etch surface face block 22	Macro etch 35 seconds 9 parts HCL to 1 part H ₂ O ₂ solution.	Eliminate "possible" masking effect of Crucible grinding operation.	Indication observed under white light. Visually W/O penetrant.
4	FPI local area block C1	P3TF2 Class "D" P-4 Penetrant Pre-rinse E-4 Hydrophilic remover ZP-4A developer Clean	To determine presence of surface cracking using what was considered best FPI inspection based on previous T700 Rene' 95 study.	Refer to Figure 2.
5	FPI local area block C1	P3TF2 Class "D" P-4 Penetrant Pre-rinse E-4 Hydrophilic remover Non Aqueous developer	Same	Refer to Figure 3.
6	Machine Slot	Slot machined .100 into OD x .200 axially block C1 slot machined .100 into ID x .600 axially block 22	To determine if machining will eliminate crack.	

TABLE III INITIAL APPRAISAL & VERIFICATION
OF SURFACE DEFECTS

BLOCK	DESCRIPTION OF INSPECTION	INSPECTION PARAMETERS	COMMENTS	RESULTS
1	Etch complete and visual	Macro etch	To improve FPI	
2	F. P. I. Inspect 100% etched condition.	P3TF2 Class "D" ZL22A Penetrant ZE-1A Emulsifier ZP-1A Developer Clean	Evaluate effects of various penetrant developer combinations especially post emulsification vs. hydrophilic.	Crack fully revealed, Figure 2, crack deeper than machined slot.

TABLE IV SONIC/FPI EVALUATION OF CRACKED DISKS

SEQUENCE	DESCRIPTION OF INSPECTION	INSPECTION PARAMETERS	COMMENTS	RESULTS
1	Resonic inspect Lynn	Face s - Variable Db circumferential - 2 Dir. (Shear) surface Wave OD variable Db Circumferential - 2Dir. Long Contact	To determine best method of detection	Face Could detect cracks at surface with circ. shear on face. If 0.125 is gated out, would not record indication. Surface wave picked up cracks but no better than shear. OD Longitudinal picks up cracks best but only rejectable at very high sensitivity and short water path (2 3/4") high surface noise because of record groove surface. Had to gate out first inch. Cracks were seen 2" to 5 1/2" deep.
2	Ultrasonic inspection by M&PTL F. Bray and J. Zurbrich	Circumferential shear at P3TF1 and 12 Db focused on 1/8" hole. Zoned 0 .125 only.	Gate start set to include surface	Identified surface cracks only signals 6% - 90%. See Figure 8.
3	Ultrasonic inspection by NDTAD A. Thompson.	On cracked face circumferential shear P3TF1 + Db Longitudinal P3TF1 + 12Db Radial shear P3TF1 + 12Db * GE NDT Specification	1) Gate start set .125 below surface using calibration hole. 2) Gate start set .100 below surface by approximation.	1) If gated to .125 perhaps 1 or 2 indications rejectable 2) If gated to .100 saw several saturated signals but nothing below 1/4" that could be considered rejectable. <u>Note:</u> The above applicable to circ. and radial shear. In longitudinal cracks not readily detectable due to noise signals of -40% -6. % at depths 0 - .3" below surface See. Figure 9.
4	FPI inspect by NDT-AD R. Wagner	ZL30A - No Developer ZL30+ Non Aqueous Developer	Compare Evendal e ZL30A/ Hydrophilic remover with Lynn system.	4 more indications observed than in Lynn Hydrophilic photo. See Figure 10 and 11.

TABLE IV SONIC / FPI EVALUATION OF CRACKED DISKS

SEQUENCE	DESCRIPTION OF INSPECTION	INSPECTION PARAMETERS	COMMENTS	RESULTS
5	Ultrasonic inspect Lynn/Evendale review A. Thompson and J. Stover with Evendale block/transducer circumferential shear.	Utilizing NSPI and Lithium sulphate transducer used in sequence #4. Instrument/transducer combo permitted 6 Db sensitivity.	Gate start set .125 below surface.	Observed nothing below .125
6	Ultrasonic inspect Lynn/Evendale review A. Thompson & J. Stover with Evendale Block and transducer Circumferential shear.	Utilizing NSPI and Lithium sulphate transducer used in sequence #4.	Gate start set to include all material including surface.	Cracks easily detectable at all levels of sensitivity.
7	FPI Lynn Hydrophilic system	Lynn Hydrophilic but with fresh can navd.	Account for four missing indications identified by Evendale.	All indications observed with no back ground problem. See exhibit
8	Ultrasonic inspect Lynn/Evendale A. Thompson/J. Stover with Lynn block/transducer.	Normal production techniques Rene' 95 test block normal P3TFI and +12Db sensitivity	Gate start set .125" below surface.	Observed nothing below .125".
9	Ultrasonic inspect Lynn/Evendale A. Thompson/J. Stover with Lab equipment.	P3TFI Calibration and P3TFI +6 Db and -12 Db.	Gate start set .100" below surface.	Crack pattern observed at all levels of sensitivity but at much lower amplitudes than in item #8.

One may conclude from this and the preceding FPI study that reliable surface inspection is better accomplished with proper FPI techniques rather than relying on special ultrasonic inspection methods. It is believed that, because of the nature of crack formation and the results of the FPI study, an etching technique and FPI would have resulted in a successful initial crack detection of the disks involved in this study.

HOLOSONICS INC. NDE EFFORT

The purpose of this project was to evaluate HIP Rene' 95 Turbine Hardware using the Holosonics System 200 Scanned Acoustical Holographic System. This equipment is capable of three major modes of operation: Intensity Mode with Coherent Pulse (similar to conventional ultrasonics but with certain equipment differences as noted in Table V), Intensity mode with Coherent Pulse and Coherent Transmit (same as above but with a transmit mode that records intensity as with conventional ultrasound but also phase shift), and full Acoustical Holography, a process using ultrasound to illuminate a sample for holographic analysis. Other special modes such as "3D" are used to better define part geometry.

The acoustical holography has the greatest potential sensitivity but it also requires the most complex software to analyze data and convert to a visual presentation. Therefore, the initial work was done using intensity mode, coherent transmit which, for the samples evaluated in this program, appeared to be sufficient to analyze for defects present. As a consequence of this early success, Holosonics Inc. performed a very limited analysis of acoustical holography as discussed later.

INTENSITY MODE HOLOSONIC EFFORT

Description Of The Process

The Holosonic equipment used in the intensity mode closely approximates conventional ultrasound in many respects. A signal generator drives a transducer whose energy impinges on the sample, usually through a water couple. The reflected energy is received by the same transducer (pulse-echo technique) or a different transducer and this signal is processed into a form for subsequent display. With the Holosonic system, this display method is usually a cathode ray tube and the display is some part outline plus signals from any defects present. Note the similarity to conventional ultrasound except for the display mechanism. Some important differences are noted below and summarized in Table V.

First, with the conventional ultrasound, narrow band transducers (those whose frequency response curves peak sharply with small frequency spread) are used by "ringing" them at their resonant frequency. These transducers cannot operate efficiently outside of their resonant value. The Holosonic system usually uses broad band transducers and drive them at a frequency that is best for the application involved. The use of a broad band transducer makes possible a selection of an operating frequency well removed from the frequency that tends to amplify "background" and interfere. Those signals from grain boundaries or other structural aspects of the base material are usually called "background".

TABLE V

COMPARISON OF CONVENTIONAL ULTRASONICS WITH INTENSITY
MODE HOLOSONIC ULTRASONIC INSPECTION

	<u>Conventional</u>	<u>Holosonic</u>
Transducers	<ul style="list-style-type: none">o Relatively Narrow Bando Ring at resonant frequencyo Pulse-short, peaking at a narrow frequency band that pulse beats at varying amplitude.	<ul style="list-style-type: none">o Relatively Broad Bando Driven at desired frequencyo Pulse relatively long-typically 10-15 beats all at same frequency and amplitude (coherent).
Energy	<ul style="list-style-type: none">o Limited by area under peaking pulse.	<ul style="list-style-type: none">o Estimated at 6-8 times energy of conventional system.
Surface Reaction	<ul style="list-style-type: none">o High surface response tends to hide defects near surface. Good inspection capability .100-.125 below surface.	<ul style="list-style-type: none">o Good inspectibility at least .030 below surface (within normal machining allowance).
Frequency	<ul style="list-style-type: none">o Max. about 5 MHz.o Rung at resonant frequency of transducer used. o Resolution limited by 5MHz frequency.	<ul style="list-style-type: none">o Capabilities 5-12 MHz.o Can choose frequency so difference between defect response and response from grain boundaries or metallurgical structure is maximized.o With higher frequency, greater resolution is possible because of short wave length .
Interpretation of Data	<ul style="list-style-type: none">o Scope blip observation of interpreting tape or graph readouts. C-scan and B-scan are separate readouts.o Defect size and location difficult to interpret.	<ul style="list-style-type: none">o Visual presentation of disk outline with any defects shown. Display can be rotated electronically to pin-point location of defects.o Defect location easily noted. Defect size evaluation appears to be improved but more work is needed.

Description of the Process (Continued)

The Holosonic signal generator gives off a square wave signal with a series of cycles all having the same amplitude. The number of cycles per signal pulse can be preset. The electronic control efficiently chops the rise and decay portion of the pulse leaving only the preset number of cycles - hence the term coherent pulse. With conventional ultrasound the ringing of the transducer yields a pulse with a sharp rise followed almost immediately by a sharp decay with a large amplitude variation per cycle and some frequency variation with time. The use of the coherent pulse permits a much larger energy input to the sample and yields a reflected signal that can be analyzed in both intensity and phase shift (coherent transmit). Thus more information is available to assess the meaning of the reflected signal.

Yet another difference lies in the available choices of operating frequency. The approximate limit with current ultrasonic equipment is 5MHz. The Holosonic equipment used for this contract was operated in the range of 5 to 11.2 MHz. With higher frequencies there are shorter wave lengths and the wave length is the factor governing resolution. Maximum resolution is approximately equal to the wave length of the signal used.

With conventional ultrasound, the ringing of the transducer yields a surface signal of intensity and base width that fogs any other signals in the first layer of material. This layer is in the range of .060 to .120 inch depending upon the technique used. The coherent pulse of the Holosonic equipment appears to reduce this interference region to less than .030 inch which is probably less than any anticipated machining allowance for years to come. The capability of inspecting near the surface could eliminate the cost adders associated with the "ultrasonic envelope" now used.

The use of shear wave techniques with conventional ultrasound can give beneficial results for two reasons. First, the impingement of the signal on plate-like defects (e.g. cracks) results in maximum response when the sequence is normal (perpendicular) to the plane of the defect. The response falls off sharply with angular variation to this normal orientation. Secondly, the shear wave propagation in the metal tends to yield an effective propagation wave length of half that from a beam normal to the surface. Thus a shear wave at 5MHz is propagating somewhat like a 10MHz signal. For the Rene' 95 powdered turbine parts, plate-like defects are not anticipated except for surface cracks. If we relegate the surface crack inspection to other processes, the only value of a shear wave may be an effective change in wave length. With the Holosonic equipment capability well within the 10MHz value, it is possible that shear wave analysis can be eliminated by use of the Holosonic system. This could sharply reduce the number of scans required to inspect the part.

Description of the Process (Continued)

Probably the most clear cut advantage and major difference of the Holosonic equipment lies in the method of presenting the inspection results. The cathode ray tube display will readily show shape and location of a defect and should contribute to ease of operation and reliability.

The various methods of image display for the intensity mode Holosonic ultrasound are illustrated in Figure 30. A C-scan involves the mapping of the top surface of the sample by the interrogating transducer, usually positioned perpendicular to the plane of the top surface. A B-scan uses a transducer perpendicular to the C-scan orientation. A simulated B-scan makes use of a C-scan interrogating transducer viewed in the B-scan direction with the aid of electronic processing of the response signal prior to reaching the cathode ray display tube. A 3-D scan uses a transducer in the C-scan position but makes use of depth as well as location measurements. The reflected signals are electronically processed to yield a view on the display tube that can be rotated permitting observation of the signal display from any chosen angle. Examples of the C-scan, simulated B-scan and 3-D scan are shown in Figures 31, 32 & 33.

Experimental Results

Because of the variety of operational modes of the System 200, it was first necessary to establish the appropriate parameters for inspection of the HIP disk specimens. Evaluation of the appropriate transducer configuration and operational frequencies were first attempted. The HIP disk specimens appear to have an extremely small grain structure acting as a very homogenous medium so that attenuation due to scattering from grain boundaries or other structures within the medium is minimal. Grain boundary scattering, which is a function of the wave length λ , is usually the determining attenuation factor in most metals, however, in the HIP disk specimens the small grain size and homogeneity of the medium appears to allow operation at very high ultrasonic frequencies for these inspections. High frequencies result in short wave lengths and hence better resolution.

The original inspection work in samples S 2 and D 1 were carried out at a frequency range between 5 and 7 MHz, however, higher frequency transducers in a different configuration were constructed to allow inspection of some of the later specimens at higher frequencies as well. In this original effort using S 2 and D 1 samples, intensity mode, coherent pulse, coherent transmit could identify the fine particles in D 1 so most of the subsequent effort for this contract was performed using these modes. See Table V.

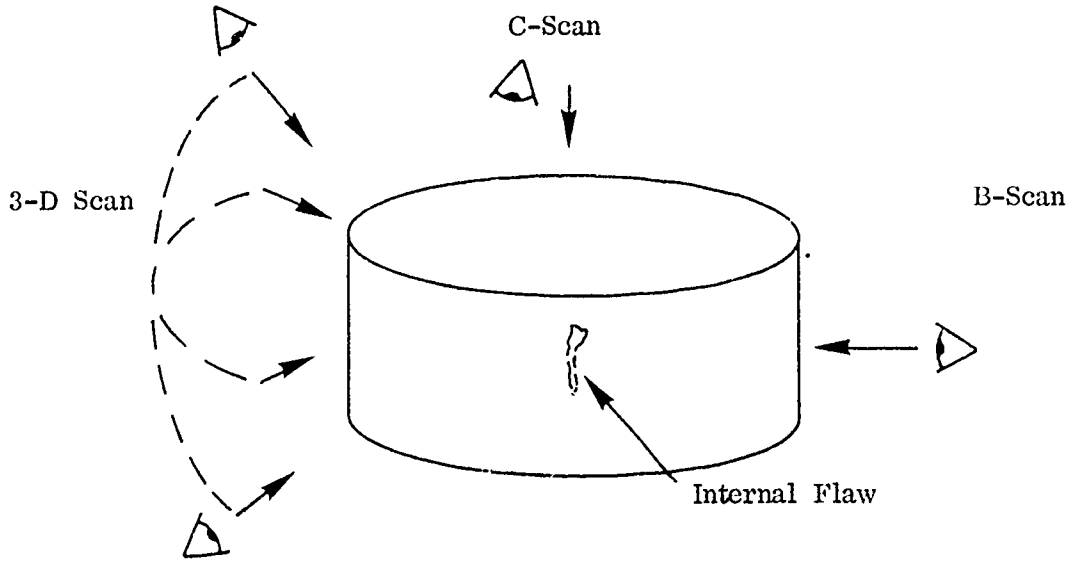


Figure 30: Schematic Drawing Of The System 200 Imaging Modes.

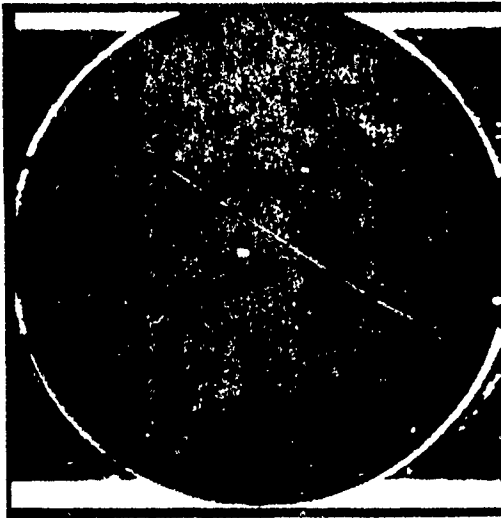


Figure 31: Plan View Or C-Scan Of Selected Region Of Specimen D-1.

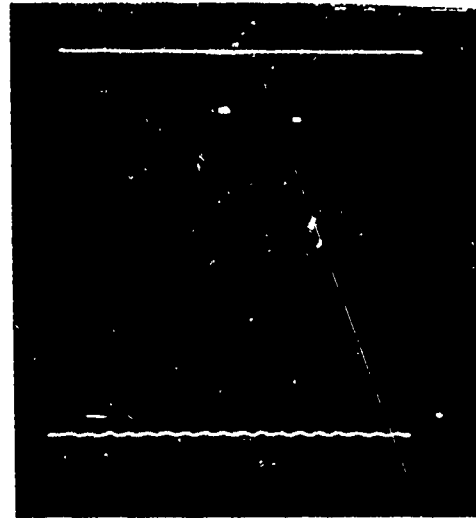


Figure 32: Electronic Section Or B-Scan View Of Selected Region Of Specimen D-1.

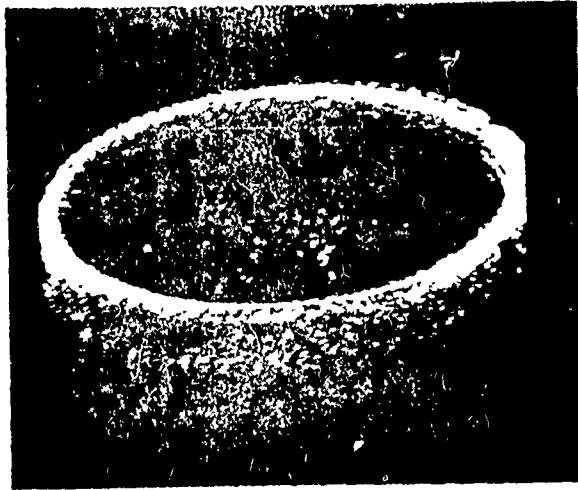


Figure 33: 3-D Perspective Image
Of Specimen D-1.

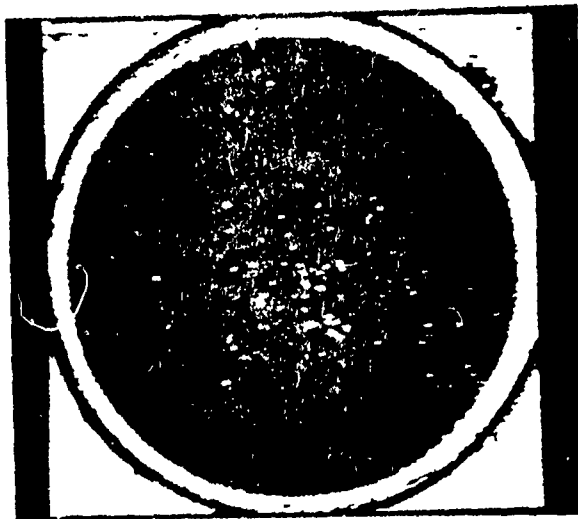


Figure 34: Plan View Of C-Scan
Of Image In Figure 33.

Test Parameters for S-2 and D-1

Transducer: 5MHz Broad Band, 4 inch focal length x 1 inch diameter
and 7.5MHz Broad Band, 4 inch focal length x 3/4 inch diameter.

System Operating Frequency: 5 MHz, 7.5MHz and 6.22 MHz, coherent.

Transmit Mode: Coherent and Pulsed.

Direction Mode: Intensity

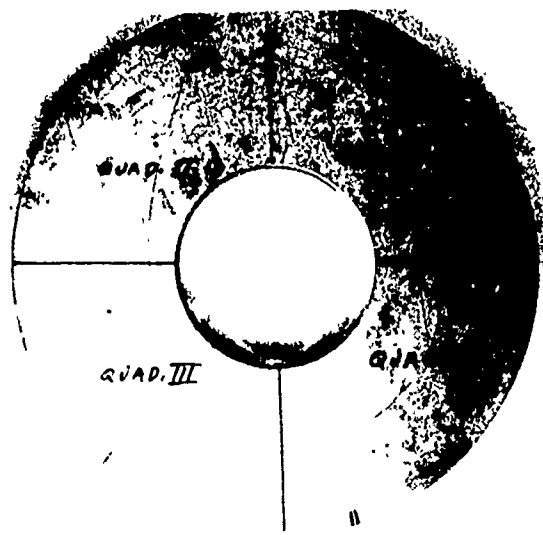
Image Presentation Mode: Plan View, Section View and 3-D Isometric Projection

Hard Copy Documentation: Polaroid Type 107 Film.

The S-2 sample is a simple disk with top-drilled and side-drilled holes .020 inch in diameter. All holes were identified using intensity mode Holographic ultrasound as indicated in Figures 36-39. A picture of the sample is shown in Figure 35 with a plan of the hole locations indicated. The plan view, with the back surface included to outline the quadrants, is shown in Figure 36. The same views with the back surface (and the front surface) gated out is shown in Figure 37. In Figure 38 is shown the quadrant III in plan view and simulated B-scan. Note that the side-drilled hole is well delineated in both location and shape. However, the end drilled holes, whose axes are parallel to the interrogating beam, is well delineated in the C-scan view (top). The simulated B-scan uses C-scan data and reprocesses it to yield a view perpendicular to the interrogating beam. This view reveals the indication denoting the bottom of the top drilled holes, but not the shape of the hole. This same response occurs in the 3-D views as shown in Figure 39. In all views, the data was collected by a typical C-scan in which the side walls of the top drilled holes are parallel to the interrogating beam. Hence, the signal fails to delineate the shape on the long axis of the holes, perpendicular to the top surface.

During the examination of resolution standard S-2 at 5 MHz and 7.5 MHz, it was determined that the difference between flat bottomed and non-flat bottomed drill holes was insignificant with regard to system sensitivity levels and gain settings. This is significant because there is a wide difference in response between flat and round bottom holes using conventional ultrasound.

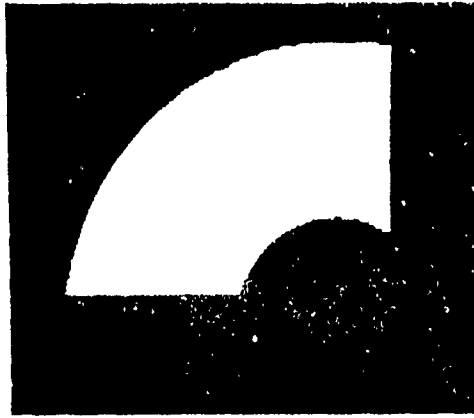
It was also determined, when making comparisons between samples S-2 and D-1, that the drill holes in specimen S-2 DO NOT approximate the defect conditions in specimen D-1. The drilled hole sample is similar to a conventional standard used to calibrate ultrasonic equipment. If we assign a number of 100% to the



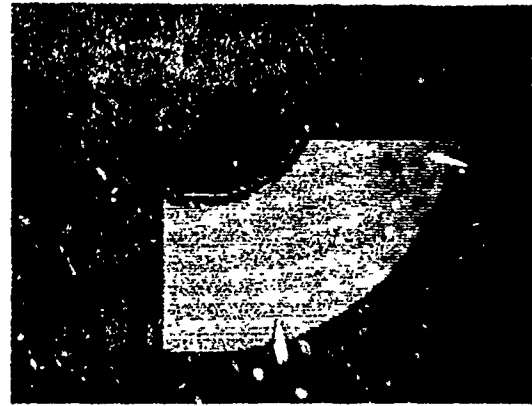
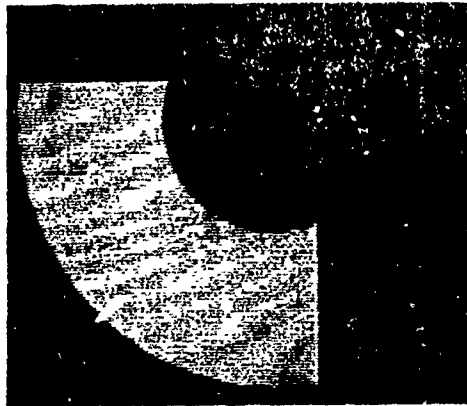
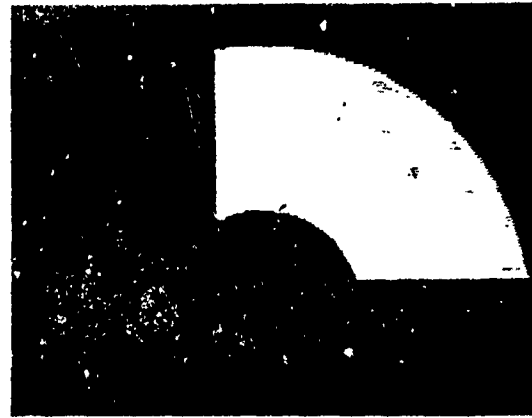
Resolution Standard S-2
6.7" O.D. X 2.5" I.D. X .75" Thick

Figure 35

QUADRANT II



QUADRANT I



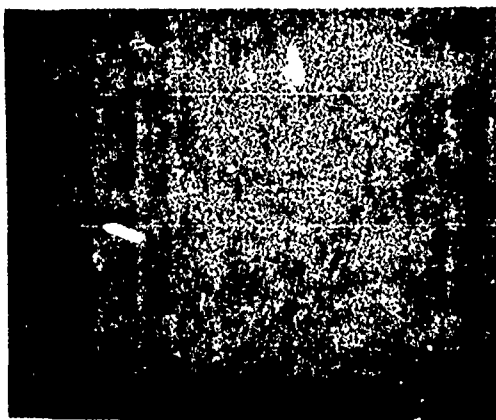
QUADRANT III

QUADRANT IV

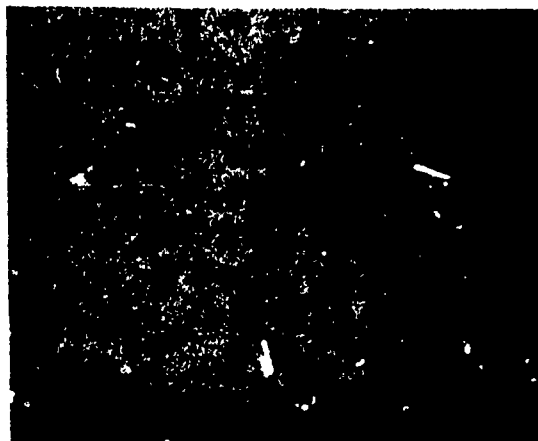
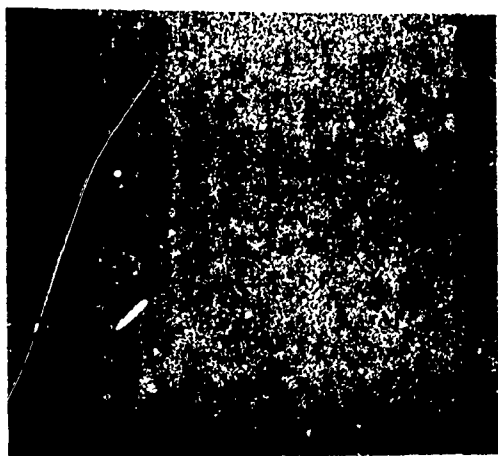
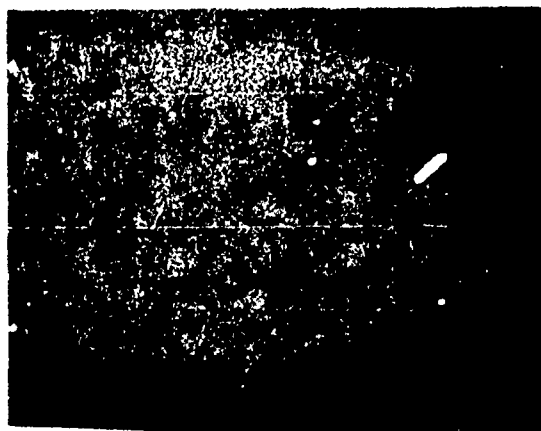
Plan View Of All (14) Drill Holes In Resolution
Standard. Back Surface Included For Reference.
Image Magnification: .45 To 1. Frequency 5MHz;
Except Quadrant IV 7.5 MHz.

Figure 36

Quadrant II



Quadrant I

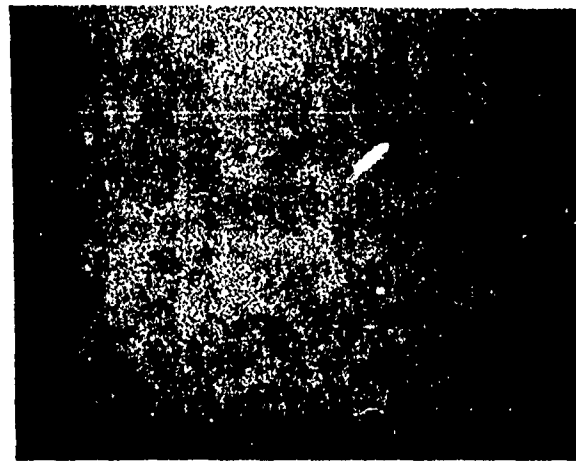


Quadrant III

Quadrant IV

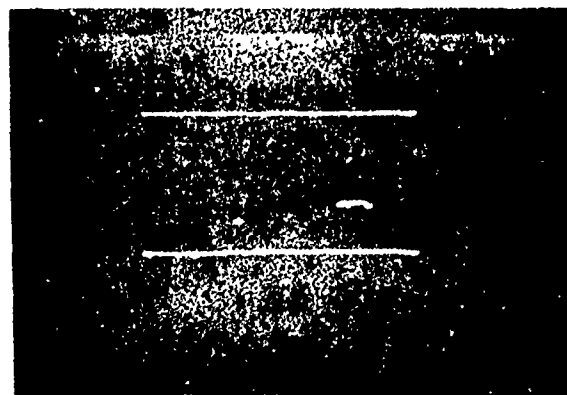
Plan View Of All (1) Holes In Resolution
Standard. Image Magnification: .45 to 1.
Frequency: Quadrants I and II; 5MHz.
Quadrants III And IV; 715 MHz.

Figure 37



(a)

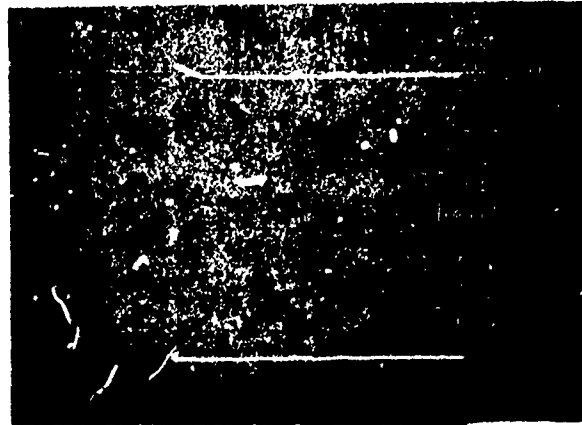
Reoriented Plan View Of Quadrant III.
Magnification: .45 To 1.



(b)

Section View Showing The Orientation
And Relative Location Of The Two Axial
And One Radial Drill Hole In Quadrant III.
Lateral Mag: .45 To 1.
Depth Mag: 1 To 1
Frequency: 5 MHz

Figure 38



(a)

2X Section View Of Quadrant III
Lateral Mag: .45 To 1
Depth Mag: 2 To 1



(b)

3-D Projected Image Of Quadrant III
At The Same Magnification As In The
Above Section View. Frequency 5MHz.

Figure 39

system sensitivity used during examination of resolution standard S-2, then the system sensitivity level necessary for detecting the inclusions in specimen D-1 is 100%. There is one exception to the preceding: one defect in sample D-1 was evident at the sensitivity level used for examination of resolution standard S-2. See Figure 44.

Since focused transducers were used for this examination, the depth of the focal point was positioned below center and examined from both sides. This positioned the focus near the slices of test samples in order to insure good resolution of all the programmed defect conditions.

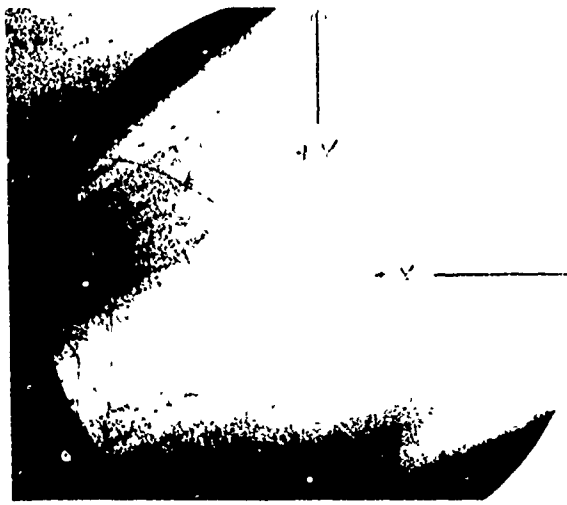
In Figure 40 is shown a picture of the doped sample D-1 with a sketch showing the slices of the disk representing the gating used to look at one slice at a time. This procedure was used because of the very large number of oxides revealed by the sweep of the total disk. Typical scans are shown in Figure 41 and 42 of #1 and #2 slice. Note that the combination of plan view and simulated B-scan (section view) in Figure 41 make it possible to accurately locate the defects. Note also that the lateral and depth magnification values differ. In Figure 42 is shown a plan and 3-D view to illustrate pictorially the defect locations. There are too many defects in this view to make mapping practical which points up a problem in sample preparation. D-1 and D-2 were to be prepared with a few intentional oxides added to permit mapping and cut-up. This would make possible an assessment of system sensitivity. The number of oxides added was excessive thus limiting the value of the samples in sensitivity evaluation.

In Figure 43 is shown the #3 slice with the only indication (1) observable at the same gain setting as that used for S-2.

The circular outline of the plan view and the lines of the section view are reflections from sample surfaces intentionally used to outline sample and reference defect signals.

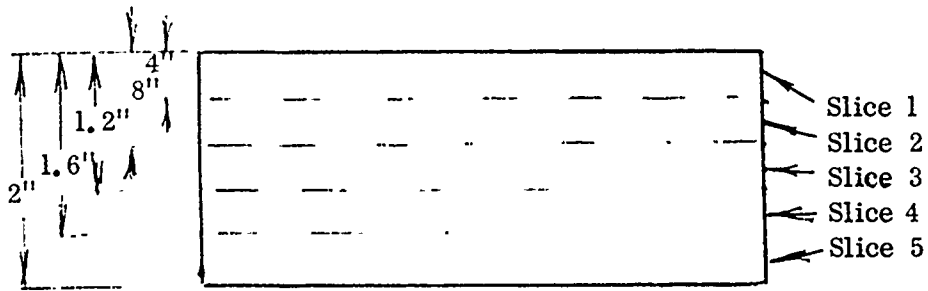
In retrospect, the good focusing procedure described above could have been improved by locating the focusing the center of each gated slice. The number of defects indicated in slices 1 and 5 are much lower than those found in 2, 3 and 4 which slices are in the proximity of beam focus. Since these disks were sectioned from larger HIP'd logs, one would not expect this type of preferred location of oxides. Thus the evidence tends to substantiate the need for more attention to optimum focus location.

A new 10 MHz broad band transducer was built with a six-inch focal length and a diameter of 0.3 inch. This transducer was used on most of the remaining NDE of this contract effort.



(a)

Doped Specimen (D-1) 6" Dia. X 2" Thick
(Top View)



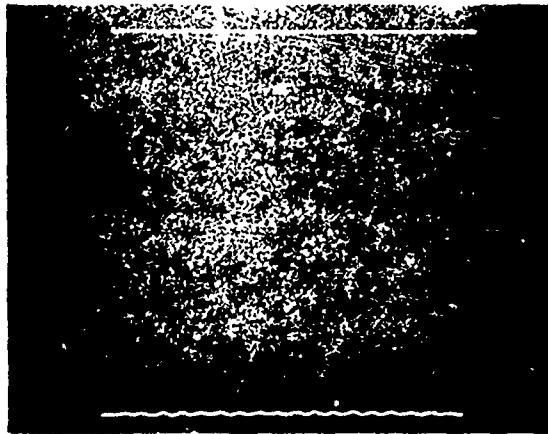
(b)

Side View Of Specimen D-1 Showing Time Gated Slices
Presented In Figure 40.

Figure 40



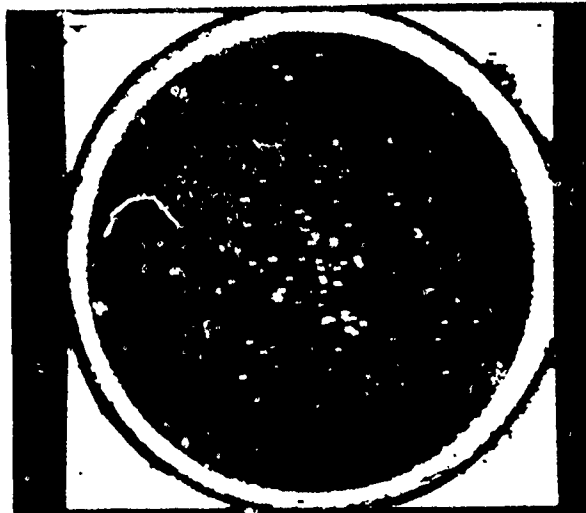
Slice 1, Specimen D-1
Magnification: .45 To 1
Frequency: 6.22 MHz



Section View Of Indications In Slice
#1 Showing Their Depth Relative To The
Top And Bottom Surfaces Of The Test
Sample.

Lateral Mag: .45 To 1
Depth Mag: 1 To 1

Figure 11

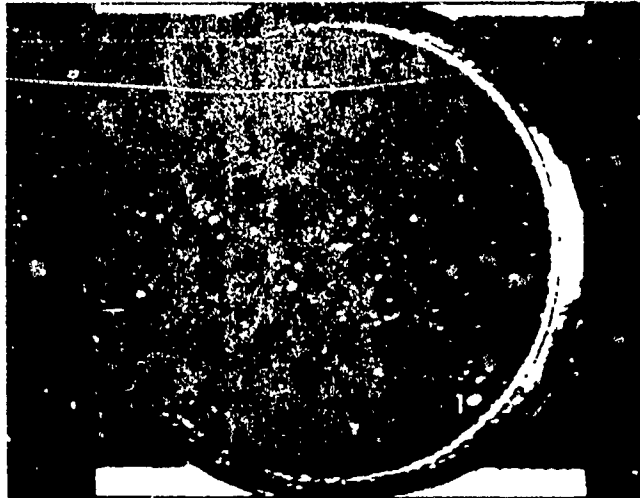


Plan View Of Specimen D-1 Showing
Indications Located In Slice #2.
Magnification: .45 To 1
Frequency: 6.22 MHz



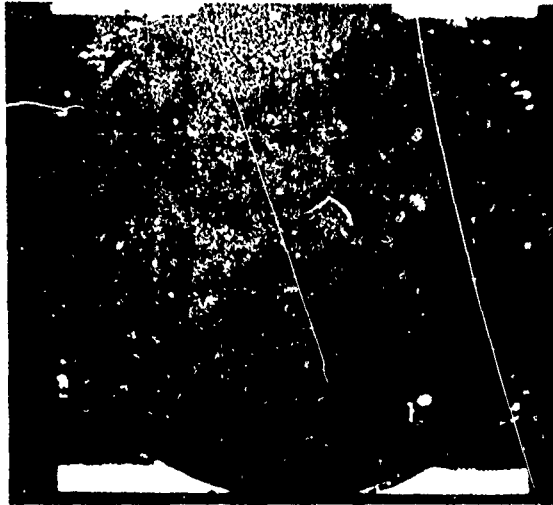
3-D Image Of Indications In Slice #2.
Lateral Mag: .45 To 1
Depth Mag: 1 To 1
30° Tilt

Figure 42

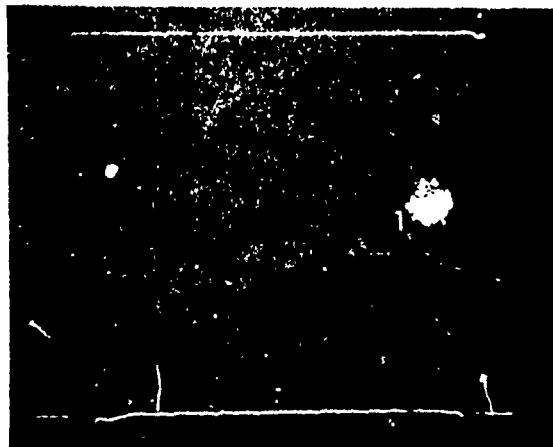


Plan View Of Specimen D-1 Showing Indications
Located In Slice #3. Note Indication 1.

Figure 43

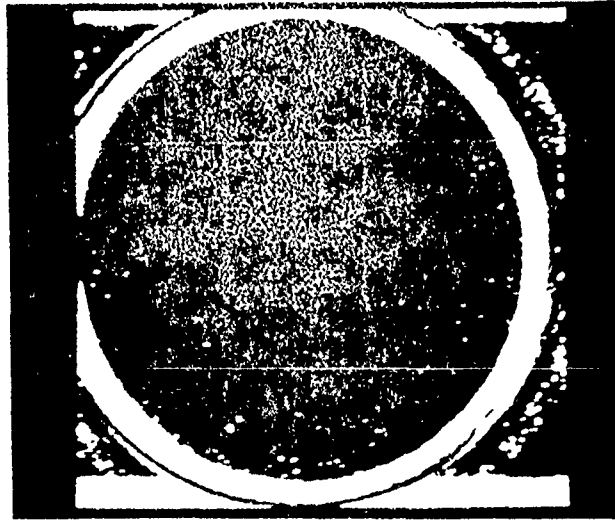


Plan View Of Slice #3 At A Lower Gain Setting
Than Shown In Figure 43
Magnification: .45 to 1
Frequency: 5 MHz



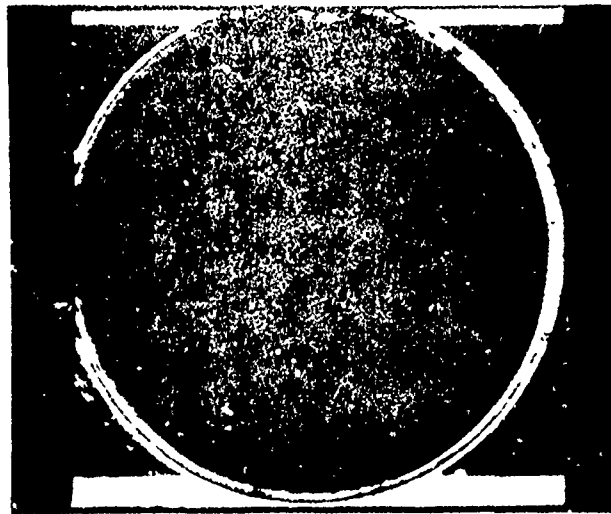
Section View Showing Relative Depth Of
Indication 1 To Top And Bottom Surfaces
Of Test Sample.
Lateral Mag: .45 To 1
Depth Mag: 1 To 1

Figure 44



Plan View Of Slice #4
Magnification: .45 To 1
Frequency: 6.22 MHz

Figure 45



Plan View Of Slice #5
Magnification: .45 To 1
Frequency: 6.22 MHz

Figure 46

The evaluation of S-2 indicated a strong definitive signal for a standard .020 inch drilled hole and insensitivity to the shape of the hole bottom. Examination of D-1 revealed a good visual presentation of oxides, many having diameters believed to be less than .010 inch. An examination of S-3 revealed excellent signals from .007 inch drilled holes, See Figure 47. For the low density sample, D-1, small voids were easily revealed. See Figure 42. All of this indicated high sensitivity but the need for calibration effort to quantify sensitivity capabilities.

A series of disk and cooling plate blanks were borrowed. These HIP'd Rene' 95 blanks were to be machined for engine qualification testing for the HIP process. Permission was given to examine these blanks using intensity mode Holosonic ultrasound. All blanks were previously accepted on the basis of ultrasonic testing using the General Electric specification P3TF1.

For ultrasonic testing, the standard calibration block is used and the signal from a .020 inch side drilled hole is set at 80% full scope deflection. No similar standard is yet developed for Holosonic equipment, and the .020 inch hole was not a challenging standard. So the gain was adjusted to readily reveal end or side drilled holes .012 inches in size, but just miss .007 inches diameter end drilled holes. These machine settings are given below:

Test Parameters

Transducer: 10 MHz broad band, 6 inch focal length x 1.4 inch diameter

Operating Mode: Intensity mode, coherent pulse, coherent transmit

Transmit Level: 65%

RF Gain: 40%

Low Frequency Gain: 50%

Using these values, the HIP'd blanks were examined and significant signals mapped. Permission was granted to cut up one cooling plate in an attempt to assess defect size. A series of pictures in Figures 48 & 49 illustrate the display of the indications. It was anticipated that the sizes of the defects illustrated here were less than .010 inch based on a comparison of indications from S-3 sample.



Figure a, S₃ Sample
in .007 Inch Hole Area

END VIEW
.007 Inch
Holes (A)

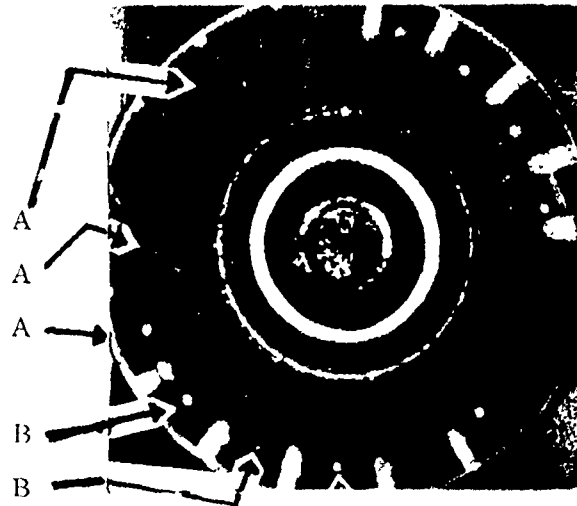


Figure b. S₃ Sample at a Lower Gain
than in Figure a Above. Note No Holo-
sonic Signal From End (.007") A
Drilled Holes But Other Holes in S₃
Identified

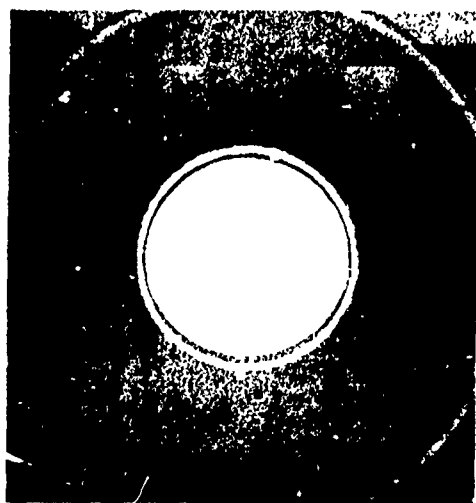
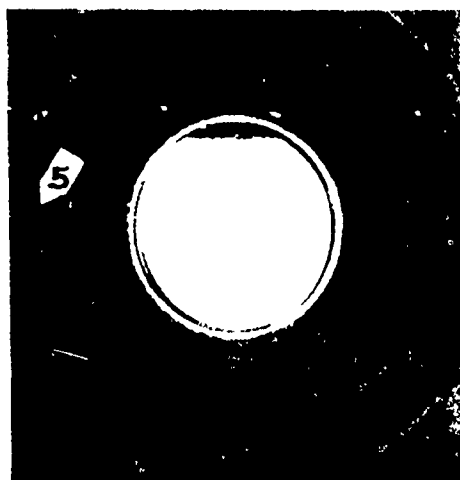


Figure c, Part No. 17A127-188
Serial COL 10045 Intensity Mode
Holo-sonic View Using Settings
Listed in Table 1.

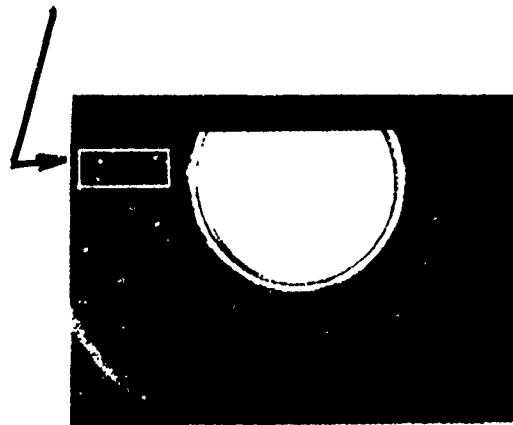
Figure 17: Intensity Mode Holo-sonic Scan of S₃ Identifying
.007 inch Holes.



a

C-Scan of Serial -46;

Delineating Box



b

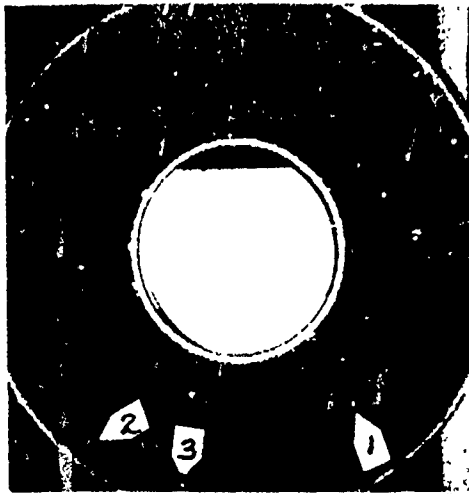
Same as (a) with Scope of Scan for
Section View Gate 2-9 μ s



c

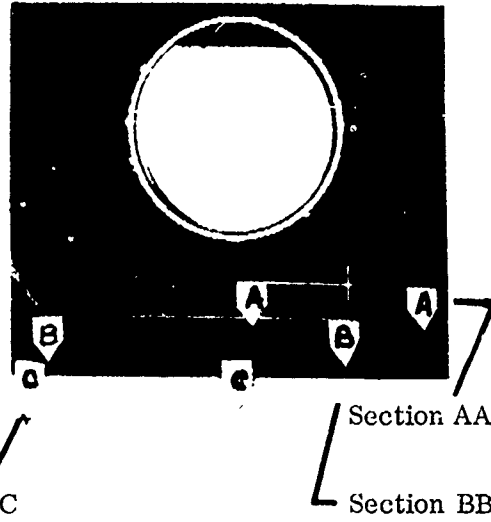
Section View Of Delineating Box
Note Multiplicity of Signal - Indication
of Many Small Defects.

Figure 48: Examples of Intensity Mode Holographic Scans Of
Serial 46 Disk



a

C-Scan of Serial -49 Gate
Set at 4-9 μ s (Total Thickness
9 μ s)



b

Same as (a) With Lines to Indicate
Scope of Section Scans



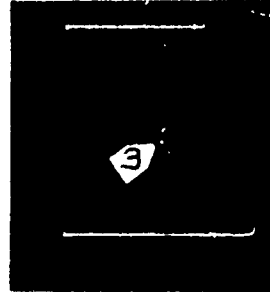
c

Line #1



d

Line #2



e

Line #3

Figure 49: Intensity Mode II Ultrasonic Scan of Serial 49 Disk.

The sample cut up had five areas identified with strong indications from the Holosonic inspection. Four of these were destructively evaluated by electrolytically machining the surface removing a thin .005 inch layer between each examination. The presence of a non-metallic particle resulted in a localized area retardation of chemical attack as illustrated in Figure 50. Another sample was exposed to metallographic polishing between examination cycles. With both methods, many .001-.002 inch particles were found, one .004 was found but none larger. Considering the care used in this evaluation, it might be concluded that:

- o There were no non-metallic particles in these areas larger than .004. - A possible conclusion but one not proved. See Figure 51.
- o The large indications noted in intensity mode inspection were due to clusters of fine non-metallic particles grouped too close to each other to be resolved as individual particles. See Figure 50. This appears to be the most probable explanation. To prove it would require quite careful mapping and small incremental metal removal between inspection cycles.
- o Lastly, larger defects could have been missed. It is possible, but not probable that a defect .010 inch was missed. It does not appear possible that a .020 inch defect could have gone undetected.

Again this evaluation gave evidence of increased sensitivity of the Holosonic intensity mode, but no solid proof. So the six disks were then evaluated in a similar manner with view to a second cut up analysis using the procedure designed to map .002 inch particle locations. The cluster concept would be evaluated.

Unfortunately, at the same machine settings, these six disks were quite clean. See Figure 53 for a typical result. So again the attempt to quantize sensitivity improvement was thwarted.

General Electric was preparing a series of intentionally doped samples with view to mechanical testing specimens with known defects. The first four disks were doped as shown in Table VI below:

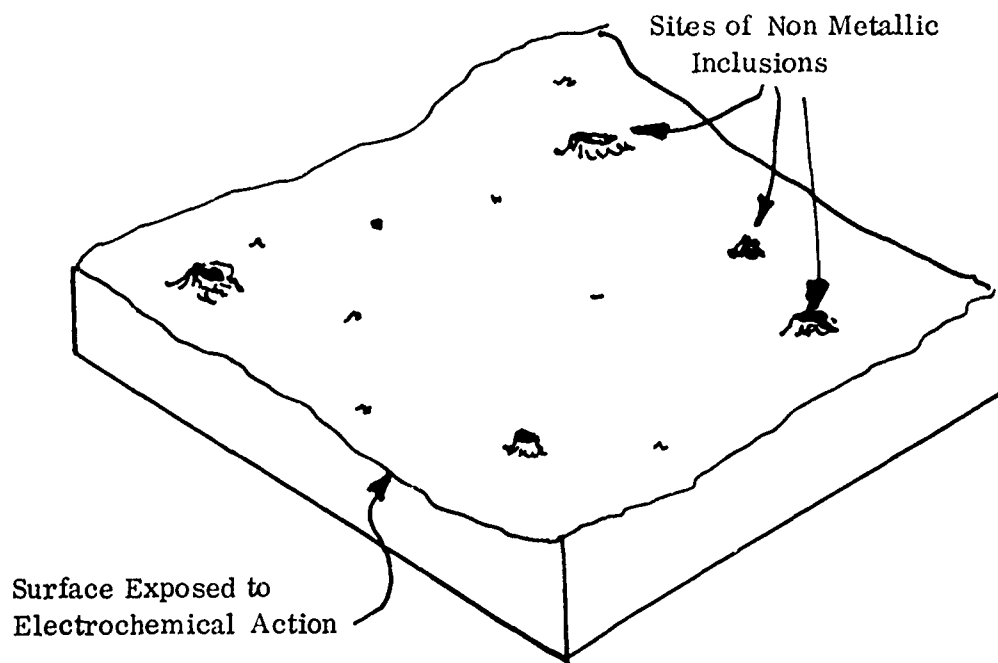


Figure 50: Diagram Showing Preferential Electrochemical Attack of a Surface With Non-Metallic Inclusions (Exaggerated)

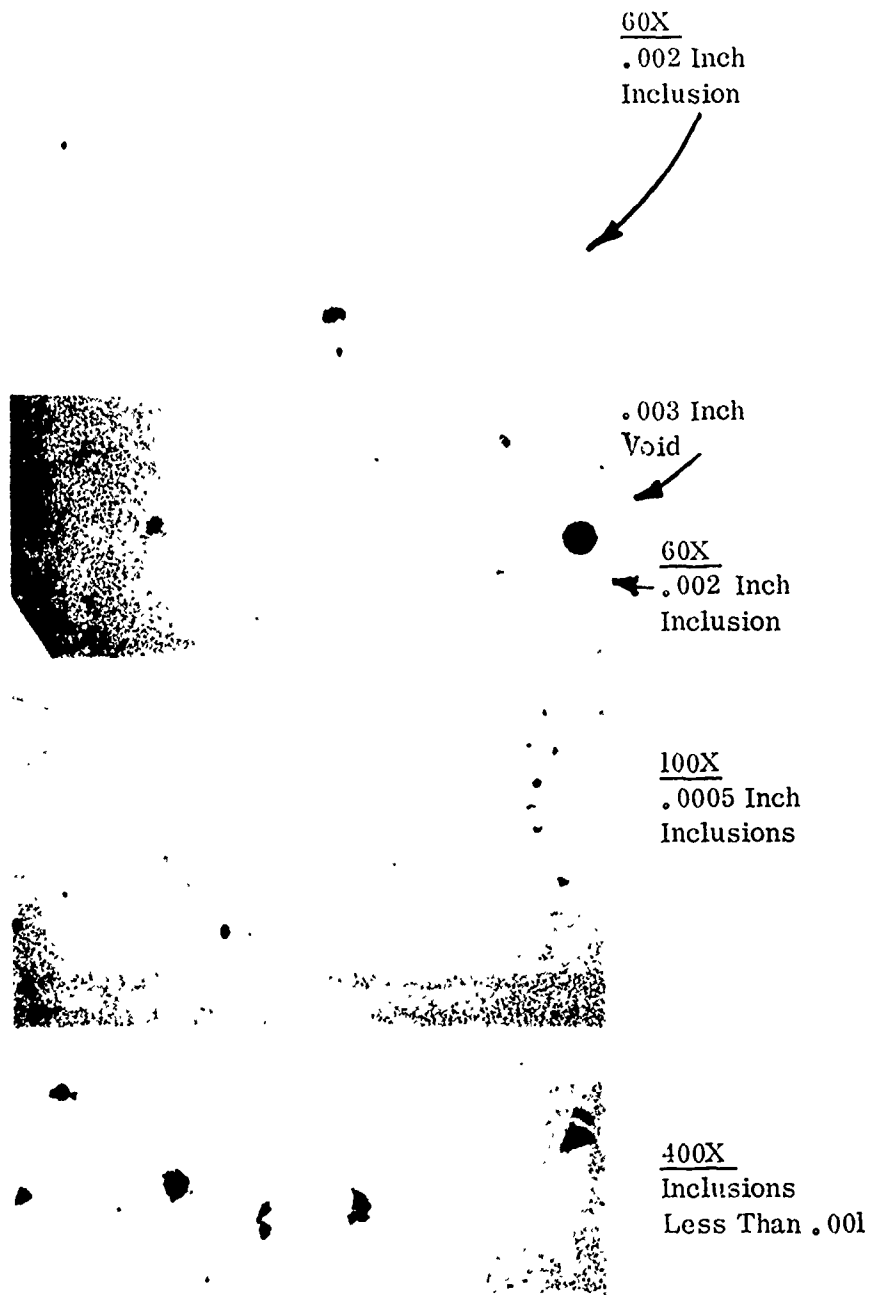


Figure 51: Examples of Small Non-Metallic Inclusions Found by Metallographic Evaluation of Sample With Holosonic Indications.



500 X

Inclusion About
.001 Inch



400 X

Inclusion About
.0025 Inch

Figure 51 (Continued)

Examples of the Larger Inclusions Found
in Metallographic Sectioning.

<u>LAYER</u>	<u>INDICATED SHAPE OF DEFECT</u>	<u>NO. DEFECTS</u>
1		2
2		0
3		3
4		0
5		2
6		0
7		3

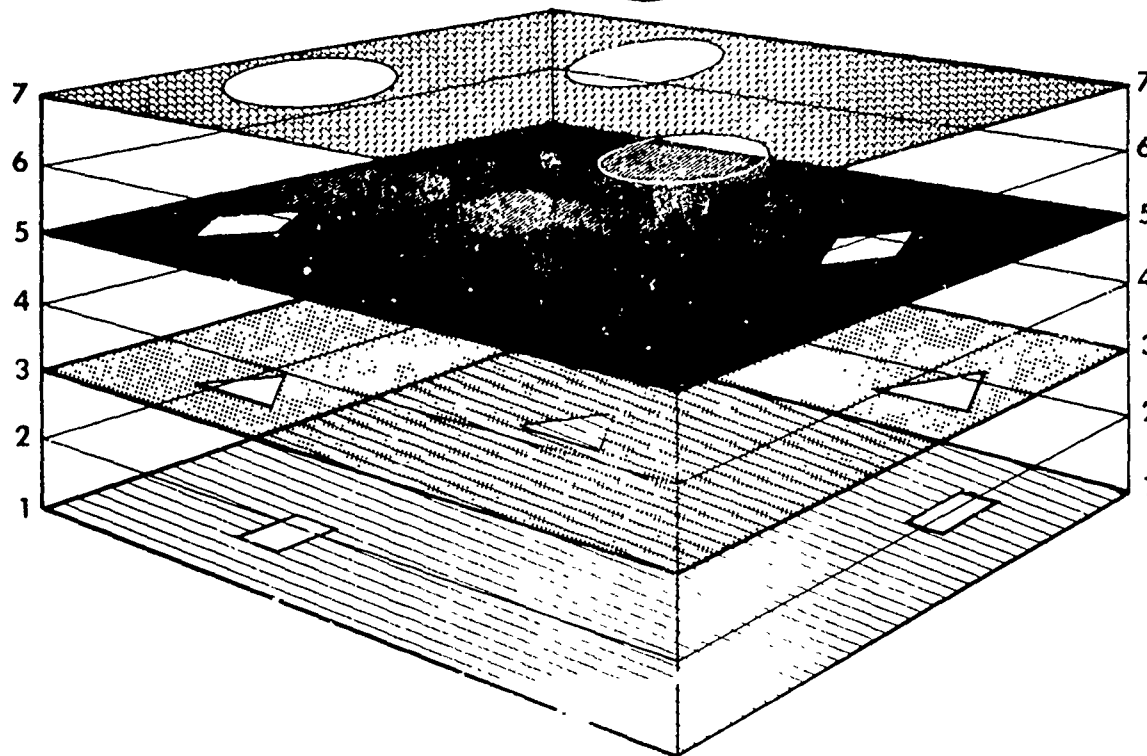


Figure 52

SPATIAL ILLUSTRATION OF DEFECTS

Assume Defect Size About .002 Inch And Layer Separation .002 Inch. All Defects In This Composite Would Appear As A Single Defect Due To Resolution Limits Of Holographic Equipment At Indicated Settings.

TABLE VI

Intentionally Doped Disks Of Rene' 95 HIP'd Material

<u>Number</u>	<u>Added Oxide</u>	<u>Size Added</u>
412	Al ₂ O ₃	.006-.010
413	Al ₂ O ₃	.020-.033
414	Al ₂ O ₃	.047-.065
416	Fe ₂ O ₃	.033-.047

All disks were inspected using conventional ultrasonics. The results are shown in Table VII along with Holosonic results. See Figures 54 to 58. There was strong evidence that identification of 412 and 414 were reversed. Compare the size defects added (Table VI) with the Figures 54 and 55. Secondly, a container malfunction resulted in oxygen pick up for #416 making this specimen useless. See Figure 58. However, the number of relatively strong indications on 412, 413 and 414 gave positive evidence of increased sensitivity over conventional ultrasonic testing. See summary in Table VII. Significant indications in 412 and 413 were mapped and attempts will be made to section these for assessment of defect size. However, the value of these samples seem limited because of the method of sample preparation. Conventional powder was used which can, and evidently did, have numerous oxides present as a result of sprue erosion during melting and atomization. Such particles smaller than .010 inch could pass through the screening (-60 mesh) used in processing the powder.

Let us assume the numbering of 412 and 414 was reversed. The Holosonic intensity mode scan of a portion of #414 is shown in Figure 54. This would be the sample to which was added .006 to .010 inch defects. Indication number 1 looks to be quite large but all of the rest appear to be quite small. Remember none were found by conventional ultrasonics. Thirteen indications were strong enough in both C-scan and simulated B-scan to permit accurate mapping. There is strong indication that these were in the range of .006 to .010 inch in size.

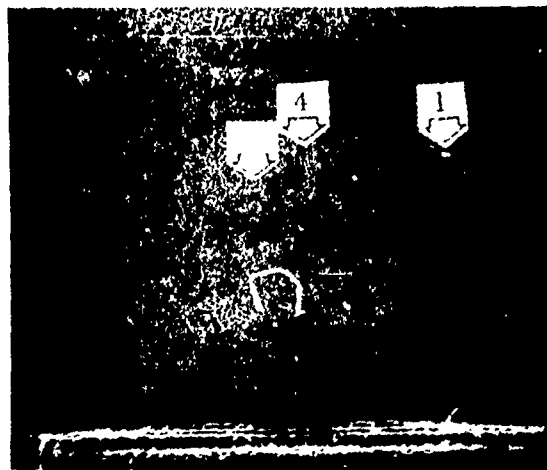
TABLE VII

Results From NDE Of Disks

<u>Number</u>	<u>Ultrasonic Results</u>	<u>Holosonic Intensity Mode</u>
412	9 significant indications	13
413	2 significant indications	16
414	None	Numerous
416	Many indications	Many



C-SCAN

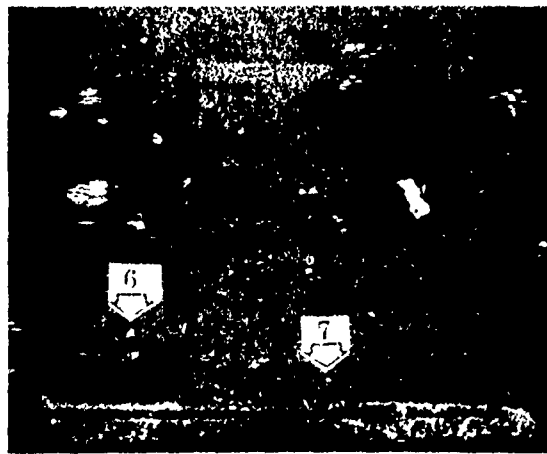


SIMULATED B-SCAN

Figure 54: Sample 414, Gated 2.8-5.5 sec. From Marked Side

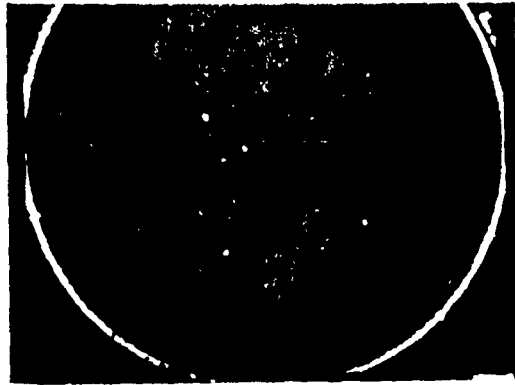


C - SCAN



SIMULATED B- SCAN

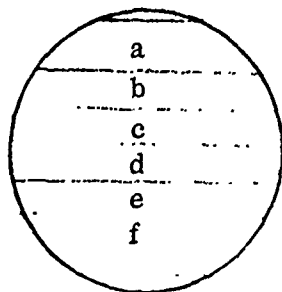
Figure 55: Sample 412, Gated 9.5 - 12.4 sec. From Opposite Side (side opposite ultrasonic indication marks)



C - SCAN



SIMULATED B - SCAN



Location of Sections

Figure 56: Full Width Scan of Sample #413 Using Settings From Table II

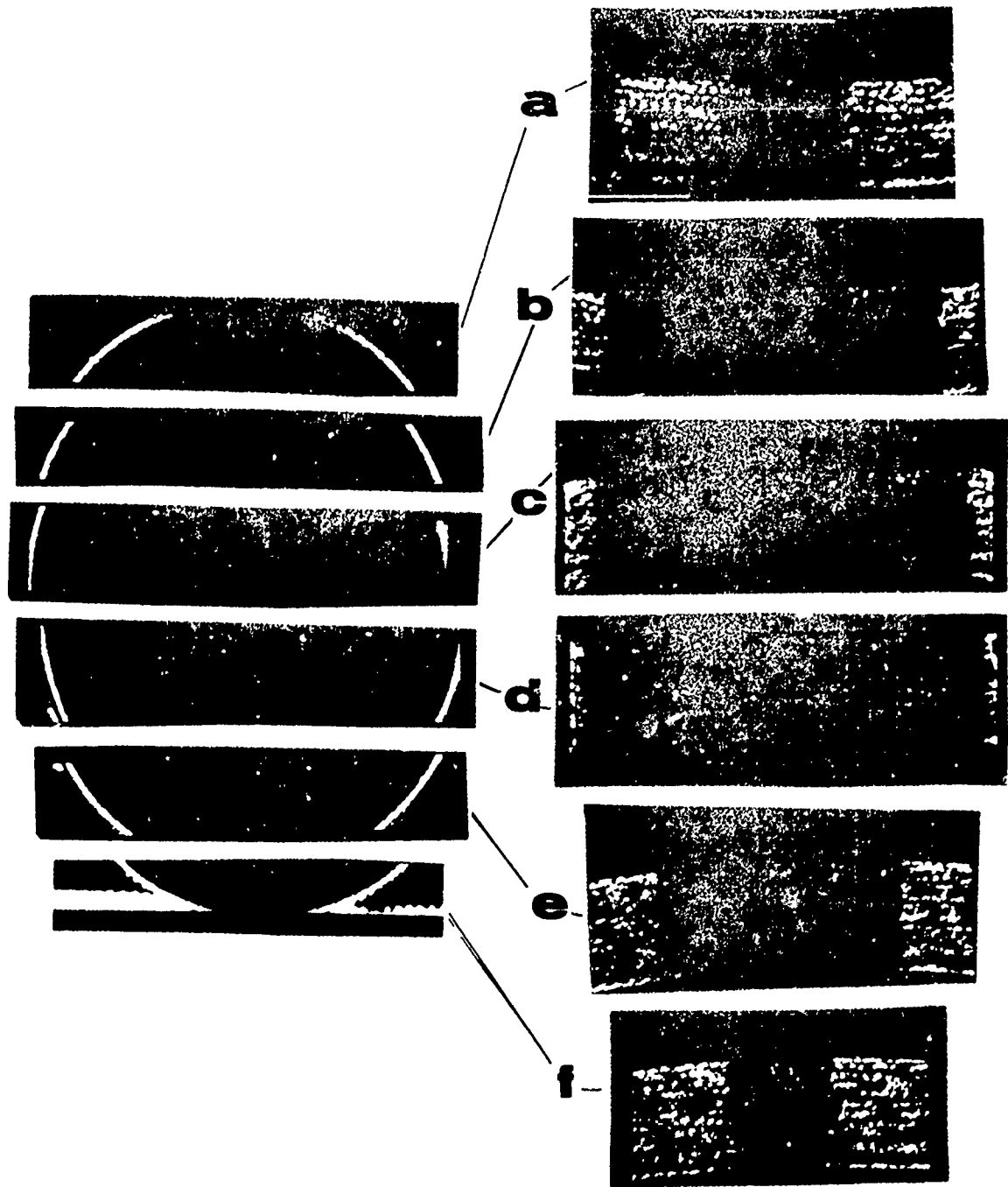
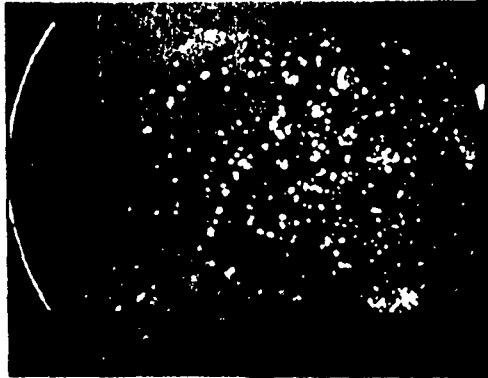


Figure 57: Continued - Sections of Scan Relative to Table II



C - SCAN



SIMULATED B - SCAN

Figure 58: Sample 16 - Partial Scan Showing Innumerable Indications. Although Fe_2O_3 Was Added, Results are Probably Due to Leakage of Can During Sintering.

Test Data On Two Cracked Specimens: #C-1 And #C-2

Specimen C-1 is 6" in diameter and 2" thick. Specimen C 2 is a rectangular block 8" X 4" X 1 1/2" thick. Both pieces contain tightly closed cracks originating at the surface.

Two techniques were used for the inspection of these test pieces. Figure 59 depicts a scanning configuration that employs a separate source and receiver. This configuration is similar to through-transmission in that the image is a shadow picture; i.e., the presence of a crack radiating from the back surface of the specimen is indicated by a lack of signal at the receiver transducer.

Figure 60 depicts a shear wave technique using a simultaneous source/receiver. In this case, the presence of a crack radiating from the back surface of the specimen is indicated by a return signal reflected from the crack. The technique shown in Figure 59 was the more successful.

Figure 61 is a 10.6MHz coherent shear wave image of Specimen C 1. This photograph is typical of those obtained during several scans of Specimen C 1, in different transducer/specimen orientations. The sensitivity was sufficiently high in this case to depict grain boundary scattering in the image. The lack of any crack indications in this image suggests that the known surface cracks in this specimen are very shallow. In reality they were quite deep.

Figure 62 is a 10MHz image of Specimen C 1 using the technique shown in Figure 59. The detection of one crack is denoted by (l). This image is typical of those obtained during inspection of Specimen C 1 with separate source and receive transducers. This image tends to confirm that the visible surface cracks are not readily identified with ultrasonic techniques due, in part, to the high dependence on ideal orientation of the beam to the plane of the crack.

Figure 63 is a 10MHz image of Specimen C 2 and was made with the set-up depicted in Figure 59. The cracks (black) seen in this figure propagate far enough below the surface to be readily detectable by this imaging technique. It is not certain that the true depth is represented by this scan.

Figure 64 is an image, of a known simulated crack, 1/4" deep, in a 1/2" thick test sample and was made using the same set-up as the image of Specimen C 2 in Figure 63.

Application of the System 200 to detection of shallow cracks in these types of specimens would require multiple scanning direction to assure that the transducer is near-normal to the crack face in order to receive a reasonable size reflected signal. Even then, reliability is questioned.

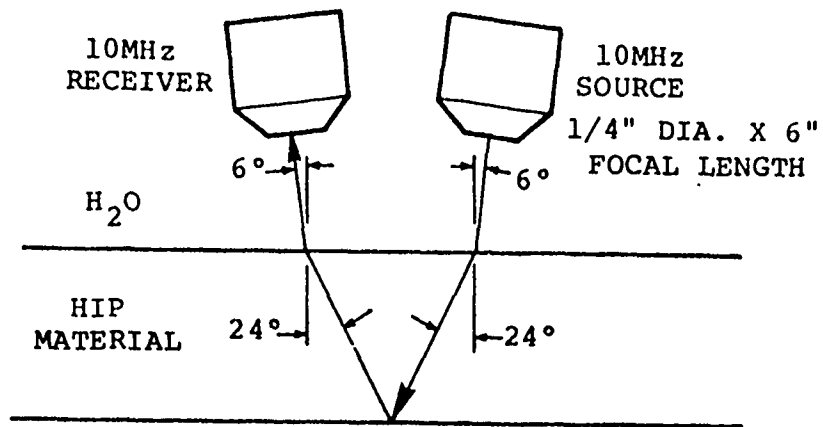


Figure 59

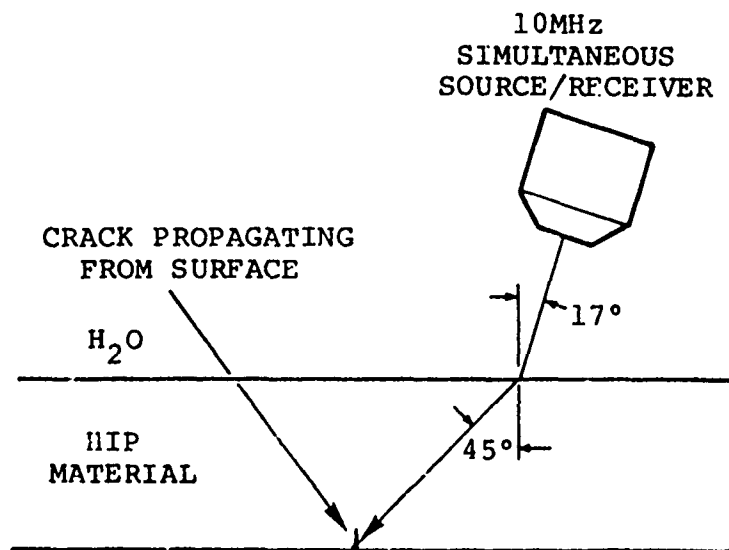


Figure 60

Two Methods Of Evaluating Cracks

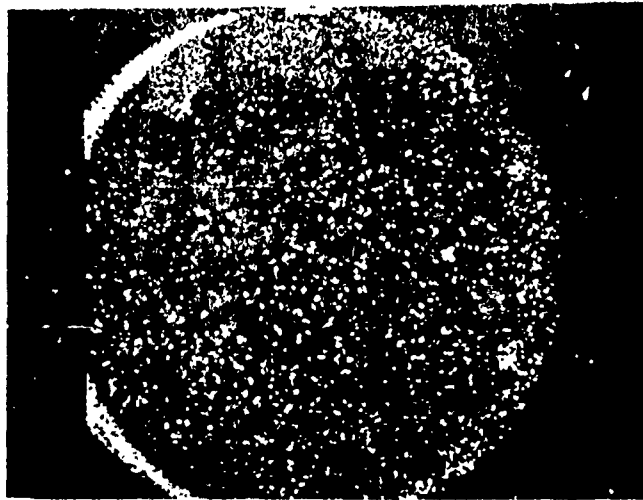


Figure 61: Holosonic Ultrasound View Of CI Specimen At High Gain
Method Of Figure 60 Was Used



Figure 62: Same As Figure 61 Except Method Of Figure 59 Was Used

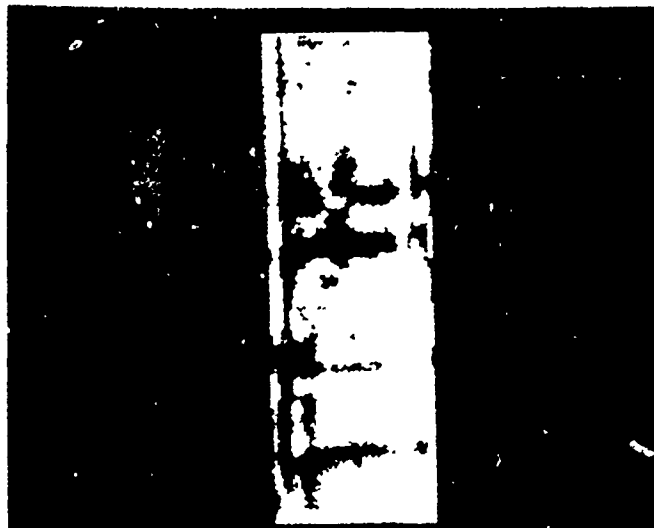


Figure 63: Specimen C-2 Inspected With Method Illustrated In Figure 59

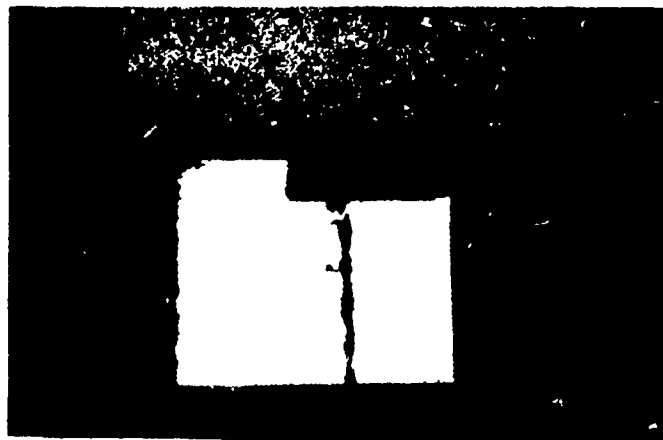


Figure 64: Image Of A Known Simulated Crack 1/4" Deep In A 1 1/2" Thick Test Sample Using The Same Set-Up As For Figure 63.

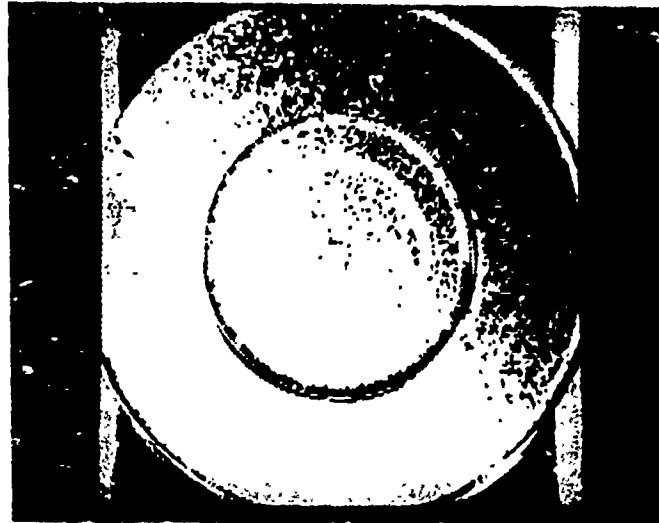


Figure 65: Sample P1 Gated To Record A Small Depth Increment.

Porosity

Results on P1 indicated ability to obtain response signals from small voids. The number of voids present made systematic evaluation meaningless.

From this work on intensity mode Holographic ultrasound we can conclude:

- o Much improved method of data presentation exists but there is the need for equipment modification to permit calibration.
- o The method of signal presentation more accurately predicts size and shape.
- o Accurate and easy location of defects is possible with cathode ray method.
- o Holographics demonstrated an ability to inspect nearer the surface than with current ultrasonic practice.
- o There are strong indications of improved sensitivity but there is a need to substantiate this claim with more cut up evaluation.
- o There appears to be no promise that this process will be a crack inspection process.

ACOUSTICAL HOLOGRAPHY

Acoustical holography, with the Holosonic equipment, makes use of all the tools used with intensity mode, coherent pulse, coherent transmit, ultrasound discussed above. Then the response signal is processed with a computer capable of handling complex Fourier formulations and reconstitutes this information in the form of a hologram. Thus one would expect all the improvements listed in Table V plus an additional apparent advantage.

There is a limited effect of signal sensitivity on the proximity of a defect to the transducer focus. As illustrated in Figure 66, defect #1 is closer to the beam focus than defect #2. If we assume the two defects are of equal size, defect #1 would absorb a larger percentage of the ultrasonic beam energy than defect #2. (The cone area at #2 is greater than #1 and the energy at #2 is more diffuse). Thus the signal from defect #1 would be strongest. In conventional ultrasound this would be reflected in an indication of larger defect size with acoustical holography, the reconstructed hologram is the summation of a series of signals from that defect representing a series of locations of the transducer. Because of the cone angle, response signals would be received from more transducer locations from #2 than #1 so the integrated or composite response from both defects would be essentially equivalent. If another modification is made in the electronic signal, the response from the two signals could be even closer making accurate calibration of defect size more probable. This modification is an amplification of the signal as a function of the depth so that wave absorption effects could be negated.

For the work on this contract, there was no computer available capable of handling acoustical holography for these samples, nor was the associated software in place. Thus the holography was done by a reconstruction method that only approximates the capabilities of a fully developed system.

Reconstructable Acoustical Holography

Figure 66 depicts typical parameters for acoustical holography imaging. In most cases, the transducer is set up to focus on the surface of the specimen being inspected. The figure depicts the transmitted ultrasonic beam shape of an F/4, lens focused transducer, i.e., the transducer focal length is four times the active element diameter. Four different transducer locations during a scan are pictured.

For acoustical holography, optimum image quality is determined by the size of the scanned aperture, transducer frequency and the distance to the object. The frequency dependency is similar to conventional ultrasound. The higher the frequency the shorter the wave length and the better the resolution.

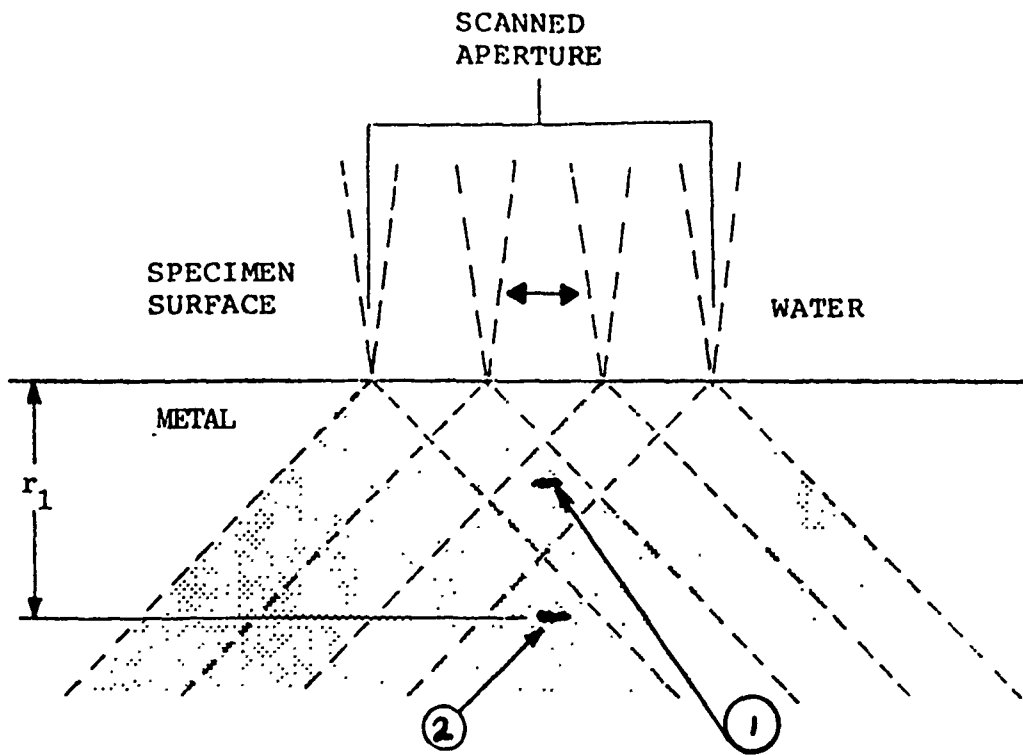


Figure 66: Transmitted Ultrasonic Beam From One Scanned Transducer Focussed At The Surface Of A Test Specimen. The Beam Shape Represents A 4 Inch Focal Length By One Inch Diameter Transducer.

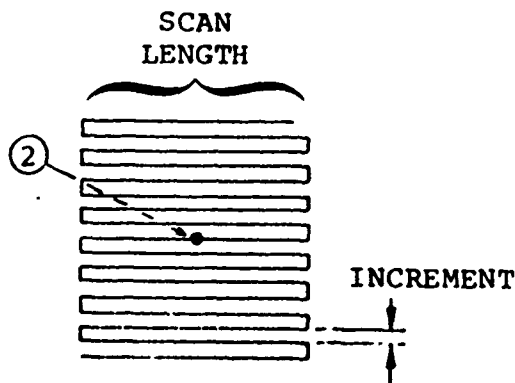


Figure 67: Typical Set-Up For Making An Acoustical Hologram Shows Object #2 (Figure 66) Centered In Scanned Aperture.

The scanning aperture is a measure of the number of discrete transducer locations contributing to the reconstructed hologram. The greater the aperture the higher the number and the sharper the holographic image. Also the greater the distance to the object (or defect within the sample) from the focus of the transducer, the larger number of transducer locations contribute to the reconstructed hologram and so the sharper the image.

This calls attention to a small problem with acoustical holography when compared to intensity mode Holosonic ultrasound. With the latter process the focus is well within the part and usable response from defects to about .030 inch from the top surface is possible. Closer approach to the bottom surface is reasonable. With acoustical holography, the focus is typically at the surface tending to ring the surface. This causes no problem when defects well within the part are imaged since the reconstructed hologram, having many contributing signals, tends to ignore that signal from the surface. But, when the defect is near the surface, the holographic signal tends to be more diffuse because of fewer contributing response elements. For such defects the ringing of the surface tends to interfere. To circumvent this problem, the hologram should be made by using two or more transducers some of which are focused below the surface.

In practice, an acoustical hologram is formed as follows:

- o Assume that Figure 67 is a plan view of Object #2 in Figure 66.
- o The transducer scans a rectilinear pattern as in Figure 67.
- o Object #2 is diffusely illuminated by scanning the diverging ultrasonic beam as depicted in Figure 67.
- o The transducer is driven by a coherent sinusoidal source at its resonant frequency. The resultant pulse of coherent ultrasound travels through the medium and is reflected from Object #2. This reflected energy pulse is received by the transducer.
- o The phase of the reflected object signal is compared to an electronically generated reference signal. The result is an electronic interference pattern.
- o Each scan line can be written as a row of dots on the face of storage oscilloscope. The dot spacing being a function of the phase comparison along the scan line, or the interference pattern.
- o The acoustical hologram of Object #2 appears on the storage scope as a pattern similar to that shown in Figure 68.
- o In a production system, the hologram information would be reconstructed by a micro-computer to provide near real-time, high resolution images of any defect condition in the production part. In this initial feasibility

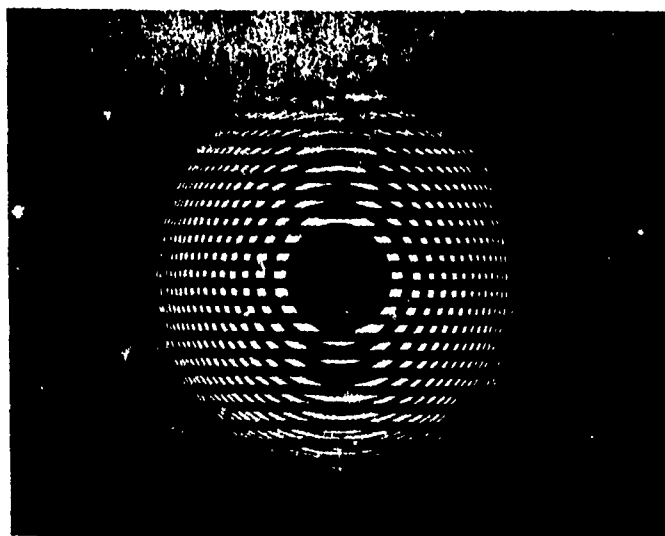
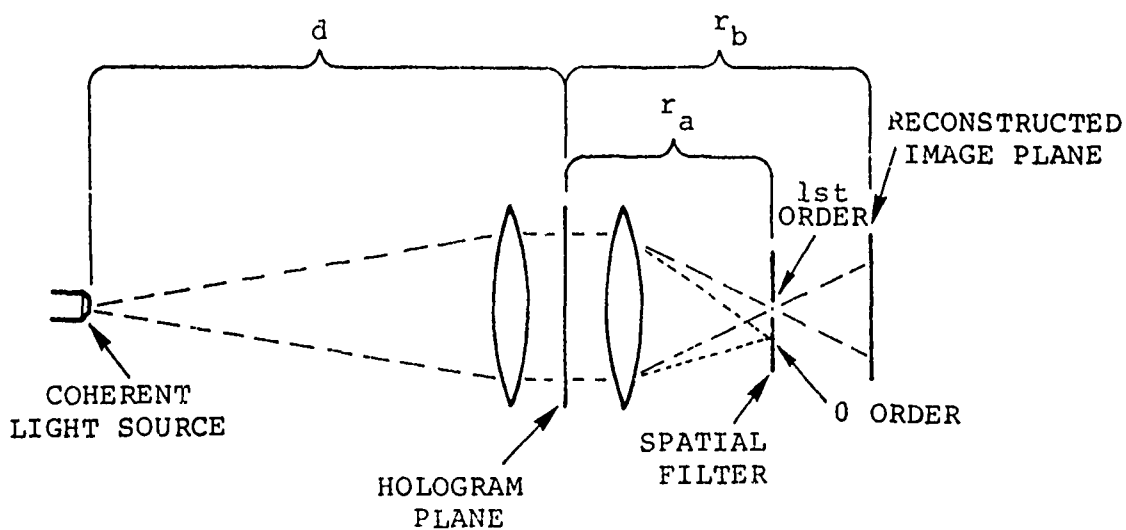


Figure 68: This Pattern Is Very Similar To That Obtained By Making An Acoustical Hologram Of A Point Source, Or A Small Diameter, Circular, Planar Defect Condition.



- r_a - Distance From Zero Order Focal Point To The Plane Of The Hologram
- r_b - Distance From The Plane Of The Hologram To The Plane Of The Reconstructed Image
- d - Variable Distance Used To Set Proper Relationship To r_a To r_b

Figure 69: Schematic Diagram - Optical Reconstruction Of An Acoustical Hologram

test, the microcomputer was not available and two step optical reconstruction was accomplished by recording the hologram on Type 46L Polaroid transparency film.

- o The transparency of the acoustical hologram is placed in an optical reconstructor (represented schematically in Figure 69) and the reconstructed image of Object #2 (Figure 67) is displayed on a video monitor. Distance in Figure 69 is proportional to the depth of Object #2, and the true size of Object #2 is as presented on the face of the video monitor, multiplied by a magnification factor based on the distance of the object from the focal point (hologram plane) of the transducer and the acoustical frequency.

The optical reconstructor schematically drawn in Figure 69 can be replaced by a microcomputer reconstruction system with TV display. The effect of the lens system in Figure 69 is to take the fourier transform to the Hologram data to obtain the reconstructed image. This same mathematical transformation may be accomplished with a microcomputer and displayed on a TV monitor. The microcomputer reconstructor has the added advantage of eliminating the film and making the inspection a one step operation. In addition, the microcomputer transforms the Hologram information using the known acoustical wavelength which helps to eliminate out-of-focus information commonly present in optical reconstructors where the optical wave length must be used. The microcomputer reconstructor is, therefore, proposed for the final configuration of this inspection system.

Figure 72 is a photograph of an 11 MHz acoustical hologram of two side-drilled holes in resolution standard S-1. This hologram was optically reconstructed as depicted in Figure 69 schematic diagram using input depicted in Figure 70. The two holes lie at different depths in the test specimen. By varying distance "d" (Figure 69) one may focus on one drill hole and then the other. See Figure 71 and 73.

The advantages of acoustical holography lie in the ability to accurately determine the lateral dimensions of objects lying in the reconstructed image plane of the hologram and to obtain the highest resolution of any defect condition regardless of its depth in the specimen. Note that with computer reconstruction, the results of Figures 71, 72, and 73 would be improved so that both holes would appear in focus as discussed below.

When a microcomputer is used to obtain near real-time acoustical holography images it must mathematically transform (Fast Fourier transform) the hologram data into the reconstructed image. Because of the flexibility of the computer, it may choose the reconstruction wavelength to be equal to the original acoustical wavelength and thereby avoid any unnecessary distortion in the reconstructed image. When an optical reconstructor is used, the reconstructed wavelength is fixed as the light wavelength.

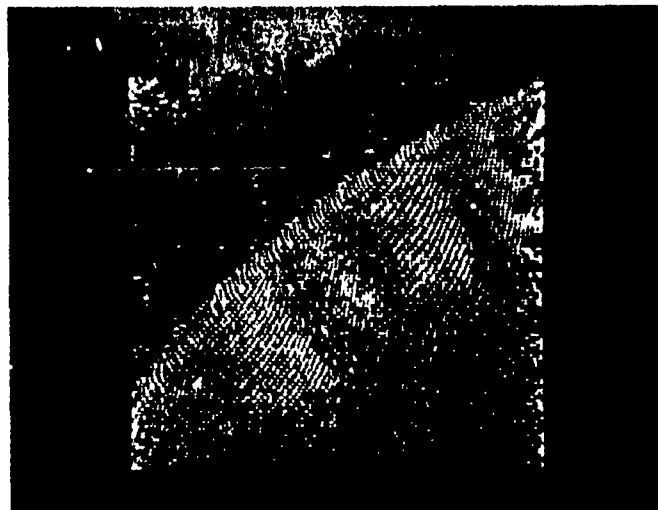


Figure 70: 11MHz Acoustical Hologram Of Two Side Drilled Holes In Resolution Standard S-1. This Hologram Contains The Phase And Amplitude Information From Which Reconstructed Images In Figures 71 - 73 Are Obtained.



Figure 71: Reconstructed Image Of Figure 70 Hologram.

r_a Set To Focus Hole #1 On Image Plane.
 $r_a = 4.08 \text{ m}$, $r_b = 10 \text{ m}$ $M = 1.08$
 (Image Mag.)
 $m^* = 1.333$



Figure 72: Reconstructed Image Of Figure 70 Hologram.

r_a Set Midway Between Hole #1 And Hole #2 Focus On Image Plane.
 $r_a = 4.12 \text{ m}$, $r_b = 10 \text{ m}$ $M = 1.07$
 $m = 1.333$



Figure 73: Reconstructed Image Of Figure 70 Hologram.

r_a Set To Focus Hole #2 On Image Plane.
 $r_a = 4.2 \text{ m}$, $r_b = 10 \text{ m}$ $M = 1.03$
 $m = 1.333$

* m is the ratio of the length of one side of the scanned aperture to the length of one side of the hologram.

The formula for calculating lateral reconstruction image magnification is:

$$M_L = (2 \lambda_L / \lambda_s) (mr_b/r_1)$$

Where λ_L and λ_s are light (6328 Å for He-Ne) and acoustic wavelengths, m is the hologram copy reduction factor (typically 4), r_1 is the depth of the object (See Figure 66) and r_b is determined from the equation:

$$1/r_b = (2 \lambda_L m^2 / \lambda_s r_1) - 1/r_a$$

The term r_a is hologram to zero order light focus distance (See Figure 69) and is generally a negative number, making the more common form of the above formula:

$$1/r_b = 1/r_a \pm (2 \lambda_L m^2 / \lambda_s r_1)$$

The two resolutions being for the true image and the conjugate image.

The large difference in acoustical and optical wavelength cause undesirable effects in the reconstructed hologram which would not be present if micro-computer reconstruction were used.

Thus, the opportunities in acoustical holography have been indicated. The capabilities appear equal or better than intensity mode Holographic ultrasound and, theoretically should be better. Additional work is required but such effort demands certain equipment modification as indicated on page .

INTERCOM RAD TEC NDF EFFORT NEUTRON RADIOGRAPHY

This process was evaluated but proved to have no application to rotating turbine hardware. There are special applications for this process and one typical use is given later in this report. Late in this contract period, work on neutron radiography was stopped and effort was transferred to a new process, Compton Scattering, which is discussed later in this section. The neutron radiography effort is described below.

DESCRIPTION OF THE PROCESS

Neutron radiography is similar to x-radiography only thermal neutrons are the energy source rather than x-rays. The source of neutrons used for this work was the Californium 252 radioactive isotope. It is housed in an appropriate shielded container. Part of the neutrons emitted from the Californium 252, which are fast neutrons at the time of emission, are reduced in energy from fast to thermal neutron energy levels with the aid of an organic moderator. (Only the thermal neutrons are effective for this inspection process.)

The thermal neutrons escaping through the aperture of the source shield impinge on the sample creating a shadow picture on the x-ray film behind the sample.

Neutron Photographic Detection Methods

The photographic detection method, most commonly used, employs the conventional x-ray film with converter screens. Since film is essentially transparent to neutrons, these screens convert the neutron image into one which can be detected more readily by the x-ray film. These converter materials are of two different types, potentially radioactive materials and prompt emission materials.

The latter type, characterized by gadolinium, has little tendency to become radioactive, but rather emits irradiation which exposes the film immediately upon the absorption of a neutron. This type of converter screen is used for a direct exposure method for detecting neutron images. The film and screen must be exposed together to get a neutron image. This direct exposure method is a relatively fast detection technique. One disadvantage, however, is that the film is present to detect other accompanying radiation, such as gamma radiation that is initially present from the neutron source or a result of prompt reactions with the piece being inspected by the neutron beam. Since gamma radiation is generally the dominant one present, one can filter the initial beam so as to attenuate the gamma component relatively more than the neutron component and obtain a high neutron to gamma ratio. A sheet of aluminum surrounding the

film can decrease gamma fogging by this selective absorption. In addition, x-ray film more insensitive to gamma rays can be used.

The main disadvantage of the direct exposure technique (gamma fogging) can be overcome by using a detection method called the transfer technique. The image is detected on a potentially radioactive screen which becomes radioactive proportional to the neutron intensity at each point of the image, and later transferred by beta emission to the x-ray film. Dysprosium and indium are two materials commonly used for the screen material.

The absorption of neutrons by the Rene' 95 disk material is quite different than absorption by conventional x-rays. Heavy metals, like chromium, nickel and iron are rather transparent to neutrons but readily absorb x-rays. Light atoms, especially hydrogen, have high absorption coefficients for neutrons but have little effect on x-rays. So the value of neutron radiography must lie in some special absorption properties.

It has already been demonstrated that corrosion products in aluminum aircraft structures are instrumental in identifying corrosion cracking. These corrosion products absorb neutrons illuminating the defects. It was hoped that similar applications could be found for disk alloys.

PROGRAM PLAN

The P, D, S and C type samples described on page 5, were to be used to establish the inspection parameters with neutron radiography. For the cracked samples, increased detectability was planned by using a gadolinium nitrate penetrant ($Gd(NO_3)_3 \cdot 6H_2O$) in back filling voids open to the surface. The neutron beam is attenuated in any material according to

$$I = I_0 e^{-\Sigma t}$$

where I is the radiation intensity transmitted through the material having a thickness t and a linear absorption coefficient Σ , and I_0 is the initial incident radiation intensity. Gadolinium has one of the highest absorption coefficients and hydrogen is also quite high. It was anticipated that cracks and other defects open to the surface would be well illuminated by the gadolinium salts.

Following the establishment of techniques with the aid of the samples mentioned above, six T700 disk blanks were to be evaluated and results compared with other NDE processes.

RESULTS

Initial attempts to inspect D1 and D2 indicated the intentionally added oxide par-

ticles were too subtle for the process. Similarly, the holes in P1 could not be identified. The holes in S2 were filled with gadolinium nitrate penetrant and the sample evaluated. The doped penetrant was effective in absorbing neutrons as illustrated in Figure 74. However, in any regions that the penetrant did not fill, the difference in film density of the exposure was subtle and identified primarily because of known defect location. See arrows in Figure 74. The holes in S2 are .020 inch in diameter.

On subsequent evaluation of S3, not all holes were observed on the films. Holes drilled in this sample varied from .007 to .030 inch in diameter. See Figure . Either the penetrant did not back fill all holes or the smaller holes were too subtle for the process.

The cracked samples C1 and C2 were examined with very disappointing results. No exposure was made with a film density contrast in the crack region sufficient to produce for the report.

Many experiments were performed to improve sensitivity of the process. These included:

- o Different film types, e.g., single and double emulsion, Type A, Type M.
- o Cutting film donuts so film could be placed in direct contact with the part surface on T700 disk shapes.
- o Use of the transfer technique with Indium sheet, to minimize gamma fogging.
- o Use of Potter Beckey grid to filter out scattered radiation from the sample and reduce film fogging.
- o Computer aided density intensification of the exposed film.

With all of this experimentation, no additional films worth reproducing were made.

CONCLUSIONS

- o Neutron radiography does not warrant further work at this time with regard to rotating turbine hardware NDE.
- o The capabilities of the process do not warrant a comparison or economic analysis since the process fails to meet minimum requirements for NDE as related to these turbine parts.
- o Even the use of gadolinium nitrate was disappointing. If drilled holes

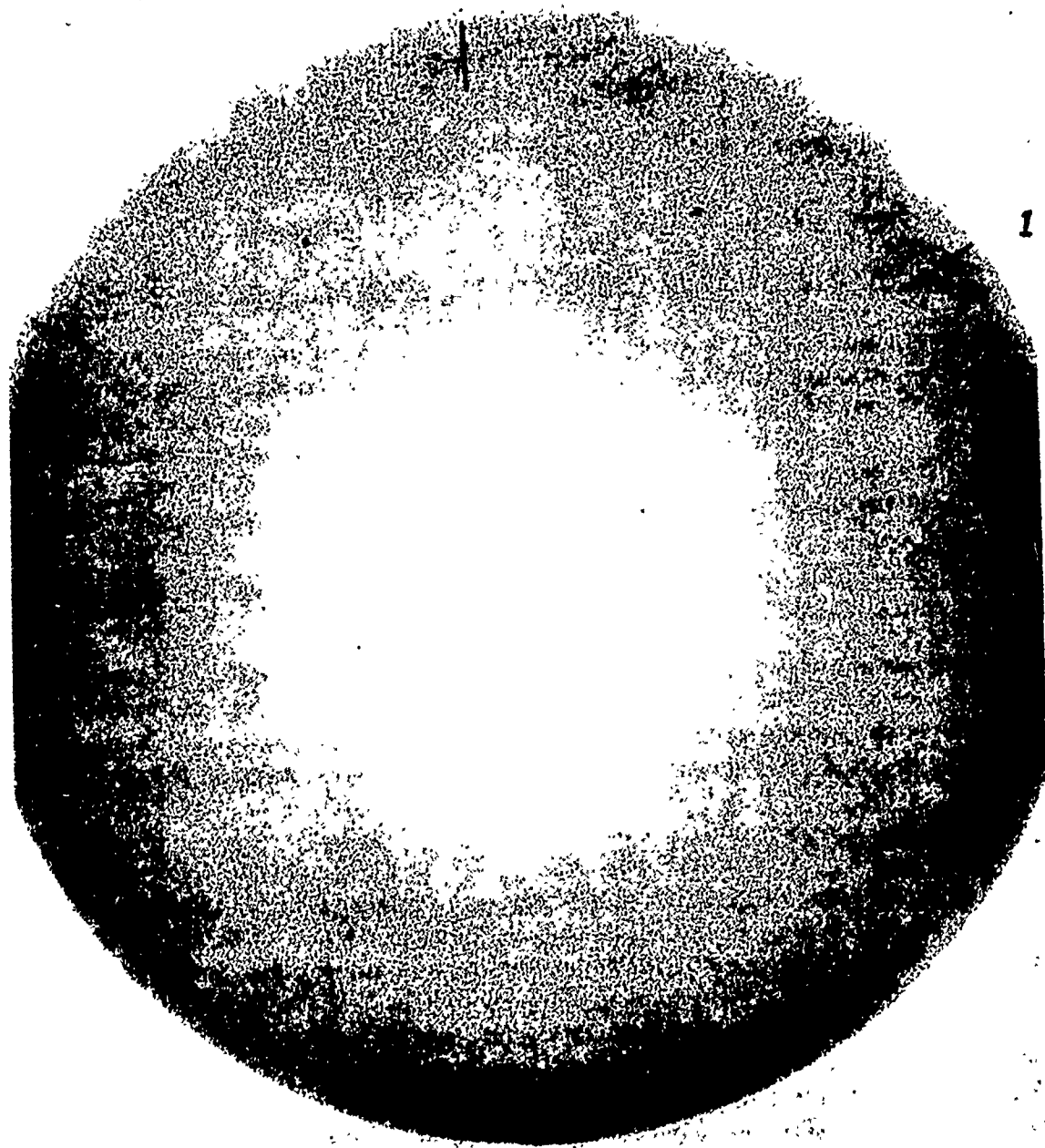


Figure 74: Neutron Radiograph Of S₂

cannot be reliably filled and inspected, there is little hope of cracks ever being reliably located by this process.

- o As a side evaluation, T700 shafts with Viton seals were inspected at overhaul to determine seal location and condition. Broken seals and seals that had shifted location could be readily evaluated in Neutron radiography films. Thus it appears that this process can be useful in inspecting organic O-rings and seals in assemblies.

No further evaluation was made of this process.

COMPTON SCATTERING NDE

Flaw Detection Of HIP Material With A Photon-Scattering Gage Introduction

As previously mentioned, the IRT effort, using neutron radiography did not prove useful in inspecting HIP Rene' 95 hardware. But, during the course of this contract, another NDE method was being explored for an ordnance application. The progress in this ordnance work warranted a modification of the HIP effort at IRT to include an evaluation of this new process. With the very limited time and money left in this contract effort, the planned evaluation was very preliminary.

DESCRIPTION OF THE PROCESS

This radiometric technique is based on a simple physical principle. By measuring the scattered radiation of a high energy source, the type, size, and location of defects in the specimen can be identified with a high degree of resolution and sensitivity, even in the presence of severe defects in other parts of the specimen.

Basic Radiation Principle

The photon-scattering gauge utilizes the fact that gamma radiation interacts with the material which it passes through by scattering a portion of the incident beam away from the incident direction. This type of interaction, known as Compton Scattering, is a well understood phenomenon. As photons exceed about 200 keV in energy, they almost exclusively interact with the electrons in the target material and transfer only part of their energy to the electron during a collision. Conservation laws require that the photon be deflected in a particular angle as a result of this collision. Energy loss and change in direction are unambiguously correlated. A small loss of energy is associated with a small angular deflection; increasing energy loss corresponds to increasing deflection, with maximum energy loss occurring when the photons are scattered 180°.

With increasing incident photon energy, a growing fraction of the scattered radiation falls in the forward direction, independent of target material, while the total probability for the occurrence of Compton Scattering depends on incident photon energy and material characteristics. Generally, photons in the energy range of 200 to 1500 keV almost exclusively interact by Compton Scattering with all but the heaviest elements. As the incident energy exceeds 500 keV, the number of scattered photons becomes practically independent of material composition and depends only on the mass or electron density of the scattering target. In other words, the number of photons scattered from a unit volume element in the target depends only on the density of electrons in this volume element. We shall see that the number of scattered photons increases linearly with the electron density in the target volume element. The energy source used for this work was a cobalt 60 isotope. Note that for the turbine materials of interest, the electron density is almost exactly proportional to the gross density of the particle being inspected.

Since scattered radiation measurements seem to be more definitive than incident beam evaluation on the bottom side of the test sample, a technique for scattered radiation evaluation was developed. A selected portion of the scattered radiation is usually measured by a radiation detector at the end of one or more collimators placed at a certain angle to the incident beam. All collimators are focused on the same portion of the incident beam. The detected scattered radiation results from Compton interactions in the volume element defined by the intersection of the incident beam and the detector collimators. Consequently, the volume element from which the scattered radiation originates appears to the detector like a source of radiation whose intensity depends on the amount of material contained in this inspection volume element. The introduction of a void into the volume element means a reduction in the amount of material available to scatter gamma rays, and consequently results in a decrease in the detector response. The introduction of an oxide increases the electron density and detector response over a void, but still oxides represent a significant drop in electron density when compared to the HIP Rene' 95 material.

If the inspection volume element is selected sufficiently small so as to represent only a small fraction of the entire sample volume, the detector response becomes highly localized, and consequently is less subject to interference from signals from the rest of the sample. The energy from the other portions of the sample is largely negated because a very small fraction is aligned with the detection collimators. The sensitivity of the process is governed by the ratio of the void size to inspection volume which is defined by the collimators.

In the schematic representation of a photon-scattering inspection device shown in Figure 75, the specimen is positioned before the source collimator. A scattering detector with a suitable collimator views the sample from the side at

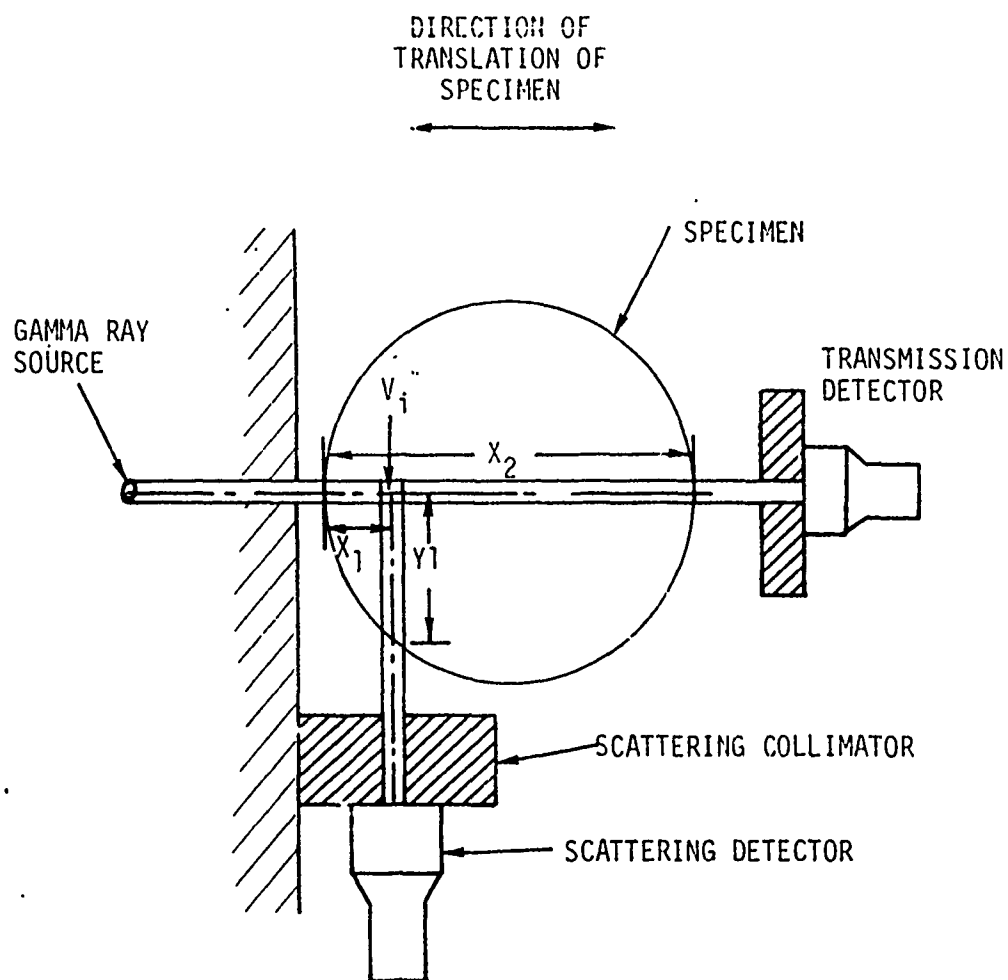


Figure 75: Schematic Representation Of A Photon-Scattering Gauge In Comparison To A Transmission Gauge.

a selected angle to the direction of the incident radiation. The 90° angle chosen for the schematic representation in Figure 75 is arbitrary, and does not imply that it is the optimum angle for a scattering gauge in general, or for this application in particular. The transmission detector shown in Figure 75 represents a measuring location to simulate conventional x-ray techniques.

The Compton scattered radiation, which is measured by the scattering detector, originates in the volume element defined by the intersection of the collimator of the interrogating gamma-ray beam and the inspection aperture determined by the collimator in front of the detector. The entire volume of the sample can be inspected by translation and rotating the sample with respect to the incident beam/detector beam intersection.

Detector Response And Sensitivity

In the following discussion a comparison is made as to the ability of two processes to detect defects. In the first process, quite comparable the conventional radiography, transmitted energy is measured. It is shown that an important factor governing detection is the ratio of defect thickness to the thickness of the part being inspected. In the second method, photon scattering is measured. The detection is governed primarily by the ratio of the size of defect compared to the size of the sample defined by the intersection of the source and detection collimators. Scattering from other regions of the sample have only minor effects.

In order to understand the characteristics of the photon-scattering gauge in some detail, we shall now develop a general analytical formalism of radiometric techniques which allows a quantitative evaluation to be made. It is convenient to use the standard transmission technique (conventional radiography) as a point of comparison, since it is easily understood and forms the basis for the well-known radiographic method. In this elementary treatment we neglect the effects of small-angle scattering of the beam and of contributions from multiple scattering in material surrounding the beam.

Transmission Gauge (Comparable to conventional radiographic techniques). See Figure 75. The energy measured by this gauge is that energy measured by normal transmission radiography using the detector rather than film. Referring to the arrangement in Figure 75, we can write the response of the transmission detector as follows:

$$R_T = I_0 e^{-\mu \rho X_2} \quad (1)$$

where

I_0 = incident gamma-ray flux the source;

$\mu \rho$ = total gamma-ray attenuation coefficient for the material of the specimen expressed for convenience as the product of the density (μ) and the mass absorption coefficient (ρ) with units cm^2/g ;

X_2 = material thickness as illustrated in Figure .

We are interested in knowing the sensitivity of the response R_T to imperfections in the material represented by changes in X_2 . These could, for example, consist of small voids which effectively cause decreases in this quantity. The fractional change of Eq. 1 can be expressed as;

$$\frac{\delta R_T}{R_T} = -\mu \rho X_2 \left(\frac{\delta X_2}{X_2} \right) \quad (2)$$

Equation (2) is derived by differentiating equation (1), dividing it by equation (1) and multiplying right side by $\frac{X_2}{X_2}$.

The left-hand side of this equation is the fractional change in the transmission response, and the right-hand side shows how this is related to changes in path length through the specimen.

That is, for a defect of width W_d in the material,

$$\frac{\delta R_T}{R_T} = -\mu \rho X_2 \frac{W_d}{X_2} \quad (3)$$

The most important generalization in the above analysis of the transmission response lies in the observation that the change in response is proportional to the ratio of the size of the imperfection to the thickness of the specimen. We shall have an occasion to return to this concept after looking at the analysis of the photon-scattering technique for gauging.

Scattering Gauge. With the background provided by the previous discussion, we can proceed directly into an analysis of the photon-scattering gauge. Again referring to Figure 75, we can write the scattering response, R_s , by stepping through the sequence of interactions which occur. The scattering detector

views a small volume at a position X_1 from the inner surface of this casing. Thus, for the assumed ideal conditions, the gamma-rays which reach this point are given by:

$$I = I_0 e^{-\mu \rho X_1} \quad (4)$$

At the inspection point X_1 , scattering events occur in the inspection volume V_i , and those which scatter into the direction of the detector can be written as

$$I V_i \rho_i \mu_i \Delta \Omega f(\theta) \quad (5)$$

where I is from Eq. 4, $\Delta \Omega$ is the solid angle subtended by the detector at the scattering volume, and $f(\theta)$ is an angular distribution function which expresses the distribution of Compton-scattered photons. We use ρ_i and μ_i to represent the values of these parameters averaged over the inspection volume V_i .

The photons which scatter in the inspection volume and are degraded in energy according to the law of Compton scattering, suffer an attenuation in reaching the detector, which is given by:

$$e^{-\mu' \rho Y_1} \quad (6)$$

where the primed mass absorption coefficient indicates that the scattered gamma rays have a lower energy than the incident gamma rays, and the overall scattering response is just the combination of the above three relations,

$$R_s = I_0 V_i \rho_i \mu_i \Delta \Omega f(\theta) e^{-\mu \rho X_1} e^{-\mu' \rho Y_1} \quad (7)$$

Now, following the same procedure as before to find the sensitivity of the scattering response to defects in the various parameters, we obtain the fractional response change;

$$\frac{\delta R_s}{R_s} = \left(\frac{\delta \rho_i}{\rho_i} \right) + \left(\frac{\delta \mu_i}{\mu_i} \right) - \mu' \rho Y_1 \left(\frac{\delta y_1}{y_1} \right) - \mu \rho X_1 \left(\frac{\delta X_1}{X_1} \right) \quad (8)$$

Equation 8 is the scattering analog of Eq. 2, and can be seen to have four terms which are similar to those of Eq. 2. These terms originate from the transmission processes which are part of the photon-scattering method, and affect the scattering response in the same manner as discussed above. In particular, their effect on the scattering response depends on the ratio of the defect size (δX_1 or δY_1) to the path length through the material. We shall concentrate our attention on the

first two terms of Eq. 8, which express the effect of changes in average density and composition of the inspection volume V_i .

a. $\frac{(\delta\mu_i)}{\mu_i}$

This term refers specifically to changes in atomic composition of the inspection volume, the most common occurrence being an inclusion of some foreign substance. This term has a negligible effect on the scattering response for any inclusion with atomic number less than tin (Sn), and rises to an effect of about 10% for lead (Pb) for 1.0-MeV gamma rays.

b. $\frac{(\delta\rho_i)}{\rho_i}$

This term refers to density changes due either to voids or inclusions. In the case of inclusions, these will typically be lower in density than the surrounding material.

The most illuminating example of the photon-scattering technique is the case of a small defect. If the inspection volume is V_i and the defect volume is V_d , the combining effect of the first two terms gives the general result,

$$\frac{\delta R_s}{R_s} = \frac{V_d}{V_i} \left(\frac{\mu_d \rho_d}{\mu \rho} \right) - 1 \quad (9)$$

In the special case of a small void in the material, we obtain;

$$\left| \frac{\delta R_s}{R_s} \right| = \left| \frac{V_d}{V_i} \right| \quad (10)$$

which says that the fractional change in response is just equal to the ratio of the defect volume to the inspection volume. This is a very important result, since it provides a concise proof of the superiority of the sensitivity of the photon-scattering technique over the transmission techniques. Simply stated, since the change in the transmission response is proportional to the ratio of the defect size to the total thickness of the specimen (i. e., Eq. 3), the above result shows that the scattering technique is more sensitive than the transmission technique by a factor approximately equal to the ratio of the size thickness of the specimen to the length of the inspection volume V_i . This can be a very large factor indeed.

CONCEPTUAL DESCRIPTION OF TECHNIQUE IMPLEMENTATION

Conceptually, a complete scan of the part is accomplished by rotating it about

an appropriate axis, translating it along a line parallel to the interrogating beam such that the scattering detector scans it from the OD to the center, and moving it up or down. The volume inspected during one revolution is a concentric annular ring with a cross-sectional area equal to that of the inspection volume element. The data are recorded as the number of gamma rays which are scattered into the detector from each inspection volume element in this annular ring, along with the three-dimensional information defining the location of that inspection volume element, viz., the angular location of the volume element, its radial distance from the center (or detector columnator position, and its vertical distance from a reference point at the base of the shell.

After one complete revolution, the part is moved horizontally by a discrete amount, depending on the size of the inspection volume element, and the process is repeated to scan another annular region at a different radius. The part is stepped in incremental amounts with each revolution, until the entire distance from OD to center has been traversed. At this point, the inspection of a thin disc whose thickness corresponds to the height of the inspection volume element is complete, and data from every volume element making up this slice is recorded, along with the three-dimensional position information. Next, the part is moved vertically by an amount corresponding to the height of the inspection volume element, and inspection of the adjacent disc begins.

The three-dimensional data array is subsequently analyzed for variations in the number of counts per data point that may indicate statistically meaningful deviations of material density as a result of defects. These deviations are then quantitatively analyzed for their magnitude, and correlated with statistically significant deviations in neighboring data points to define the size, shape, and orientation of the defects.

The photon-scattering gauge is thus seen to be an inspection device which provides a high-resolution, three-dimensional scan profile of the entire part. It performs a differential measurement which, with an appropriately small inspection volume element, not only identifies the presence of discontinuities (such as voids, cracks, and inclusions), but also provides data about their size, three-dimensional location and orientation.

Experimental Arrangement

IRT assembled a conceptual model of the scattering gauge to demonstrate the capability of the photon-scattering technique.

In Figure 76 is shown in a schematic representation of a photon scattering rig. It consists of four major sub-assemblies: the Co^{60} isotopic source with shield and collimator, the photon-scattering detector with associated shield and collimator, the

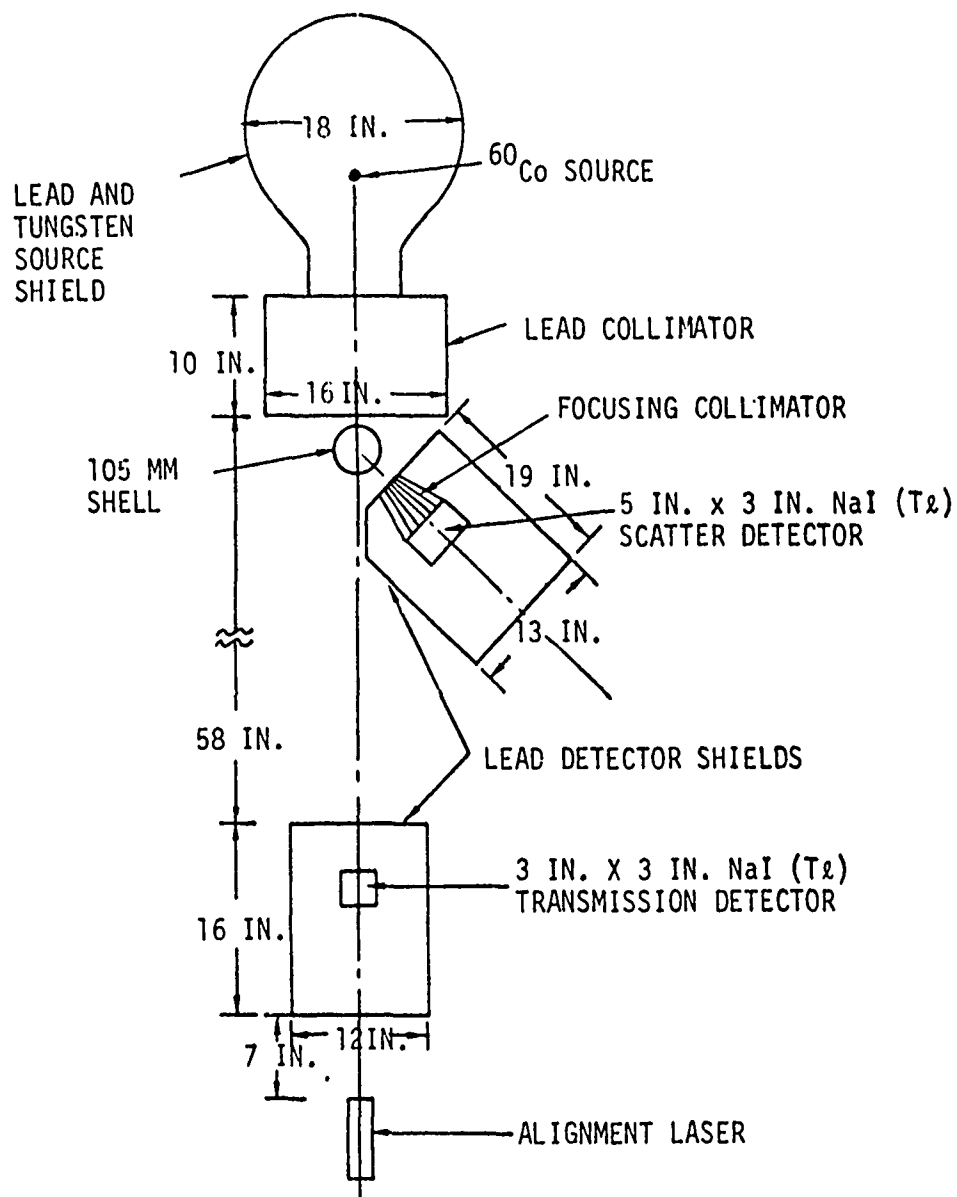


Figure 76: Schematic Representation Of Geometrical Arrangement Used For The Conceptual Model. Rene' 95 Disk Was Placed In The Location Of The Shell For The Evaluation For This Contract.

associated electronic data acquisition instrumentation, and the mechanical scanning device allowing inspection of the entire volume of the specimen.

Isotopic Source Assembly

Co ⁶⁰ is an isotopic source widely utilized in industrial and medical applications as a gamma-ray emitter because of a number of favorable characteristics. Every disintegration results in the emission of two energetic gamma rays at 1170 and 1332 keV. Its half-life is relatively long at 5.24 years, resulting in a theoretical specific activity of 818 Ci/g (curies per gram). High intensity teletherapy sources with specific activities of up to 400 Ci/g are commercially available (about 50% of theoretical maximum intensity).

Source Collimator

The source is surrounded by a thick lead shield in which is placed a small hole that acts as a collimator. The efficiency of the collimator in eliminating unwanted diffused radiation is increased by increased length of the collimator. Since radiation passing through a given diameter hole varies as the square of the distance of that hole from the source, collimators should be near sources. Using similar reasoning, the part being inspected should be as close as possible to the source collimator and the interrogating collimators should also be as close as possible. The interrogating collimators should be numerous, small in diameter and cover as much of the spherical envelop around the inspection volume as practical. All of these factors should be optimized for the particular size and shape being inspected for maximum cost effectiveness.

Photon - Scattering Detector

The photon-scattering detector consists of a NaI (TI) scintillation detector, a collimator, and a cylindrical lead shield, as shown in Figure . All components are arranged axial to the axis of the detector. The axis of the detector assembly was placed at a 45° angle relative to the direction of the source beam for this particular experiment.

Sample Scanning Device

The time and funds available did not permit a construction of an optimum sample manipulator. Rather a simple saddle was constructed with provisions for rotation and translation of the sample with relation to the focal point of the scattering detector. Inspection involves rotation and translation of the sample so that all volume elements pass through the focus of the system. This is to be done rapidly and automatically. When manipulating by hand, the accuracy of sample movement is degraded and times for inspection are sacrificed.

Thus for the evaluation of the holes in sample S3, only the inspection of hole #10 represented near optimum orientation of detector focus and hole location.

A total of 11 holes were examined on sample S3. These were numbers 1, 5, 6, 10, 12, 14, 17, 26, 29, 30 and 32.

Inspection Procedures

The response to each hole was measured by following the same basic sequence of steps. First, the sample was placed on its side on the saddle shaped holding fixture described earlier. Secondly, a determination was made of a suitable angle of the sample relative to the radiation beam. Thirdly, the horizontal and vertical positions of the sample relative to the beam and focal point were selected such that the focal point fell directly at the location of the hole. Finally, five one-minute counting periods were conducted at this location as well as at locations to the left and right of the hole, rotating the sample on its stand. Typically, the stepwise rotational motion was performed in steps registering 1/8 inch on the circumference of the sample.

This process was rather time consuming since it frequently involved several trial runs to find a reasonably suitable sample orientation for the inspection of a particular hole. This somewhat cumbersome procedure was necessary only because the geometry of the existing Photon Scattering Gauge, which has been tailored for a different inspection task, did not provide for efficient placement and inspection of the sample which would have required placing the sample either horizontally or vertically on a motor driven shaft to permit a more automated scan procedure than the one improvised for this study. As it was, the scanning operation had to be completely conducted by hand with the experimenter manually setting the sample for each data point.

As a result of time limitations not all holes could be scanned with the same thorough pre-scan positioning preparations. Instead, special attention was paid to holes 5 and 10. While a series of three measurements for hole 5 was made to demonstrate how the technique provides unambiguous data about the size of a hole, a special effort was expended on hole 10 to place the sample relative to the beam in such a way that the focal point truly fell on the defect as the sample was scanned, thereby maximizing the response. Therefore, only hole 10 can be used for quantitative statements about the resolution capabilities of the system. The remaining measurements primarily serve to demonstrate that defects are discernible over the range of different sizes and locations.

It should be noted that any of these positioning considerations only apply in this special case of a feasibility study with equipment designed to address only the basic measurement parameters and not any operational aspects. Importantly, in a gauge designed for routine inspection of certain components, a motorized scan control system would conduct a full scan sequence, automatically positioning every volume element of the sample to the inspection point. There would be no need for searching for the best orientation of defining the presence of a defect with the least number of data points, as was the case in this study. The complete data set would automatically contain complete information, within system resolution limits, about any defect in the part.

Inspection Results

The inspection results are shown in Figures 77 through 80. For each hole, the response is displayed as the average number of counts per minute from the total of five one-minute runs, as a function of the position of the focal point relative to the hole. The data points reflect the total number of detector counts per minute at each position of the inspection volume element, without any correction for contributions from background or secondary scattering radiations. Even though such a correction would increase the magnitude of the fractional response deflection due to a hole, it would not in any way improve the statistical precision of the measured deflection. In other words, if the magnitude of the deflection is expressed in terms of the number of standard deviations of the data points, there is no improvement for the case of the corrected net response.

Also displayed with the response to each hole is a schematic representation of the sample orientation selected for the measurement.

Studying the gauge response to each hole in some detail, it is apparent from Figure that the presence of hole 1 is clearly discernible. The pronounced slope in the non-defect part of the response is thought to be due to the fact that sample S3 was not rotated in a regular manner with relation to the beam. The resulting effect on the measurement was that the upper edge of the sample experienced a slight vertical displacement as the sample was rotated. This vertical change caused a slight variation to take place in the length of travel through the sample of the exiting beam on its way to the detector. This, in turn, resulted in a change of absorption experienced by the exiting beam. The fact remains, however, that despite this change in sample position the hole is clearly discernible as a highly localized response deflection.

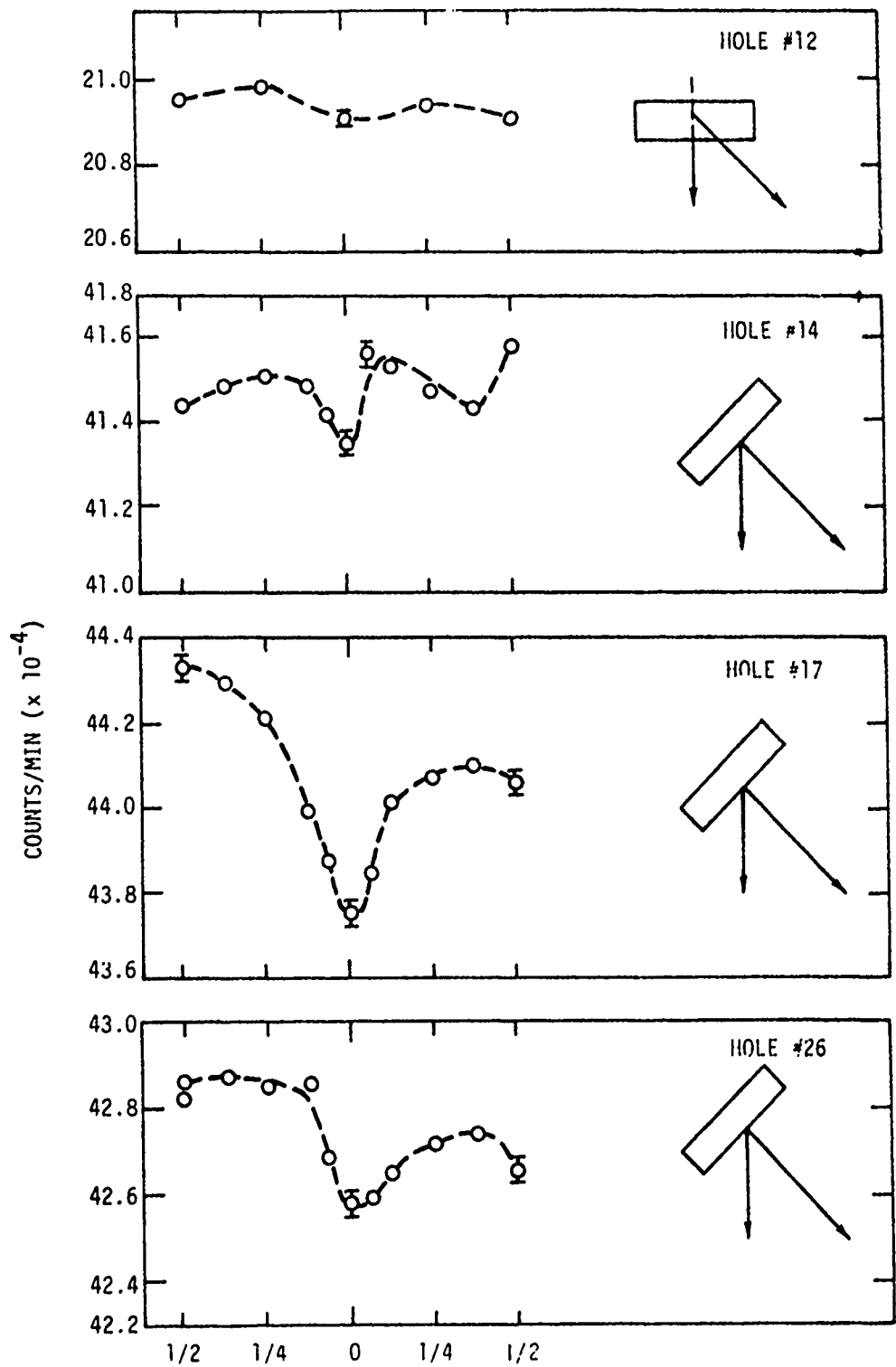


Figure 77: Photon Scattering Measurements of S3

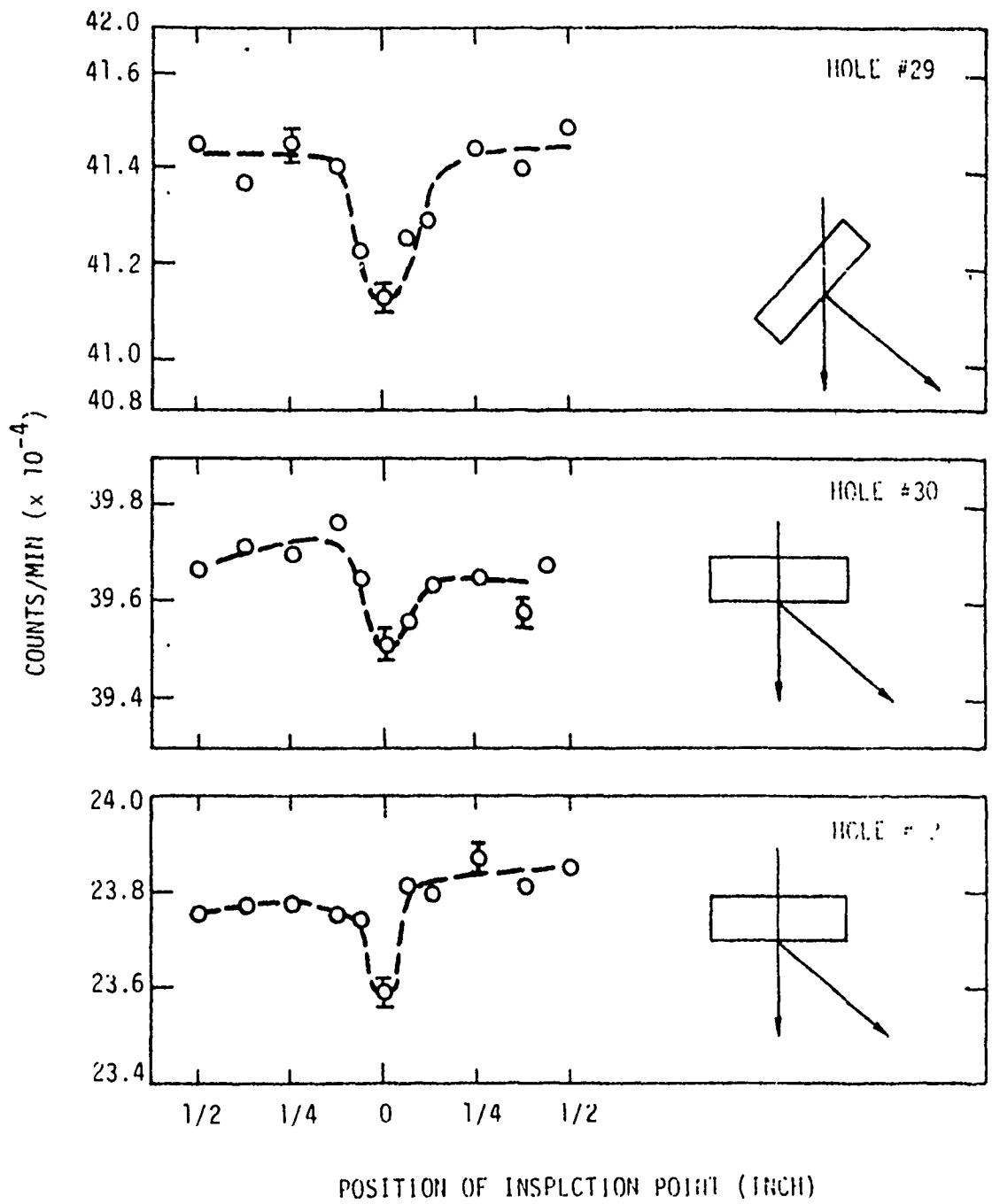


Figure 78: Photon Scattering Measurements of S3

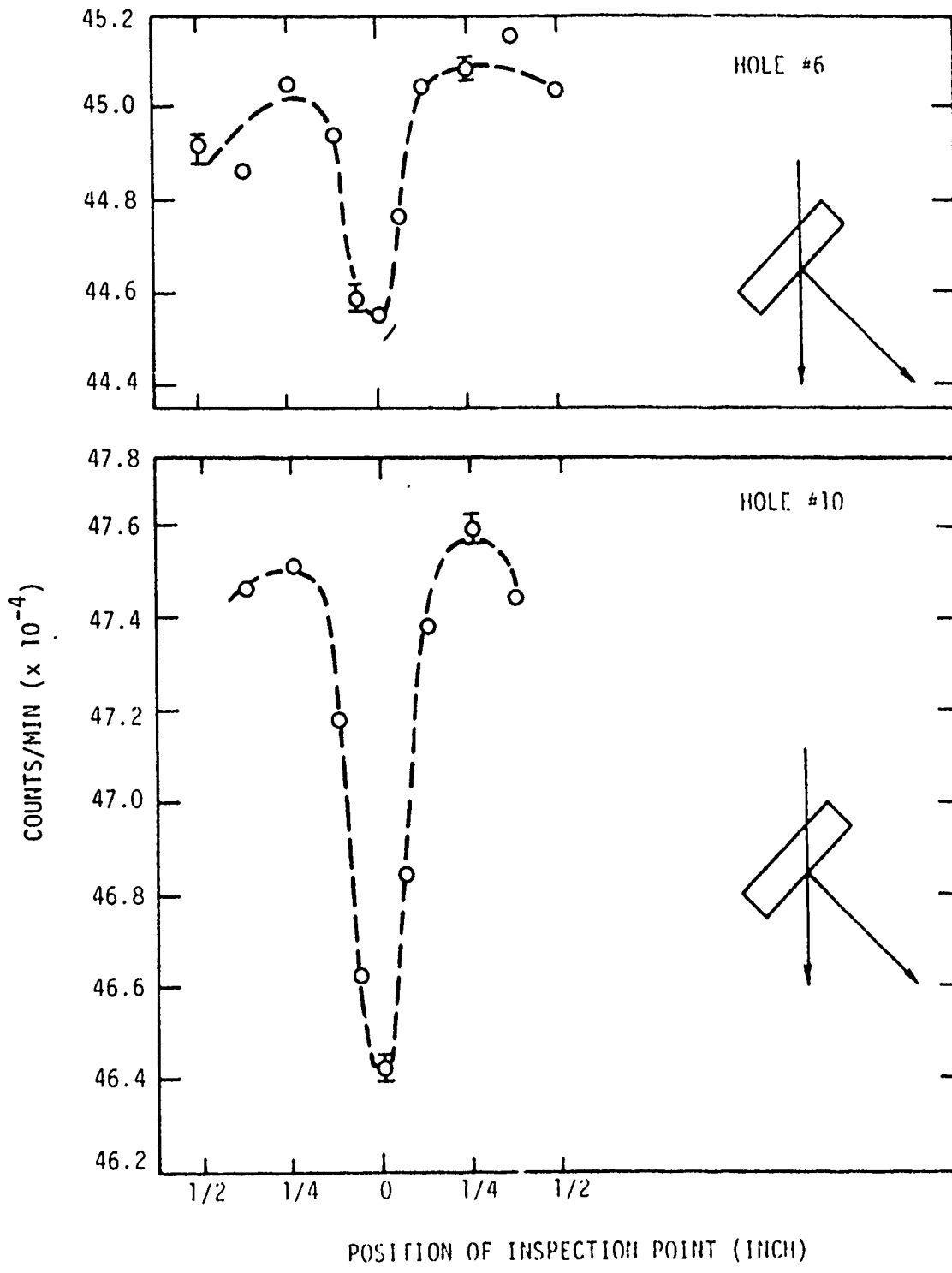


Figure 79: Photon Scattering Measurements of S3

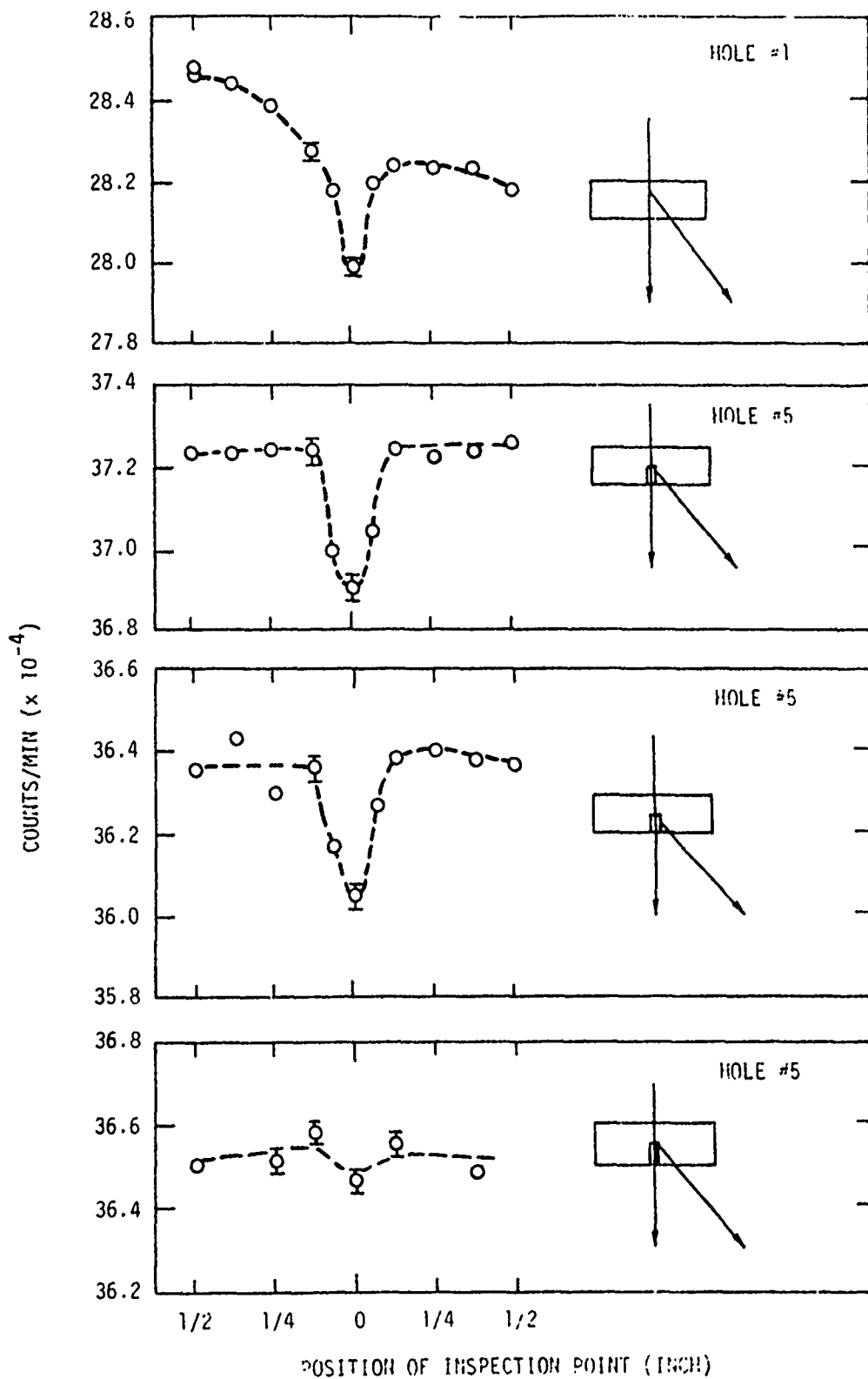


Figure 80: Photon Scattering Measurements of S3

The response to hole 5 was measured in three different places; 0.25 inch, 0.375 inch and 0.500 inch from the surface. As expected, there is no noticeable difference between the first two responses since the hole clearly extends through the inspection volume element in both cases. In the third case, however, the response deflection is greatly reduced, indicating that the inspection point is near the end of the hole. Since the coordinates for any inspection point are uniquely defined with production inspection procedures, the latter measurement pinpoints the location of the bottom of the hole. In a complete scan, in which data for the entire sample is available, the size, direction, and location of any defect are thus defined.

The response to hole 6 is quite pronounced. It also shows the edge deflection effect seen in the case of hole 1.

Hole 10 provides a clear example of how well the response to the holes can be defined if the data is taken in such a manner that the inspection point is moved right through the hole. As stated earlier, considerable effort was expended under the constraints imposed by the available equipment to optimize the response to hole 10. Since hole 10 is of the same size relative to the inspection volume element as holes 1 and 5, the response of the latter could be optimized to the same magnitude of deflection.

The response to hole 12 was not optimized since it was nearly impossible to physically locate the sample within the geometric system confines in an appropriate measurement position.

The responses to the remaining holes, 14, 17, 26, 29, 30, and 32, all clearly show the presence of the hole. They are usually also subject to the edge effect.

DISCUSSION OF RESULTS

All holes are clearly discernible in the gauge response. The smallest hole inspected is 14 with a clearly recognizable response deflection. It has about 1/3 the volume of 12 but was measured with a stronger response. This is further evidence of the fact that the sample could not be properly positioned for the scan of 12.

From a quantitative point of view the response of hole 10 is analyzed since this is the only response which is close to demonstrating the true potential of the technique. Hole 10 was selected on a completely random basis. There are no geometric considerations favoring it over any of the other defects, except 12. The measured, uncorrected response of 10 shows a deflection of 2.2%, corresponding to 15 standard deviations, comparing very favorably to the theoretical prediction

of 5% based on the ratio of void to inspection volumes. This demonstrates that the total response is not overly affected by background and secondary effects, thus easily lending itself to parametric projection. It also indicates that a 0.6% deflection would be clearly discernible as a 4-sigma deviation from the average response. It would correspond to a hole with a 0.016 inch diameter and a length of at least 0.125 inch. Yet hole 14 is only .007 in diameter and yields a solid defect indication.

If even smaller holes are to be detected the inspection volume element must be reduced in size. For example, a halving of the length, width, and height of the inspection volume element would result in a volume reduction by a factor 8, which translates into an increase in resolution capability by a factor 8. In other words, continuing the discussion of the previous paragraph, a hole with half the volume of hole 14 would require a smaller inspection volume for reliable identification.

It would be feasible to reduce the volume size of the inspection volume element by another factor 4 to 8, increasing resolution capability by roughly the same amount. Whether further reduction could be realized is not quite certain at this time. A study would have to determine if secondary scattering effects did not tend to put a practical lower limit to the amount of resolution that could be achieved. Such an improvement in resolution would of course result in a commensurate increase in the number of data points that describe a given sample and, therefore, an increase in inspection time. The latter can be compensated to a degree by the selection of more intense radiation sources.

The Photon Scattering Gauge results clearly indicate the power of this technique. The defects are discernible roughly within the theoretical prediction and a parametric projection showed that the resolution can be improved.

To further explore the feasibility of the projected resolution improvement it is important to consider count rates and inspection times. A detailed quantitative parametric analysis in report INTEL-RT 6115-001, prepared under contract DAAG46-76-C-0019 for the U.S. Army Materials and Mechanics Research Center⁵, demonstrated that the feasibility demonstration unit could be projected into an optimized gauge with a total detector improvement factor of 1.5×10^4 . In other words, the improved system would have a total combined count rate from an improved detector arrangement which was estimated to be 1.5×10^4 higher than the one achieved with the testbed. A further improvement of a factor 2.4, as described in the above report, is achieved by suitable three-dimensional data smoothing which improves the statistical significance of the data. The proprietary discussion related to the improvement factors is given in appendix iii. In order to provide a quantitative framework for a projection of the potential of the Photon Scattering Gauge for the flaw inspection of HIP components, it was assumed

5 - See Bibliography

that the model underlying the referenced projection identically applies to this case. This assumption should be reasonable since the referenced system has been used for measurements on a HIP sample. However, the space requirements of the HIP samples might be quite different from those of the 105 mm projectile sample used for the referenced report.

The combined improvement factor of $2.4 \times 1.5 \times 10^4 = 3.6 \times 10^4$ means that the total scan time of 5 minutes for the inspection of each hole would be reduced to 8.3 milliseconds. As mentioned earlier, the size of the inspection volume element for these measurements was 0.002 cubic inch, resulting in an estimated 50,000 data points for a complete scan of a T700 disk with about 100 cubic inches of material. With a measurement time of 8.3 milliseconds per data point a total scan time of 6.9 minutes would result.

If this hypothetical, improved system, which would have resolution characteristics identical to the ones applying to the test measurements, were altered by reducing the size of the inspection volume element by a factor 4 and keeping all other parameters unchanged, the following measurement time projection results.

- a) A reduction of the inspection volume element by a factor 4 results in 4 times as many inspection points. The total inspection time becomes 4 times longer.
- b) In order to reduce the size of the inspection volume element, the collimator dimensions have to be altered. This results in a total estimated effect of a decrease of the available count rate by a factor 4.

The total penalty is thus a factor of $4 \times 4 = 16$. This means that the total inspection time will grow from 6.9 minutes to 1.8 hours.

In such an optimization, use would be made of the fact that a HIP sample similar to S3 is of rather compact size and shape. An S3 type sample could practically be surrounded by a collimator-detector arrangement for about one half of the available sphere of scattered photons and this half in the more forward direction.

It is important to note that a system optimized for the inspection of HIP samples would more fully utilize the source radiation than the present system by placing one inspection station on either side of the source, rather than just on one. This factor was not included in the above projection. In other words, in terms of the most expensive component of a photon scattering gauge, the intense radiation source, another factor of two improvement is realized. Further improvements may well be realized if maximum advantage is taken of the geometric char-

acteristics of HIP samples.

On the basis of the positive results of the measurements conducted under the subject report and the fact that a quantitative, parametric projection to an optimized inspection system for HIP samples indicates that such a system appears to be feasible from a technical point of view, it is recommended that such a system be developed as a fully automated high resolution inspection device. The photon scattering technique naturally lends itself to automation since it routinely provides a data set in which the density of every inspection point is uniquely correlated with its three dimensional coordinates. Thus, the data analysis needs to be merely concerned with a direct evaluation of the density data and not with a sophisticated tomographic type analysis as required for all conventional transmission type inspection techniques.

RADIOGRAPHIC TOMOGRAPHY

Introduction

Radiographic tomography was evaluated as an NDE process for rotating turbine hardware and was found to offer no promise. The process and brief experimentation is described below.

The "Dynatome" System for continuous dynamic X-ray film tomography was created by CFC Products, Inc. and is marketed through Medicom for medical and industrial applications. While applications engineering for medical uses is essentially complete, the engineering for industrial uses has just begun. Primary technical problems being solved center around the wide range of X-ray absorptions involved and the special high resolution sought from industrial X-ray films. This project is a small effort to focus specific engineering studies on the tomographic imaging of reference holes or oxide inclusions contained in thick-section Rene' 95 powder metallurgy T700 engine disks.

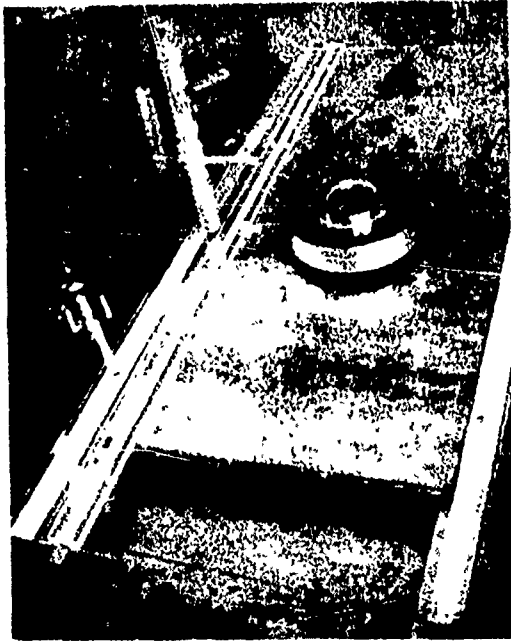
Description Of The Process

"Tomo" means "thin slice" and for X-ray film imaging purposes this refers to a thin plane of focus or image "slice" orthogonal to the path direction of X-ray beam travel.* "Dynatome" dynamic tomography uses silver halide emulsion film as the image producing medium and the geometrical/mechanical manipulation of three subsystems; exposure table, film parallelogram trimmer, and film-sliding viewer, Figures 81, 82, and 83. The observer is able to operate the film viewer to see the entire three-dimensional volume of the object radiographed.

The three-dimensional image effect is obtained by taking a series of X-ray exposures at a number of angles as illustrated in Figure 81. These angles are selected by the radiographer to best accomplish the image presentation on the set of films taking into account section thicknesses, regions of interest, materials, and absorption coefficients. The focal spot of the X-ray generator must travel parallel to the film plane as each angle is set (not in an arc). Two vertical markers (dots) and a straight line marker provide the geometrical alignment information directly in the film image of each exposure.

Each film is trimmed to a parallelogram shape in the Dynatome trimming unit, Figure 82. The two vertical markers and the straight line are aligned with mechanical guides moved by the operator. This step establishes the proper angle

*Note: Not to be confused with "computer tomography" used in medicine where the X-ray beam is scanned around the head, and the image produced is a section view of the brain parallel to the X-ray beam travel path.



Sliding Table



X-Ray Machine

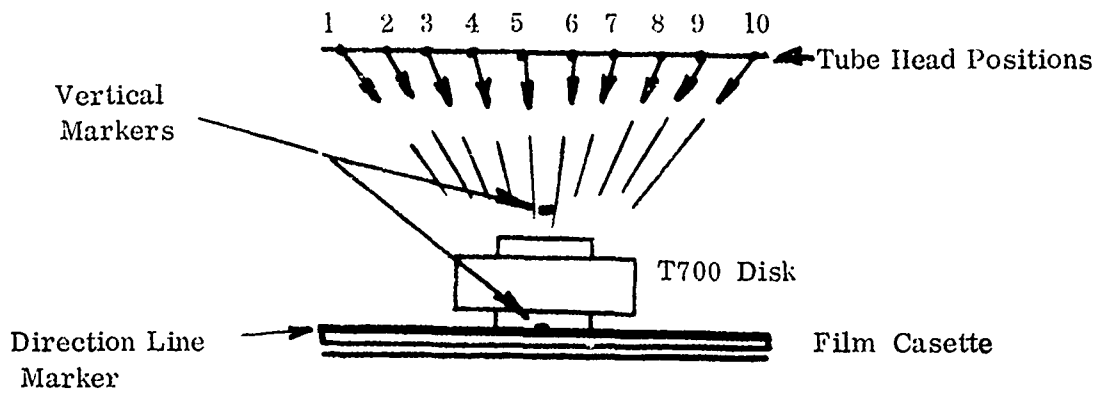
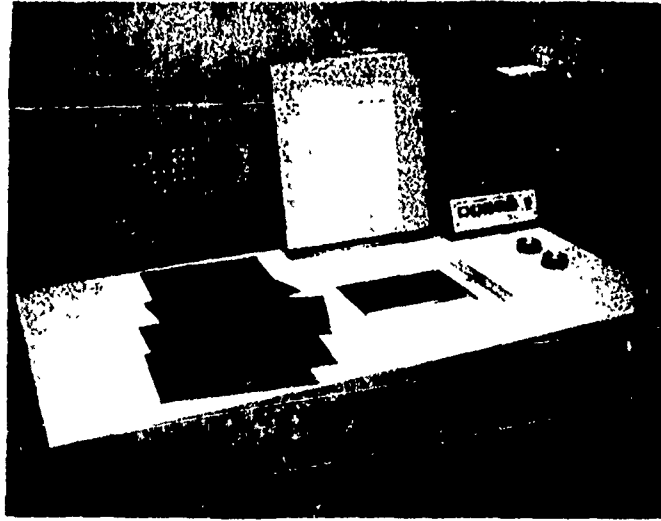
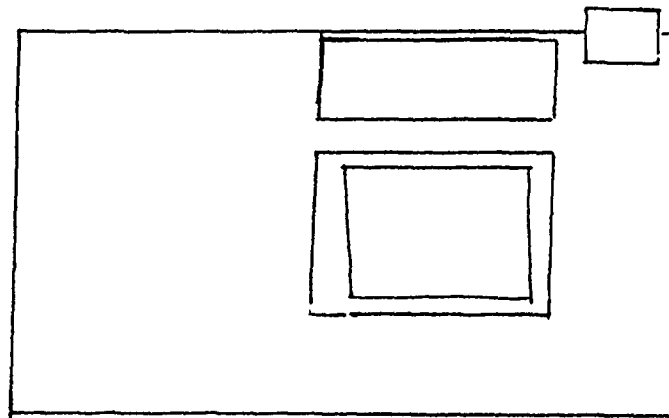


Figure 81: Exposure Table And Schematic Of Multiple Exposures For Tomography

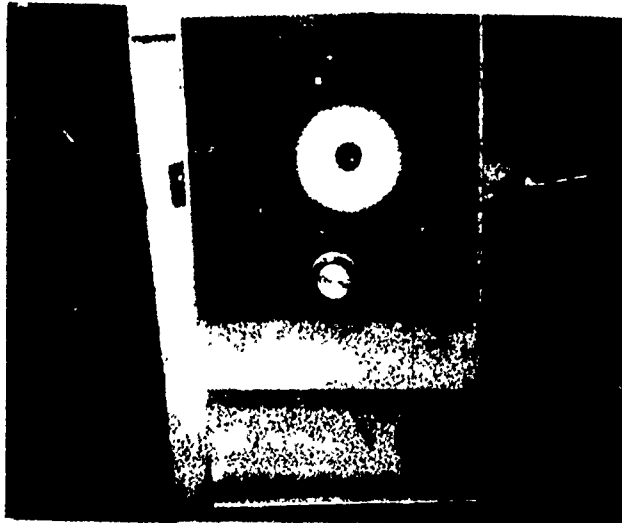


Picture of Trimmer

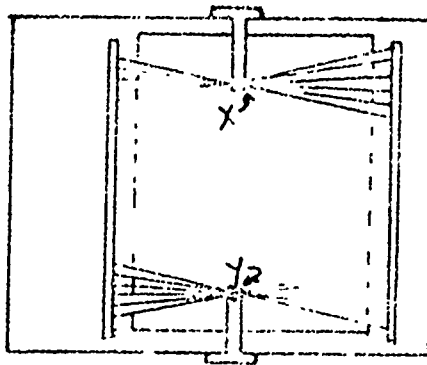


Trimmer Sub System
Unit Trims Film To A Parallelogram
With Reference To Two Marker Dots

Figure 82: Tomography Parallel Trimmer



Picture Of Viewer



Viewer Sub System
X-Y Mechanism Slides To
Rearrange Relative Position
Of Film Stock

Figure 83: Tomography Film Viewer

and spacing of the film cutters. Vacuum holds the film on a small pedestal while two stages of cutter wheels trim opposing edges. The film edge angles are proportionally related to the tubehead exposure angles, thereby building the necessary geometrical information directly into each film.

The parallelogram shaped films, thus produced, are stacked together and placed between the straight vertical edge guides and movable horizontal fingers of the Dynatome viewer, Figure 83. By moving the dial-controlled fingers left or right, the operator can move the apparent focal plane image smoothly through the entire volume of the object radiographed. The sequential order of each film in a film stack is of no general consequence, and the stack is usually assembled quite arbitrarily. Where helpful in viewing, one or more films may be removed from the stack.

X-Ray Exposure Conditions

Exposure conditions for industrial tomography applications thus far have been empirically obtained by referencing all images to results on Kodak single-emulsion R industrial X-ray film, using normal exposure procedures and film densities. Once satisfactory conditions have been established, rule-of-thumb ratios are used to set an appropriate exposure time for each film in a tomographic set using lithographic film.

Images in these films result from the interactions of X-rays, which pass through the engine part, with the silver halide salts in the film emulsion. Auxiliary intensifiers such as lead foil "screens" aid in this process. The amount of X-rays, measured in RADS, to create a given film density (darkness) is the exposure, and the actual quantity is also a function of the X-ray spectrum of energies actually hitting the film. In general, for a narrow range of exposure conditions, the "Exposure" is expressed as follows:

Exposure = \log_e (milliamps * time)
or more exactly:

Exposure = \log_e (radiation intensity * time)

This X-ray exposure is usually plotted versus optical density for a given film designation and associated image development chemistry schedule.

$$\text{LEAD } \mu = 10.7 \text{ CM}^{-1} \quad 1 = 11.34 \text{ grams/CM}^3$$

$$\text{RENE' 95 } \mu = 1.465 \text{ CM}^{-1} \quad 1 = 8.1926 \text{ grams/CM}^3$$

using the relationship:

$$d_{\text{lead}} = \left(\frac{\mu_{\text{R95}}}{\mu_{\text{Lead}}} \right) d_{\text{R95}}$$

$$d_{\text{lead}} = (1.465/10.7) (1.25)$$

$$d_{\text{lead}} = .171 \text{ inch}$$

A 1/8 inch thick sheet of lead was placed over the travel line and the lower marker. This proved satisfactory for marker imaging.

A study was conducted to learn an effective means for adjusting exposure conditions from one shot to the next in the technique evolution process. Starter exposures at $D = 2$ operate on the high slope (gamma) portion of the film curve above the "knee". Tomographic exposures at $D = 0.2$ operate on the low slope portion below the knee. However, the majority of gray tones occur across the knee. The distinctly different curves for industrial X-ray film further complicated the analysis.

Considerable development trial-and-error effort was expended relating single -R film exposure times at 310KV, 10MA for $D = 2$ (Time = 8 minutes) and MP4557 tomographic exposures at $D = 0.2$ processed through DuPont 42G machine chemicals at 4 inches per minute. Once this exposure time range had been bracketed (Time = 1 to 6 minutes), the calculation of refined time settings was begun. First trial used the simple ratio of the gamma curve expression.

$$\frac{D_1}{D_2} = \frac{\ln(\text{Time } 1)}{\ln(\text{Time } 2)}$$

which gave obviously long exposure times for reasonably small changes in density. The second trial used an empirical, straight-line approach where film-base density (D_0) was accounted for:

$$\frac{D_1 - D_0}{D_2 - D_0} = \frac{\text{Time } 1}{\text{Time } 2}$$

This relationship proved very satisfactory for small adjustments in optical density over the range $D = 0.10$ to $D = 0.50$ with the MP4557 film, whose base density was $D_0 = 0.06$ (clear). Similar success was had with the SR-54 film, whose base density was $D_0 = 0.16$ (blue), over the image density range $D = 0.20$ to 0.80 .

Film Considerations

CFC Products, Incorporated and Medicom have pursued the need for a water-clear plastic film base for the purposes of medical and industrial tomography.

The medical case was solved by a special arrangement with Kodak to produce a medical-appropriate emulsion on a 7-mil thick clear base. An industry-appropriate emulsion (single or double) on clear base film has not yet been accomplished although initial inquiries by Medicom have been made. In the interim period, they have identified one lithographic film, single emulsion on a 7-mil clear base, which meets the general requirements of industrial X-ray tomography. This is Kodak MP Lithographic Film 4557. Using the companion Kodak MP chemicals, an Exposure vs. Density curve typical for this film is presented in Figure 84. The sharp "knee" of the curve represents a rapid change from clear to black with a small change in exposure (light) which is ideal for lithography. The typical curve for Kodak single R film is shown in Figure for comparison. Note the soft "knee" or broad gray-tone range with change in exposure (X-ray). The two curves are separated horizontally in proportion to their relative "speed", with "slow" MP film being to the right (longer exposure for equivalent black). Note that single-R is the slowest industrial X-ray film, yet is markedly faster than MP film when both are exposed to X-rays. Most industrial radiography uses double emulsion film to reduce exposure time and cost (1/2).

A separate image on each film, related to the angle of X-ray beam passage through the object is the primary data obtained. Experience has taught that 10 separate film images, provides the best balance between defect resolution and quantity of light transferred through a stack of such films. The process works with as few as two films and as many as 15. The average blackening or optical Density (\bar{D}),

$$\begin{aligned} D &= \log_{10} \left(\frac{1}{T} \right) \\ T &= T_1/T_0 \\ T_0 &= \text{Incident light from film viewer box} \\ T_1 &= \text{Light reaching the observer's eye} \end{aligned}$$

on each film (D_1) in the region of interest is essentially derived from a suitable viewing total density $D_T = 1.5$ to 3 (with best visual acuity between $D_T = 2$ to 2.5) divided by the number of films in the stack (n).

$$D_1 = D_T / n$$

Therefore, one individual film from a stack of 10 films, where $D_T = 2.5$, would exhibit a $D_1 = 0.25$, and appear to be considerably underexposed to the casual observer. The additive effect of all 10 films, as they are coordinated geo-

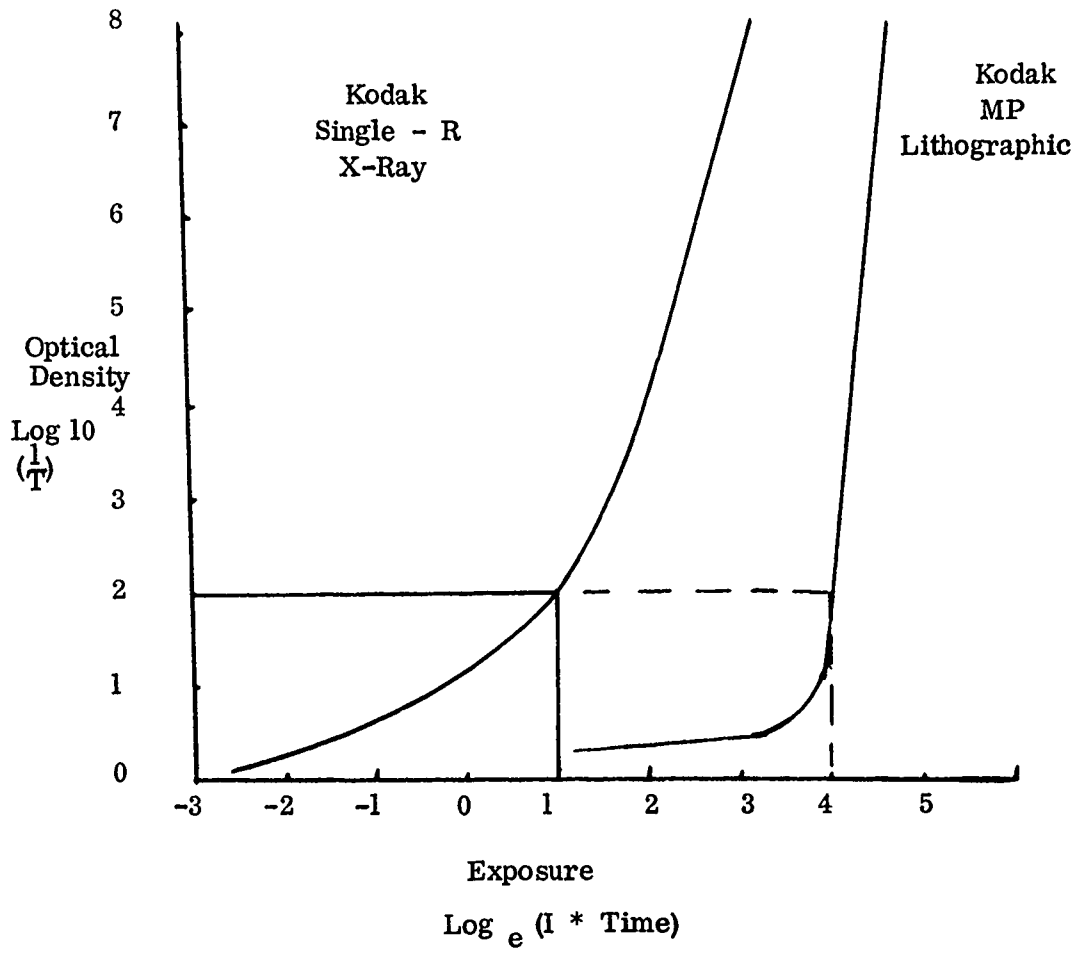


Figure 84: Density Vs. Exposure Curve Comparison

metrically by the Dynatome viewer, is the image of the focal plane selected by the observer at the familiar $D = 2.5$.

The portion of the object thickness in focus at any given relative orientation of the film stack is claimed to be 2 mm. That portion of the object out of focus contributes to overall graying without, (according to claims) appreciably effecting intensity and resolution of the region in focus. Thus, if the X-ray exposure is capable of 1% sensitivity and the object thickness is one inch, a conventional X-ray could identify a defect .010 inch in size. A Tomographic exposure would reveal 1% of 2 mm or about .001 inch defect. However, graying of the film stack by those areas out of focus is almost certain to reduce capabilities to some intermediate defect size.

Three phenomena are claimed to improve detection of defects. First, is the focal plane thickness:

$$\% \text{ Sensitivity} = \frac{\text{Defect height dimension}}{2 \text{ millimeters}} \times 100 *$$

where the 2 millimeters is usually much smaller than engine part section thickness. Second, the lithographic film is a high contrast imaging medium which provides a natural enhancement in each film of the set. Third, the stack of films add in Density which further enhances defect indication contrast. The first and third claim are closely related.

* (assuming no degradation by graying of film by out-of-material focus)

Equipment

The following equipment was used in this project for evaluation of dynamic X-ray film tomography:

- T700 Reference Standard Disk S-3
- Picker 310KV X-ray Generator
- Jib Crane for vertical and horizontal motion
- Exposure table frame
- Film cassette tray and marker subsystem
(special unit supplied by Medicom) - Figure 81
- Automatic Film Processor
- Dynatome Shaper - Figure 82
- Dynatome Viewer - Figure 83

Procedure

The following procedure was used to produce individual radiographs and tomographic sets:

1. Place S 3 on cassette tray with axial holes opening to surface toward film.
2. Adjust upper vertical marker to 4 inch position.
3. Cover upper and lower vertical markers and edge line with enough lead sheet to match X-ray absorption through engine part section of interest.
4. Adjust X-ray tubehead to O, X position. (In the Picker system O scales and illuminated crosshair reference lines were provided in the frame to establish position).

TABLE OF ANGLES USED

S = 0

TABLE VIII

F = 40 inches

<u>O degrees</u>	<u>P inches</u>
20	14.56
16	11.47
12	8.50
7	4.91
2.5	1.75
-2.5	-1.75
-7	-4.91
-12	-8.50
-16	-11.47
-20	-14.56

5. Load film cassettes in total darkness for MP film (X-ray film safelights are not suitable).
6. Perform exposures at 310 KV, 10 MA for desired time.
7. Process, develop, fix, rinse, dry film.
8. Place film emulsion down on shaper platform.
9. Align direction-of-travel line and two vertical-marker pinholes.
10. Apply vacuum and assure exact alignments
11. Cut film
12. Reset machine and remove parallelogram

13. Repeat shaping for all films in a set
14. Assemble the set of films in a stack (the order of each film is arbitrary).
15. Place film set in guide slots and between guide fingers of Dynatome viewer.
16. Turn on viewer, rotate control knob, and search for defect indications.

Results

Installation of the "Dynatome" dynamic X-Ray Tomography equipment in the Visual NDE Systems Laboratory was completed November 24, 1975, and Medicom's specifications for geometric accuracy were met using the existing X-Ray generator and boom. Initial exposure trials established that maximum X-Ray output (310KV, 10MA) was required to penetrate the 1-1/4 inches of Rene' 95, and prove the adequacy of the exposure procedure. It was soon discovered that success in this project was controlled by film emulsion/development chemistry/processor machine conditions associated with the clear-base Kodak MP lithographic film (slow, high contrast using standard processing relative to Kodak single -R X-Ray film which has a blue-tint base) recommended for Dynatome. In-house processing proved inadequate, and outside inquiries resulted in a smooth gratis relationship with Bell and Hortenstine, a top Cincinnati color lithography house. In fact, their production manager recommended running the Kodak MP film through his DuPont chemistry-processor set for broadest gray range, resulting in lithographic film speed and gray tone behavior very close to single -R film, giving economical 4-minute per film X-Ray exposure times, rather than 60 minutes per film as with standard processing.

Because Medicom had never encountered film/chemistry problems, they had never explored this avenue, and, as a result of our studies, the use of MP film for thick-section industrial X-Ray tomography has been significantly advanced.

Once this technology barrier had been overcome, we were able to make valuable use of Dr. Gary Cochran's expertise (President of CFC Products, Inventor, and Consultant on this project). A total of 126 exposures were completed during these studies. The long exposure times associated with the Rene' 95 S-3 disk, 1 to 60 minutes as compared with a few seconds in medical exposures, at much higher energy and intensity (310KV, 10MA) caused difficulties in imaging the upper and lower markers and travel line. To solve this problem, linear absorption coefficient (μ) values were calculated for lead and Rene' 95 at 200 keV (peak intensity for 310KV setting on X-ray generator). These were combined to calculate the equivalent thickness of lead for 1.25 inches of Rene' 95.

The most successful ten-film tomographic set on MP4557 film was produced with a 4 minute exposure time and the DuPont 42G processor. The cassette was loaded emulsion side down between 5 mil (top) and 10 mil (bottom) lead screens. Depth-position of the side-drilled holes imaged and the end position of the axially-drilled holes imaged was readily observable, and measurable using a drawn scale along the upper guide finger on the viewer. Table I lists the holes observable in the 10-film tomographic set of MP4557.

The most clearly defined hole images were produced on single-R film SR54 using a 5 minute exposure and all other exposure conditions same as above. Individual-film images were purposely dark $D \approx 0.8$ for best hole/background contrast. Under these conditions of dark films with blue base only two or three films could be stacked for observation on the viewer at one time. The better contrast and additive effect of image coincidence aided in resolving hole no. 29. The soft "knee" of SR54 film resulted in a much narrower band of "undercut" blackening around the edge of the disk cylinder image, allowing holes 18 through 22 to be observed. The sharp "knee" of the lithographic film created almost 1/4 inch width of "undercut" blackening around the disk edge, and thereby obliterated the short (shallow depth) images of these holes.

The difficulties with MP4557 film exposure and processing emphasized the need for an industrial X-ray emulsion on clear-base material .007 inch thick before further evaluation of the Dynatome process could continue. Also, the basic question of image contrast and contrast enhancement was opened, because it was found that the hole must image on each individual film before the best images in a tomographic set could be obtained. For a relatively simple shape as the S 3 disk a single film offered essentially the same information as a two- or three-film tomographic set.

CONCLUSIONS AND RECOMMENDATIONS

Conclusions:

1. X-ray Film Tomography provides no real advantage for the inspection of regular cylinders such as the T700 turbine disk.
2. Lithographic film such as Kodak MP4557 is unsatisfactory for industrial X-ray Film Tomography applications at GE/AEG, due to processing and exposure control.

TABLE IX
DESCRIPTION OF S 3 DISK AND RESULTS OF INSPECTION

Hole	Diam. (mils)	Depth (mils)				Angle (degrees)	Observable	
			x *	y *	z *		4557	SR54
1	29	500	---	---	---	(Ref.) 0	Yes	Yes
2	29	500	---	260	---	17	Yes	Yes
3	29	500	---	375	---	39	Yes	Yes
4	30	500	---	500	---	60	Yes	Yes
5	29	500	---	620	---	78	Yes	Yes
6	38	100	490	---	---	5	Yes	Yes
7	31	300	490	---	---	27	Yes	Yes
8	31	500	470	---	---	49	Yes	Yes
9	30	700	405	---	---	70	Yes	Yes
10	29	890	508	---	---	90	Yes	Yes
11	27	25	---	---	150	45	N/A	N/A
12	28	50	---	---	150	78	N/A	N/A
13	7	15	435	---	---	109	No	No
14	7	125	420	---	---	130	No	No
15	7	75	420	---	---	153	No	No
16	7	100	465	---	---	173	No	No
17	14	200	485	---	---	198	No	No
18	7	90	---	200	---	100	No	Yes
19	7	90	---	275	---	121	No	Yes
20	7	90	---	450	---	141	No	Yes
21	7	90	---	512	---	163	No	Yes
22	7	165	---	615	---	185	No	Yes
23	7	100	---	---	255	142	N/A	N/A
24	7	100	---	---	310	173	N/A	N/A
25	15	100	475	---	---	219	No	No
26	14	290	475	---	---	242	No	No
27	14	375	475	---	---	264	No	No
28	*	20	540	---	---	286	No	No
29	14	500	490	---	---	306	No	Yes
30	15	500	---	110	---	209	Yes	Yes
31	14	500	---	250	---	231	Yes	Yes
32	14	550	---	340	---	251	Yes	Yes
33	14	500	---	515	---	276	Yes	Yes
34	14	500	---	635	---	296	Yes	Yes
35	15	40	---	---	339	241	N/A	N/A
36	16	50	---	---	277	274	N/A	N/A

15 21

N/A - Not Attempted, Beyond exposure capacity of X-Ray Generator.

* - About .011 inch at bottom of hole and .030 inch at surface.

Recommendations:

1. Concentrate applications for X-ray Film Tomography on complex-shaped, solid or hollow engine parts, e.g. castings.
2. Combine an industrial X-ray emulsion with a 7-mil clear base in a non-standard run in order to provide a fine-grained controllable film for further development.

COMPARISON OF NDE PROCESSES

Radiographic Tomography and Neutron Radiography failed to offer any promise as an NDE process for rotating gas turbine hardware. The processes do not demonstrate capabilities equivalent to conventional production ultrasonics and thus do not warrant further consideration. The inspection times are also predicted to be greater than for ultrasonic inspection. All discussion which follows will concentrate on the promising processes.

A modified ultrasonic method using Holosonic equipment, acoustical holography and Compton scattering evaluation all showed promise in that equal or better sensitivity to defects are strongly indicated. In addition, the two latter processes are readily adaptable to fully automatic NDE and so offer cost effective processes.

Surface Defects

Cracked samples C1 and C2 were used in this program to evaluate inspection of surface defects. The standard production processes used today are conventional ultrasonic inspection using the shear mode and FPI (fluorescent penetrant inspection) to the G.E. specifications P3TF1 and P3TF3. The cracks in the samples were very tight which represents a problem in inspection.

With ultrasonic inspection, a well developed production inspection procedure includes shear wave analysis of the disk face from four directions (shear clockwise, counter-clockwise, radial out, and radial in). Yet the sensitivity of signal response to orientation was demonstrated with C1 in that only a portion of the crack was revealed using normal P3TF3 standards.

The maximum signal response occurs when the plane of the crack is perpendicular to the direction of ultrasonic wave propagation. As the angle between the wave direction and direction perpendicular to the plane of the crack increases, the signal response falls off sharply. One would normally expect a crack open to the surface to approximate an orientation perpendicular to the surface plane of the part. Thus a shear mode would more closely approximate the ideal perpendicular orientation. The failure to delineate the total crack by ultrasonics indicates a very great sensitivity to orientation and questionable reliability as an NDE process for surface defects. Use of ultrasonics for this type of defect could lull one into a false sense of security as to product reliability.

However, production FPI inspection also failed to reveal the total crack. It was necessary to go to an advanced method of FPI using ultra high penetrant solution with a hydrophilic remover and a non-aqueous developer. Thus, if we are to assume the possible presence of such tight cracks in Rene' 95 HIP'd

product, an improved FPI constitutes the minimum NDE process requirement.

The improved ultrasonic process using Holoson' equipment and acoustical holography both use transducers and have some sensitivity to orientation as described above. Experiments also revealed erratic results as typified by Figures 6 and 63. It seems reasonable to assign the same risk factor to these processes for surface crack evaluation as one would for conventional ultrasonics.

Two possible processes were not evaluated. Eddy current testing was not within the scope of this contract. Eddy current testing has been very effective in inspecting some types of surface cracks, primarily in service hardware with which service induced cracks occur in a predicted direction. When orientation is unknown, eddy current testing suffers from similar sensitivity dependency on orientation of propagating wave to the plane of the crack.

The second method not evaluated is Compton scattering. This NDE contract was modified late in the program to include a minimal survey effort using this scattering process. From the survey, a hole .007 inch in diameter was readily identified using an inspection volume approximating a 1/8" cube. The ratio of defect volume in this test to the inspection volume is 1/300. This ratio is the governing factor of sensitivity for Compton scattering. It has been projected that an inspection volume approximating a cube .05 inch on a side can be used in a cost effective surface inspection. A tight crack with a gap of approximately .0002 inch and effective area of .015 inch in diameter would have a void volume to inspection volume ratio of about 1/300 as above. Thus we could predict a sensitivity to surface cracks which would exceed any current process. It is noteworthy that the Compton scattering process would respond to such a defect solely on the basis of ratio of void size to inspection volume. Thus an inclusion or crack barely subcutaneous would be identified. Such a defect would be missed by FPI. Yet the effect on life of such a defect at the surface and just below the surface would be about the same. Both locations are predicted to reduce life more than the same size defect deep within the part. Using a similar analysis, the Compton scattering process would easily identify a surface or subsurface oxide about .005 inch in diameter. No other process would even project such capability close to the surface.

In summary, there are strong arguments for using the advanced FPI system described on page 28 on Rene' 95 turbine hardware. This is predicated on the possible existence of a tight heat treat quench crack similar to the example in disk C1.

Secondly, there is good justification for pursuing the Compton scattering method in that its predicted sensitivity would equal or better current NDE capability for detecting internal defects. It concurrently permits inspection of finished disks to assess presence of surface or barely subsurface defects in selected critical zones. This projection assumes sensitivity already demonstrated and inspection zone size linearly reduced 60% from the value used in current work. The risk of this projection should be low.

Non Metallic Inclusions

In the process of making metal powders, there is some erosion of sprue during the atomizing. Thus the amount of non metallic inclusions in powdered product exceeds that commonly found in cast plus wrought product. Although most of these inclusions are quite small, below .010 inch, two efforts are underway to assess and improve product quality. First, techniques are being developed to separate most non metallic particles from the powder. Secondly, work is underway to assess the effect of various non metallic inclusion morphologies on mechanical properties. In this latter effort, there is much difficulty in locating small defects and assessing size by correlating indications to actual defects. This correlation problem is inhibiting accurate evaluation of the effect on mechanical properties.

This same correlation difficulty interfered with attempts to evaluate sensitivity of these emerging NDE processes. Thus some of the sensitivity claims in the following comparisons are based on available evidence and some projections.

Consider the work of intensity mode ultrasound using Holosonic equipment as described in the section on page 53. All drilled holes, including .007 inch X .050 inch long, were easily identified by this process. The D1 and D2 specimen revealed many defects but the gain settings required were about ten times that used on the S series of samples. This indicates that many of the defects must have been smaller than the drilled holes. Remember most of the particles had passed through a 60 mesh screen indicating a .010 inch maximum diameter.

In the evaluation described on page 72, strong indications were obtained on disks having no questionable indications with the conventional ultrasonic process. When cut up evaluations were made, many .002 inch oxides were found but the maximum size was .004 inch. The cut up techniques used should have found larger defects if they were there. Thus, there is an indication that the NDE process identified small defects or maybe clusters of small defects located in an array too close to resolve. In the evaluation described on page 81, many more indications were found by Holosonic ultrasound than were noted with conventional ultrasonic inspection, thus there is strong evidence that defects smaller than .010

inch in size yielded bright response signals. However, more effort is required to calibrate equipment and correlate defect size using a more extensive cut up analysis.

This intensity mode Hologonics equipment, like the other emerging processes requires some modifications to make it more adaptable to production inspection. The recommended actions for this process include an increase in memory and conversion from analog to digital information processing. This will aid in equipment calibration in that more definitive signal response analysis will be possible. In the following discussion, these new processes are compared assuming the equipment modifications necessary to make them a production process.

Sensitivity

The sensitivity of intensity mode Hologonics ultrasound equals or exceeds the capabilities of conventional ultrasound. As discussed in the previous paragraphs one could claim an improvement in sensitivity, but, since difficulties have occurred in cut up analysis, these claims must be based on evidence, not proven fact. This same strong evidence can be applied to acoustical holography since the same basic signal is used. The only change between the Hologonics intensity mode and acoustical holography is that with the latter method the data is reprocessed making more use of the phase shift information to form a hologram. This reconstituted signal, using the holographic transmit mode, yields a comparable signal for the given defect size regardless of the location of the defect within the part. It is also less sensitive to shape and orientation. Conversely, conventional ultrasound will demonstrate a very great difference in signal response when viewing the end of a flat bottom versus round bottom drilled hole.

Compton scattering evaluation also indicates sensitivity equal to or better than conventional ultrasound. All such evaluations of this process must represent projections from very limited test data base. In the single series of tests made on a Rene' 95 disk with drilled holes, easy identification was made on a .007 inch diameter hole in an inspection volume described by the intersection of 1/8 inch diameter collimators.

This represents a ratio of defect/inspection volume of 1/300. By simple mathematics, factoring all known limitations of the process, the use of a smaller inspection volume (\cong .050 inch collimators) would make it possible to reliably inspect an inclusion .005 inch in diameter. This exceeds capabilities of conventional ultrasonics by a considerable margin. In actual practice one would use as large a collimator system as possible to minimize inspection time. Thus the collimator size would be determined on the basis of the smallest acceptable defect size.

So in the following analysis, it is assumed that these three emerging NDE processes equal and probably exceed sensitivity capability of conventional ultrasound. The risk in using this assumption appears low in light of the evidence, however, additional experimentation is required to fully substantiate these claims.

Now consider total product costs, assuming equal or better inspection capabilities when compared to current production ultrasonics. The base point for comparison assumes conventional ultrasonics and an ultrasonic envelope machined to obtained good surface quality and inspected by a series of normal and shear scans from various surfaces of the part. (Present procedure).

The intensity mode Holosonic process promises equivalent inspection with the use of fewer scans. This assumes the elimination of shear scans. These scans, with conventional ultrasonics, have two major values; they increase the chance of orienting the interrogating beam to the surface of a crack-like defect, and, the propagating wave length in shear is half that in the normal (perpendicular) scan so the beam behaves somewhat like a higher frequency signal. With conventional ultrasound equipment, 5 MHz is the approximate limit of frequency. Thus, one might claim that the signal behaves in shear similar to a 10 MHz signal. The higher frequency results in shorter wave length and so better resolution. But the Holosonic equipment can operate well above 10 MHz. Also, for HIP'd Rene' 95, any cracks would tend to be at the surface and such defects are identified better by improved FPI or possibly eddy current or Compton scattering methods. Thus if the equipment used can operate at 10 MHz and orientation is not important in the absence of sub surface cracks, normal scans alone could be used to interrogate the parts. This could reduce the number of scans required by an average factor of three or more.

There is one technique that could increase sensitivity of both conventional ultrasound and Holosonic intensity mode ultrasound. With both processes, the sensitivity near the depth of beam focus is better than a region in the sample well removed from the focus. The difference in sensitivity can be approximated by comparing the ratio of defect area to beam cone slice near and well removed from the focus. The difference can vary widely as a function of focus size and cone angle. However, this variable suggests a value to multiple pass gating a portion of the part depth as illustrated in Table γ but also adjusting the beam focus to the center of each slice. Although this is not a new concept, it appears to have limited use. The most probable reason is the proliferating of scans suggested by such a process. But, if the normal (perpendicular) scan were used at 10 + MHz and shear scans eliminated, such an inspection process warrants consideration.

When considering acoustical holography, the location of the defect to the depth of focus is of limited importance. Since the signal describing a given defect represents the combination of responses from several transducer scan locations, the integrated intensity from the same size defect in different locations appears to be the same. A signal at a given scan location from a defect near the focus may be stronger than one well removed but the number of scan locations contributing to the reconstructed hologram is fewer for the defect in the proximity of the beam focus. Thus it appears feasible to inspect a sample with acoustical holography by using a single scan. This scan could have a single or multiple transducers. The transducers could move in a radial direction while the part rotates continuously keeping an orientation normal to the surface and maintaining a uniform water path length. Using existing experimental transducer manipulators, the inspection of a T700 disk blank in a single sweep would require about 10 minutes. This assumes completely automatic inspection. The current equipment needs some revision to have this capability and these revisions are given in the following recommendations. See page 146 .

Due to the ability to inspect near the surface, as demonstrated in the work performed on this contract, no "inspection envelope" is required. If we allow normal machining tolerances of .060 inch, there appears to be no difficulty in inspecting within this framework.

Currently a HIP'd disk is machined after the can is removed to yield a rectilinear inspection envelope. In addition to the difficulty in inspecting near the surface, additional problems occur at the disjunctures of the surface with present inspection processes. If a single scan is used, there will be an advantage to using smooth curves joining regions of varying disk thickness. This eliminates the disjunctures that are difficult to inspect. These smooth contours are also easier to make with a HIP process. Thus less waste is anticipated by the reduction of the inspection envelope to the machining envelope requirement and by using a shape that parallels the shape most easily HIP'd. It may be possible to remove the processing HIP can and inspect after chemically treating the surface to insure removal of can material. This would save pre-inspection machining costs.

For the Compton-scattering process, the economics are directly related to the speed of inspection. Also, the sensitivity is directly proportional to the inspection volume defined by intersecting collimators.

Since the inspection time varies inversely as a power function of the inspection volume, clear delineation of acceptable limits of non metallic inclusions is necessary to avoid multiplying inspection costs needlessly. With the absence of such a defect limit at this time, some assumptions will be made in order to have a basis of comparing inspection costs. First consider the factors controlling inspection time.

The reduction of inspection volume by using one half the diameter of collimators is a factor of 8. Thus the scan time is increased 8 times to just traverse the volume. But, since the volume contributing to scattered radiation is reduced by a factor of 8, the time to sense a given number of photons (a measure of reliability) is increased by a factor of 8. So halving the diameter of collimators increases inspection time by a factor of 64 without more subtle considerations. Thickness of the part being inspected is also an important factor affecting inspection namely the absorption of X-ray energy as a function of metal thickness.

Assuming reliable inspection of a .016 inch diameter defect, the projected time to inspect a disk the size of the T700 is about 15 minutes. Extending this to .005 inch would increase inspection time to about 2 hours. This still could be satisfactory since it represents an automatic process and two parts could be inspected concurrently per radiation facility.

To summarize, again refer to Table V. It is assumed all three processes are capable of the sensitivity of conventional ultrasound. If we assume the current NDE is adequate, only costs are important. With such an assumption, the elimination of shear sweeps with intensity mode Holographic ultrasound could reduce inspection times by a factor of 3 or more. Acoustical holography, based on a single scan, has a predicted capability of a completely automatic inspection of a typical T700 disk in 15 minutes. With both of these processes, ease of interpretation is a real benefit. In addition accurate location of defects is readily obtained and this could save scrapping a disk in which there is a defect that would be removed by machining. With both processes, material savings could occur by eliminating the inspection envelope.

For Compton scattering and the same requirements as above, a 15 minute automatic inspection appears to be attainable. Again the inspection envelope could be eliminated. The process is probably the least sensitive to geometry. There is a practical limit to part thickness and this is probably less than 4 inches. Any part with a high percentage of the disk over 2 inches thick may require too much time.

The comparison can take new dimensions if we assume a requirement to inspect reliably to a smaller size defect than is now possible with conventional ultrasonic testing. With this assumption the three emerging processes have much more promise than seems possible with conventional ultrasound.

Probably the most fascinating projected capability of the Compton scattering process is the ability to inspect surface and near surface regions of critical zones of rotating parts. With life extension programs being emphasized, this offers an enticing new tool. Overhaul base inspection possibilities exist.

Future Possibilities

It appears that both acoustical holography and Compton scattering have a potential place in future NDE. Acoustical holography and Compton scattering both promise improved sensitivity, reliability and automation adaptability. Acoustical holography may excel for thick sections, large parts and simple shapes. The time to inspect would increase in proportion to the plan area. Contour following introduce complexity in data handling. The Compton scattering would tend to excel with more complex parts, smaller parts and inspection of surface and barely subsurface portions of finished components in regions of critical stress requirements. The time to inspect is proportional to the volume being inspected. Contour complexity introduces a minimum of programming to handle efficiently.

EQUIPMENT MODIFICATIONS FOR PRODUCTION CAPABILITY

This contractual work revealed the need for equipment modifications for cost effective NDE processes. For acoustical holography and intensity mode Holographic ultrasound, the existing analog data handling does not permit definitive signal intensity analysis. In order to have a method of relating signal strength to defect size, a digital approach is recommended. Holographics has developed a digital memory bank capable of 256 X 256 X-Y location scanning with each location capable of 64 levels of intensity and 64 levels of phase shift. This advanced memory system is applicable to HIP'd inspection.

Rotating engine parts have circular symmetry so the scanners should be based on a $\rho-\theta$ rather than x-y grid. Attempts have been made to develop $\rho-\theta$ scan approaches but the complexity in the subsequent holographic transmit mode seems excessive. This problem has been circumvented by use of a mathematical conversion of x-y to $\rho-\theta$. This appears to be a solution to this problem.

For actual engine hardware, software needs to be developed to be used with encoders to coordinate manipulator movements with the response signals and feed into the signal processor. This software must be compatible with contour following elements of the manipulator.

Finally, for the acoustical holographic mode only, a much larger process computer is required to handle the complexity of input information, process the Fournier wave forms and deliver output information to generate the holograms. This would have been difficult to do even two years ago. The quantity of data to be handled and the myriad of conversion operations that are made require very large memory banks and extensive computer processing. Without the recent advancements in preprogrammed subsystems and microprocessor chips the cost of the software and hardware would be prohibitive and there is doubt that the data could be handled within a reasonable time frame.

For Compton scattering evaluation, the process is adaptable primarily to automation. The early work on this concept was performed on crude laboratory equipment so much work is necessary to develop a cost effective system. The requirement to inspect a very small volume at one counting sequence almost demands automatic manipulation and data handling to permit cost effective scanning of an entire part. Recent advancements in scintillation counters, microprocessor chips and systems, and precision manipulators all contribute to capabilities of designing a cost effective system. Much of the interface software programs being developed for the acoustical holographic systems could be applicable to the Compton scattering approach.

However, the complicated information of the acoustical holography is reduced to a single photon count per measuring location for the Compton scattering approach. This greatly reduces information processing requirements.

However, there is an additional hardware problem unique to the Compton - scattering system. The total economics of the process is governed primarily by inspection time. The greatest contributor to a cost effective system is the efficiency of the scattering collimator system, an area requiring equipment development to capture the maximum percentage of the scattered photons from the inspection volume.

CONCLUSIONS AND RECOMMENDATIONS

- o Radiographic Tomography demonstrated limited value for the aircraft engine. The process is not sensitive enough for rotating hardware. If problems are solved relative to the proper X-ray film, there may be some value in inspecting castings. It is recommended that no additional work be done with this process at this time.
- o Neutron Radiography was quite inadequate in sensitivity required for engine hardware. Even when using penetrants designed with high capture cross section, results were inadequate. Exposure times were excessive indicating a high cost even if sensitivity were acceptable. A small use is possible in identifying non-metallic rings and seals in assemblies. However, if other uses for equipment cannot be developed, it would be difficult to justify a facility for this application only. No additional work with this process is recommended.
- o Advanced FPI Systems - An improved FPI system was explored using an ultra-high penetrating fluid, hydrophilic remover and non-aqueous developer. The system proved very useful in examining tight surface cracks and is recommended for this type of defect.
- o High Gain Ultrasonics - Some high gain ultrasonic effort indicated a possibility of improving conventional ultrasonic capabilities. Use of such a process as an interim measure may be beneficial if improved sensitivity is required. However, even improved ultrasonics appears to be quite limited in sensitivity and quite inferior to some new processes in identifying size, shape and location of defects. With the additional promise of fully automatic, cost effective inspection with acoustical holography and Compton scattering, it seems reasonable to consider this at best, an interim process. Effort that could be spent on this process could probably be better invested accelerating acoustical holography.
- o Intensity Mode Holographic Ultrasonics - This process promises immediate improvement in defect location and sensitivity. With certain equipment modifications (see page 146) accurate defect size assessment seems probable. However, since the same equipment, with an additional Fourier transmit computer could yield full acoustical holography, the intensity mode Holographic ultrasound would also be considered an interim step. It seems reasonable to develop acoustical holography using intensity mode only to perfect this more advanced approach.
- o Acoustical Holography - This process has great promise but much effort is required to modify existing equipment for production capabilities of aircraft turbine hardware. The pay off in automatic cost effective inspection and improved sensitivity (if required) give adequate justification

for pursuing this process. Its application would be primarily in inspection prior to final machining. Economics would favor large parts and relatively simple shapes. Effort is recommended to pursue equipment modifications discussed on page 146.

- o Compton Scattering - This process compliments acoustical holography. It is a new process requiring much effort to reach production capabilities for aircraft turbine hardware but this effort appears to be justified. This NDE process promises equal or better sensitivity of any of the other processes. It appears to have capabilities of inspecting finished machined surfaces and service hardware for small defects and this is an unique capability. There is strong argument for specific inspection of high stress regions of rotating hardware. The process is also capable of inspecting complex shapes. Conversely, it does not appear to be cost effective for inspecting the complete volume of large parts or very thick parts. Additional effort is recommended to substantiate the claims which presently involve extrapolation of limited test data.

BIBLIOGRAPHY

1. Contract No. DAAJ02-73-C-0106; Development of Hot Isostatically Pressed Rene' 95 Turbine Parts, P.S. Mathur and J.L. Bartos - General Electric Co.; Final Report Aug. 1976.
2. Contract No. DAAJ01-75-C-0894 ; A Comparison of Various Non-Destructive Inspection Processes Using Hot Isostatically Pressed Powder Turbine Parts, D. Nulk Dec. 1975
3. Avscom Report No. TR76-25 - An Evaluation of Real and Programmed Defect Conditions in HIP Discs Using Hologonics System 200 Scanned Acoustical Holography Imaging System N.J. Knuter, June 1976
4. Avscom Report No. TR-76-24 - Evaluation of Calcium 252 Based Neutron Radiography and Photon Scattering Techniques for the Inspection of Hot Isostatically Pressed Components of T700 Aircraft Engine. Aug. 1976 H. Harper et al
5. Contract No. DAAG-76-C-0019; Fully Automated Systems for Inspection of Explosive Charge of 105mm M-1 Projectiles Under the U.S. Army's Ammunition Base Modernization Program. Hans Weber et al Jan. 7, 1976.

APPENDIX I

Portions of Rene' 95 hot isostatically pressed powder G.E. specification
C50TF64.

3. REQUIREMENTS

3.1 Raw Material

3.1.1 Parts shall be produced from powder of a nickel base alloy known as Rene'95.

3.1.2 Chemical Composition, Percent

Carbon -----	0.04-0.09	Columbium -----	3.30-3.70
Manganese -----	0.15 Max.	Zirconium -----	0.03-0.07
Silicon -----	0.20 Max.	Titanium -----	2.30-2.70
Sulfur -----	0.015 Max.	Aluminum -----	3.30-3.70
Phosphorus -----	0.015 Max.	Boron -----	0.006-0.015
Chromium -----	12.00-14.00	Tungsten -----	3.30-3.70
Cobalt -----	7.00-9.00	Oxygen -----	0.010 Max.
Molybdenum -----	3.30-3.70	Nitrogen -----	0.005 Max.
Iron -----	0.50 Max.	Hydrogen -----	0.001 Max.
Tantalum -----	0.20 Max.	Nickel -----	Remainder

3.1.2.1 Powder from each powder lot shall meet the carbon, hydrogen, oxygen, and nitrogen limits before blending to form a powder heat. If the powder heat is to be made up by blending several powder lots, procedures for blending and sampling for chemical analysis shall be as agreed upon by Purchaser and powder suppliers.

Appendix I (Continued)

	<u>Room Temperature</u>		
	<u>CLASS A</u>	<u>CLASS B</u>	<u>CLASS C</u>
Tensile Strength, psi -----	230,000	220,000	208,000
Yield Strength (0.2% offset), psi	180,000	170,000	166,000
Elongation, % in 2 inches or 4D --	10	10	10
Reduction of Area, % -----	12	12	12

	<u>1200F</u>		
	<u>CLASS A</u>	<u>CLASS B</u>	<u>CLASS C</u>
Tensile Strength, psi -----	207,000	197,000	186,000
Yield Strength (0.2% offset), psi-	167,000	161,000	153,000
Elongation, % in 2 inches or 4D --	8	8	8
Reduction of Area, % -----	10	10	10

SI UNITS

	<u>Room Temperature</u>		
	<u>CLASS A</u>	<u>CLASS B</u>	<u>CLASS C</u>
Tensile Strength, MPa -----	1586	1517	1434
Yield Strength (0.2% offset), MPa-	1241	1172	1145
Elongation, % in 50.8 mm or 4D ---	10	10	10
Reduction of Area, % -----	12	12	12

	<u>649C</u>		
	<u>CLASS A</u>	<u>CLASS B</u>	<u>CLASS C</u>
Tensile Strength, MPa -----	1427	1358	1282
Yield Strength (0.2% offset), MPa-	1151	1110	1055
Elongation, % in 50.8 mm or 4D ---	8	8	8
Reduction of Area, % -----	10	10	10

3.3.1.2 The location and CLASS of the required tensile specimens shall be as specified on the drawing.

3.3.2 Stress Rupture

3.3.2.1 Test specimens shall be tested at 1200F (648.9C) and 150,000 psi (1034 MPa) and shall meet the applicable minimum life requirement specified below. Tests shall be continued to rupture, and elongation after rupture, measured at room temperature, shall be not less than three percent in 4D.

	<u>Minimum Life, Hours</u>
CLASSES A and B:	50
CLASS C:	35

Appendix II
Portions of GE Specification, P3TF1 for Neltrasonic Testing

3.8 Test Procedures

3.8.1 Material shall be inspected by the immersed technique at five megahertz frequency or above, except four megahertz frequency may be used for shear mode. Both longitudinal and shear types of inspection shall be performed unless otherwise specified.

3.8.2 For inspection on flat surfaces, transducers shall be no larger than .75 inch (19.0 mm) diameter. A reflector may be used for thin sheet if desired. Shear wave inspection of plate, sheet and strip shall be performed in both longitudinal and transverse directions.

3.8.3 CLASS B: For diameters less than 10 inches (254 mm), focused transducers shall be used. The focal zone shall not exceed .3 inch (8 mm) in the circumferential direction at the point of entry into the material and shall also not exceed one inch (25 mm) in length in the axial direction. Alternate transducer configurations may be used with prior approval of the Purchaser. Automatic equipment which traverses a spiral path is satisfactory, but the following two traverses shall be made unless otherwise specified:

- (a) With the transducer in the circumferential shear position.
- (b) With the transducer in the longitudinal wave position.

3.8.4 Place a reference point or identifying mark on the material so that any indications found on the initial inspection may be defined in terms of the reference point in the inspection reports and may be readily located during future inspections.

3.8.5 CLASS B: Maximum scan spacing (or one helix) shall be no greater than 75 percent of the effective beam width.

3.9 Calibration

3.9.1 If equipment has been off for more than 15 minutes, allow the manufacturer's recommended warm-up time on equipment, or 15 minutes whichever is greater.

3.9.2 Calibration shall be performed before and after the ultrasonic inspection of each part, or at least at the beginning and end of each work shift. If the magnitude of the indication from the post-test calibration differs 10 percent or more from the pre-test calibration indication, all material inspected since the pre-test calibration shall be reinspected. Calibration may be performed on artificial defects cut into the actual material if that portion of the material is later trimmed and scrapped, or on material of the same type in test blocks per 4.3.2 or with geometry similar to the material to be inspected. Water travel shall be recorded and shall be maintained for inspection with flat transducers within .25 inch (6.4 mm) of that used for calibration; water travel for focused transducers shall be as specified on the applicable scan plan.

Appendix II (Continued)

3.9.3 CLASS A: Shear Wave

3.9.3.1 With the search unit directed at the near surface of test block, change the transducer position until the calibration defect deepest from the incident surface produces a maximum signal response at approximately 45 degree shear wave sound path in the material. The magnitude of this indication shall be adjusted to 80 percent of full amplitude, and the gain setting recorded for comparison with periodic or post-test calibration. Each of the other calibration defects shall have their signal response adjusted to 80 percent amplitude, and the gain setting recorded. Evaluation shall be done with the gain setting for the most applicable calibration defect, but inspection shall be done at the highest of the above gain settings.

3.9.4 Longitudinal Wave

3.9.4.1 CLASS A: An attenuation check shall be made on the maximum thickness region of the material by first confirming that sound transmission is possible. If one full back reflection cannot be attained in this region, calibration shall be made to half thickness and inspection shall be performed from both sides. If the gain setting is 30 percent greater than that required for a similar distance in the calibration test block, then a calibration test block which has similar attenuation shall be used or an approved attenuation correction shall be made. Calibration settings to achieve 80 percent full scale amplitude of the above holes shall be recorded along with the magnitude of other applicable calibration defects. For example, on cylindrical forgings, the hole nearest the near surface should be set at 80 percent and the amplitudes recorded for the indication from the holes nearer the far surface. The gain settings should be recorded. Similarly, gain settings should be recorded to achieve 80 percent full scale as above on each of the other applicable calibration holes at each gain setting.

3.9.4.2 CLASS B: Holes C and E (GE drawing 9064M16) shall be used to obtain appropriate sensitivity setting for longitudinal inspection. With the transducer directed normal to the surface, scan along the bar axis until the transducer is directly over hole E. The gain shall be adjusted to achieve an 80 percent full scale amplitude. Record this setting. Repeat this procedure for hole C. Inspection shall be performed with the instrument set at the maximum of the two gain settings recorded above.

3.9.5 CLASS A: Surface Wave

3.9.5.1 Whenever thickness is less than .050 inch (1.27 mm) or whenever the geometry precludes shear inspection, calibration for surface wave inspection shall be performed. Notches perpendicular to the surface and of depth three percent of thickness, or .001 to .010 inch (0.03 to 0.25 mm) width not greater than .003 inch (0.08 mm) and length not to exceed .5 inch (13 mm) shall be placed in a position not closer than .5 inch (13 mm) of edge or other major surface deviation. Where possible, the notches shall be placed in the front and back surface, unless the calibration piece is readily inverted.

Appendix II (Continued)

3.9.5.2 The surface wave search unit shall be placed so that the beam is directed toward the broad side of the notch. Sensitivity of the unit shall be adjusted until the indication of the notch is clearly defined and is 80 percent amplitude. This sensitivity setting shall be recorded. The search unit shall be moved backward until the image disappears from the screen, and then forward until the image maximizes on the screen. Distance shall be measured from some reference on the search unit to the notch so that distances may subsequently be measured properly on the material being inspected.

3.9.6 CLASS B: Circumferential Shear Wave

3.9.6.1 In shear wave calibration of bars 2.75 inches (69.8 mm) in diameter and greater, test blocks shall be equipped with holes B, D, and F; to GE drawing number 9064M16. In bars under 2.75 inches (69.8 mm) in diameter, hole F only may be used to obtain the appropriate sensitivity setting for the circumferential shear inspection. The transducer may be angled or offset to achieve the 45-degree sound propagation within the bar. An offset of 1/6th bar diameter is a good starting point to establish the proper angle. Appropriate gain setting shall be recorded for future calibration checks.

3.9.6.2 Calibration configurations other than flat bottom holes may be approved by the Purchaser as working calibration standards provided it can be proved that the alternate configuration establishes equal or greater sensitivity, resolution and penetration.

3.9.7 CLASS B: Dynamic Calibration

3.9.7.1 The calibration defect used for the specific inspection being performed shall be recorded or monitored at operating speeds. This verification of calibration shall be performed at least every four hours. If more than 10 percent change in calibration is evidenced, all material inspected since the previous calibration shall be re-inspected.

3.10 Inspection

3.10.1 Testing shall be conducted so that all material in the required zone is scanned during each type of inspection. This can be done by advancing the search unit or part no more than three-fourths of the minimum effective beam diameter of the specific transducer in use.

3.10.1.1 CLASS B: A system utilizing gate monitoring without recording (C-scan or strip-chart) shall be set so that when an indication other than the end of the bar activates the alarm, the system will shut down, or will alarm continuously. The sensitivity shall not be reduced near the end of each bar. The gate shall be placed between the front and back reflections, as close to the front reflection as noise will allow to enable recording or monitoring of defects. In no case may the gate monitor less material than included between the outer diameter and the center of the bar.

Appendix II(Continued)

3.10.2 Both shear wave and longitudinal wave ultrasonic inspection shall be performed, except where surface wave inspection is indicated in 3.9.5 above. In such cases, surface wave inspection replaces all or part of the shear wave inspection.

3.10.3 Inspection shall be performed at a rate compatible with sensitivity and resolution required for the specific material being inspected with such things as pulse repetition rate, effective beam diameter, lineal surface speed, etc., being taken into consideration. Focal distance during inspection shall be maintained equal to that used in the calibration for such material.

* 3.10.4 Inspection shall generally be performed at the maximum of the calibration sensitivity settings, but evaluation of an indication shall be to the most appropriate calibration defect; that is, surface wave indications shall be compared to the surface calibration notch on the proper surface, and internal indications shall be compared to that calibration hole which has metal travel equal to the indication or the next greater metal travel than that of the indication.

3.10.4.1 CLASS A: Amplitude, location, and depth of all indications 10 percent of full scale less than drawing requirement or 60 percent of full scale, whichever is smaller shall be recorded and reported. The length or area dimensions of indications which are relatively continuous [.250 inch (6.35 mm)] at magnitude of 30 percent amplitude of full scale or greater shall be recorded.

3.11 Rejection

* 3.11.1 CLASS A: Indications which exceed the magnitude obtained from the appropriate calibration defect and any indication of a continuous nature (i.e., continually of greater than 25 percent magnitude) which has any dimension over .5 inch (13 mm) shall be cause for rejection. For longitudinal wave inspections on material less than .125 inch (3.18 mm) thick, reduction of the magnitude on fourth back reflection, or from the reflector, to 50 percent or below shall be cause for rejection.

CLASS B: Unless otherwise specified, acceptable limits shall be 60 percent of full scale for bar stock under 2.75 inches (69.8 mm) in diameter and 40 percent for bar stock 2.75 inches (69.8 mm) and over in diameter. Evaluation of those indications which are within five percent of the acceptance limit shall be made in comparison to the calibration hole of equal or next greater metal travel. The appropriate calibration hole being used for comparison shall have its indication set at a screen amplitude of 80 percent of the full scale during the evaluation.

3.11.2 Unacceptable indications which can be removed without affecting the usability of the material may be resubmitted for ultrasonic inspection after rework.

Appendix III

A portion of GE Specification P3TF2

APPROVED FLUORESCENT PENETRANT INSPECTION SYSTEMS

P3TF2 Class	Inspection Systems	Oil Soluble Penetrants	Emulsifiers	Dry Powder Developers	Classes A+B		Solvent Mixed Developers	Penetrant Removers
					Water Mixed Developers	Water Mixed Developers		
A, S	Tokushu	OD-1700A	OD-1700B	DN 600P	DN 900B	-	-	-
	Ardrox	985 P1	9PR3, 9PR4	9D3	9D71	-	-	-
	Dubl-Chek	FP-22	ER-82	D-90	D-110	-	ER-82	ER-82
	Fluro-Chek	P-21	EB, E4	DD2	WD	NAD, NAD-NF	-	EW
A, B, C	Tracer-Tech	P-148A	E157A	D493A	D492C	D495A, D499A, D499C	-	-
	Zygo	ZL2, ZL2A	ZE4B, ZE4A	ZP4A	ZP-13A, ZP-5	SKD-S, SKD-NF	-	ZR1, ZR10
	Ardrox	985P2, 985P3	9PR3, 9PR4	9D3	-	-	-	-
	Dubl-Chek	FP-30A	ER-82	D90	-	-	-	ER-82
D, E, F	Fluro-Chek	P40-B-GE	EB, E4	DD2	-	NAD, NAD-NF	-	EW
	Tracer Tech	P-149	E157A	D493A	-	D495A, D499A, D499-C	-	-
	Zygo	ZL2-ZL2A	ZE4B, ZE4A	ZP4A	-	SKD-S, SKD-NF	-	ZR1, ZR10
	Tokushu	OD-6000	OD-1700B	DN 600P	-	-	-	-
C, D, E, F	Fluro-Chek	P-41	E-41	DD-2	-	NAD	-	-
	Zygo	ZL30A	ZE4A	ZP4A	-	ZP9	-	ZR1, ZR10

Higher Sensitivity for Classes D & E Hardware

Appendix III (Continued)

APPROVED WATER WASHABLE FLUORESCENT PENETRANT INSPECTION SYSTEMS

P3TF2 Class	Inspection Systems	Water Soluble Penetrants	Dry Powder Developers	Water Mixed Developers	Solvent Mixed Developers
A, B, C, D, E	Dubl-Chek	HM-440	D-90	-	-
A, B	Fluro-Chek	WP-100	WD, DD-2	-	-
C, D, E	Fluro-Chek	WP-169	DD-2	-	-
A, B, C	Insta-Viz	PSF4	D-1	-	-
A, B, C, D, E	Tracer-Tech	P134A	D-493A	-	-
C, D, E	Tracer-Tech	P136	D-493A	-	-
A, B	Zygio	ZL-60	-	ZP-5	-
A, B, C, D, E	Zygio	ZL-60	ZP4A	-	ZP-9
A, B, C, D, E	Zygio	ZL-54	ZP4A	ZP-5	ZP-9
A, B	Tokushu	OD-2800-1	-	DN-900	-
C	Tokushu	OD-2800-1	DN-600P	-	-
D, E	Tokushu	OD-2800-2	DN-600P	-	-
A, B, C	Ardrox	970P10	9D3	-	-

DISTRIBUTION LIST
 US ARMY AVIATION SYSTEMS COMMAND
 PRODUCTION ENGINEERING MEASURES PROJECTS
 FINAL OR INTERIM REPORTS

<u>No. of Copies</u>	<u>To</u>
	Commander; US Army Aviation Systems Command; PO Box 209; St. Louis, Missouri 63166
10	ATTN: DRSAV-EXT
1	ATTN: DRSAV-FE (Cliff Sims, Maint Engr)
1	ATTN: DRSAV-EQ (C. Crawford, Sys Dev & Qual)
1	ATTN: DRSAV-FES (H. Bull, Corpus Christi)
2	ATTN: DRSAV-ZDR (Ref Library)
1	ATTN: DRSAV-LEP (Mr. D. Fleming)
1	Project Manager; Advanced Attack Helicopter; ATTN: AMCPM-AAH, TM; P.O. Box 209; St. Louis, Missouri 63166
1	Project Manager; Utility Tactical Transport Aircraft System; ATTN: AMCPM-UA-T; P.O. Box 209; St. Louis, Missouri 63166
1	Project Manager; CH-47 Modernization; ATTN: AMCPM-CH47M; P.O. Box 209; St. Louis, Missouri 63166
1	Project Manager; Advanced Scout Helicopter; ATTN: AMSAV-SIA, P.O. Box 209; St. Louis, Missouri 63166
1	Product Manager; Aircraft Survivability Equipment; ATTN: AMCPM-ASE-TM; P.O. Box 209; St. Louis, Missouri 63166
1	Product Manager; Cobra; ATTN: AMCPM-CO-T; P.O. Box 209; St. Louis, Missouri 63166
1	Product Manager; Iranian Aircraft Program; ATTN: AMCPM- IAP-T; P.O. Box 209; St. Louis, Missouri 63166
4	Commander; US Army Material Command; ATTN: AMCRD-TE; 5001 Eisenhower Avenue; Alexandria, Virginia 22333
1	Director; Eustis Directorate; US Army Air Mobility R&D Lab; ATTN: SAVDL-EU-TAS; Ft. Eustis, Virginia 23604 (Mr. Haselbauer)
1	Director; Ames Directorate; US Army Air Mobility R&D Lab; ATTN: SAVDL-AM; Ames Research Center; Moffett Field, (Mr. Andre) California 94035

<u>No. of Copies</u>	<u>To</u>
1	Director; Langley Directorate; US Army Air Mobility R&D Lab; ATTN: SAVDL-LA; Mail Stop 266; Hampton, Virginia 23365
1	Director; Lewis Directorate; US Army Air Mobility R&D Lab; ATTN: SAVDL-LE; 21000 Brook Park Rd; Cleveland, Ohio 44135
2	Director; US Army Materials & Mechanics Research Center; Watertown, MA 02172 ATTN: AMXMR-PT (Mr. Fahey) ATTN: AMXMR-MQ
1	Director; Production Equipment Agency; Rock Island Arsenal; ATTN: AMXPE-MT; Rock Island, IL 61201
	Air Force Materials Laboratory; Manufacturing Technology Division; Wright-Patterson Air Force Base, Ohio 45433
1	ATTN: AFML/LTM
1	ATTN: AFML/LTN
1	ATTN: AFML/LTE
1	Commander; US Army Electronics Command; Ft. Monmouth, NJ ATTN: AMSEL-RD-P
1	Commander; US Army Missile Command; Redstone Arsenal, AL 35809 ATTN: AMSMI-III
1	Commander; US Army Troop Support Command; 4300 Goodfellow Blvd.; St. Louis, MO 63120 ATTN: AMSTS-PLC
1	Commander; US Army Armament Command; Rock Island, IL 61201 ATTN: AMSAR-PPR-IW
1	Commander; US Army Tank-Automotive Command; Warren, MI 48090 ATTN: AMSTA-RCM.1
12	Commander; Defense Documentation Center; Cameron Station; Building 5; 5010 Duke Street; Alexandria, Virginia 22314
2	Hughes Helicopter; Division of Summa Corporation; ATTN: Mr. R.E. Moore, Bldg. 314; M/S T-419; Centinella Ave & Teale Street; Culver City, CA 90230
2	Sikorsky Aircraft Division; United Aircraft Corporation; ATTN: Mr. Stan Silverstein; Section Supv, Manufacturing Tech.; Stratford, Connecticut 06497

No. of
Copies

To

- 2 Bell Helicopter Co.; ATTN: Mr. P. Baumgartner, Chief,
Manufacturing Technology; P.O. Box 482; Ft. Worth, Texas 76101
- 2 Kaman Aerospace Corp.; ATTN: Mr. A.S. Falcone, Chief of
Materials Engineering; Bloomfield, Connecticut 06002
- 2 Boeing Vertol Company; ATTN: R. Pinckney, Manufacturing
Technology; Box 16858; Philadelphia, PA 19142
- 2 Detroit Diesel Allison Division, General Motors Corporation;
ATTN: James E. Knott; General Manager; P.O. Box 894;
Indianapolis, Ind. 46206
- 2 General Electric Company; ATTN: Mr. H. Franzen; 10449 St.
Charles Rock Road; St. Ann, MO 63074
- 2 AVCO-Lycoming Corp.; ATTN: Mr. V. Strautman, Manager
Process Technology Laboratory; 550 South Main Street; Stratford,
Conn. 08497
- 2 United Technologies Corp.; Pratt & Whitney Aircraft Div.;
Manufacturing Research and Development; ATTN: Mr. Ray Traynor;
East Hartford, Conn. 06108